A NEW DIGITAL BANDPASS FILTERING SCHEME FOR THE EFFICIENT IMPLEMENTATION OF THE SPLIT SPECTRUM TECHNIQUE FOR ULTRASONIC NONDESTRUCTIVE EVALUATION

Thesis

Submitted to

Graduate Engineering and Research
School of Engineering

UNIVERSITY OF DAYTON

In Partial Fulfillment of the Requirements for

The Degree

Master of Science in Electrical Engineering

by

Orlando J. Canelones

UNIVERSITY OF DAYTON

Dayton, Ohio

December 1991

To my parents Benjamin and Isabel and to my wife Dawn Marie Canelones

A NEW DIGITAL BANDPASS FILTERING SCHEME FOR THE EFFICIENT IMPLEMENTATION OF THE SPLIT SPECTRUM TECHNIQUE FOR ULTRASONIC NONDESTRUCTIVE EVALUATION.

APPROVED BY:

Frank Scarpino, Ph.D
Advisory Committee, Chairman

Franklin E. Eastep, Ph.D.
Associate Dean/Director
Graduate Engineering and Research
School of Engineering

Patrick J. Sweeny, Ph.D.
Dean, School of Engineering

ABSTRACT

A NEW DIGITAL BANDPASS FILTERING SCHEME FOR THE EFFICIENT IMPLEMENTATION OF THE SPLIT SPECTRUM TECHNIQUE FOR ULTRASONIC NONDESTRUCTIVE EVALUATION

Name: Canelones, Orlando J.
University of Dayton, 1991

Advisor: Dr. Prasanna Karpur

Split spectrum processing (SSP), based on the decomposition of ultrasonic signals by multiple narrow-band filtering, has been proved efficient in the suppression of backscattering noise in the nondestructive evaluation of materials in order to enhance the signal-to-noise ratio of such signals for flaw detection and characterization purposes. However, SSP is a computationally intensive technique requiring long processing times. Industrial inspection procedures often demand fast acquisition and processing rates making a real time or near-real time implementation of the technique very appealing. SSP is currently performed by means of Fast Fourier Transform techniques which can be very efficiently implemented with digital signal processors; despite the fact that, strictly speaking, the FFT is a non-real time instrument since it requires the availability of all points before processing. This thesis investigates the efficient finite impulse response (FIR) as well as the frequency domain (FFT)

implementation of SSP from two standpoints. First, it considers a reduction in the size of the bandpass-filter bank by employing bandpass filters with flat-top frequency responses (Hanning windows), as opposed to the more conventional Gaussian filters. This allows to concentrate more energy within the filter's bandwidth without substantially increasing the correlation between adjacent filters. Secondly, it advances a computationally efficient approach towards the design of FIR narrow-band bandpass filters for SSP based on a two branch structure of cascaded lower-complexity subfilters. This work demonstrates that it is, indeed, possible to greatly reduce the computational load of the technique with smaller filter banks without compromising SNR performance and that a very efficient tapped-delay line (VLSI) implementation is also within reach. This document presents the results from simulations and experiments on ultrasonic signals based on signal-to-noise ratio performance and a comparison between this approach and the more traditional Gaussian-filter scheme.

ACKNOWLEDGEMENTS

I would like to express my sincere gratitude to Dr. Frank Scarpino for introducing me to the world of digital filters, and to Dr. Prasanna Karpur for his continued support and guidance both technical and moral during the course of this work. Also, I would like to extend my appreciation to the Structural Integrity Division people of the University of Dayton Research Institute, especially Dr. Joseph Gallagher, whose moral support for this effort has been invaluable. Last, but not least, I would like to thank my wife Dawn whose enduring patience and understanding have made this work possible, and whose technical assistance was crucial in the creation of this manuscript. To those not mentioned, allow me to express my heartfelt thanks. This work was supported by and performed on site in the Nondestructive Evaluation Branch, Materials Directorate, Wright Laboratories, Wright-Patterson Air Force Base, Ohio 45433-6533 under contract F33615-89-C-5612.

TABLE OF CONTENTS

LIST OF ILLUSTRATIONS

LIST OF TABLES

CHAPTER I

SPLIT SPECTRUM PROCESSING

1.1 Introduction

Ultrasonics is of great importance in the nondestructive evaluation (NDE) of engineering materials and noninvasive diagnostic medicine. Defects and anomalies can be detected, located, sized and classified by means of ultrasonic signals provided the backscattering noise or interference patterns contained within the received signals can be suppressed to acceptable levels; that is to say, the signal-to-noise ratio (SNR) must be adequately enhanced.

Split spectrum processing (SSP) was introduced in the late 1970's as a technique adapted from radar applications[18] to improve the signal-to noise ratio in ultrasonic signals. Figure 1.1 depicts the filtering scheme for SSP. The spectrum of the received ultrasonic signal is split into different overlapping frequency bands by means of equally spaced Gaussian bandpass filters with constant bandwidth. The split frequency bands so obtained have time domain representations called spectral decomposition components which can be compounded using techniques such as minimization[18], polarity thresholding[1], or both[4], etc. Excellent SNR enhancements have been reported with SSP in the literature[1,2,4]. As an example, figure 1.2 shows an ultrasonic signal containing a great deal of

clutter which completely hides or obscures the flaws or defects within the material sample. The signal is, once again, shown in figure 1.3 after the application of the split spectrum technique. It is quite evident that this backscatter-reduction technique is very efficient in the removal of material clutter for the detection of flaws and defects. The SNR performance of SSP is very sensitive to processing parameters such as the number of filters used for the spectral splitting, the filter bandwidth, the frequency separation between adjacent filters and the location of the filter bank within the available bandwidth of the transducer. The proper selection of these parameters for optimal SNR performance has been recently studied and established by Karpur *et al* [1,4,5].

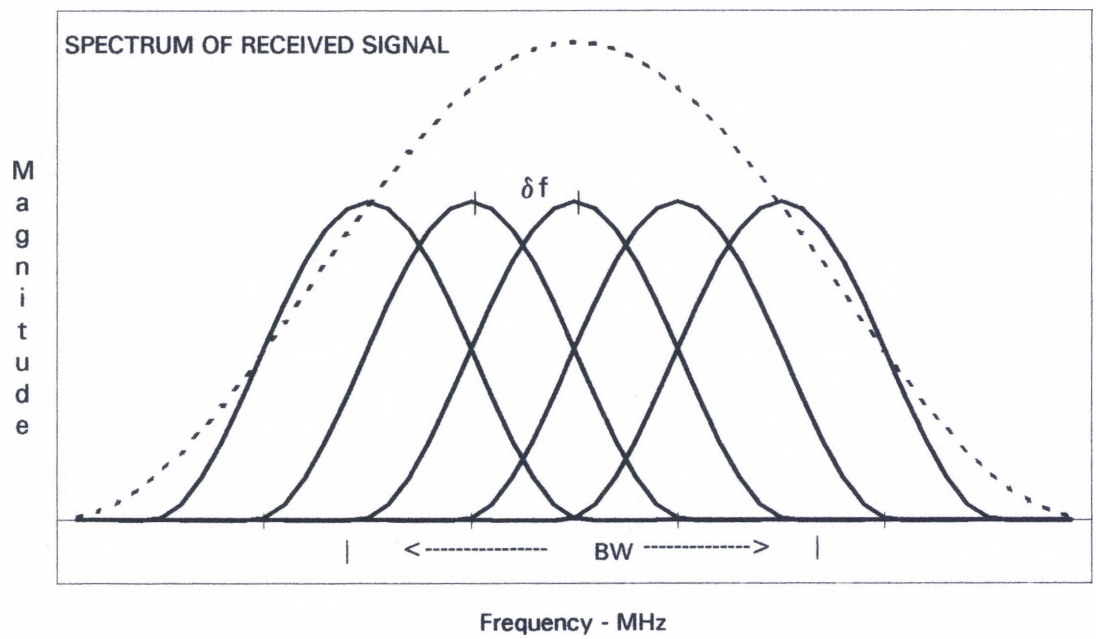

Fig. 1.1 Conventional Filtering Scheme of the Split Spectrum Technique.

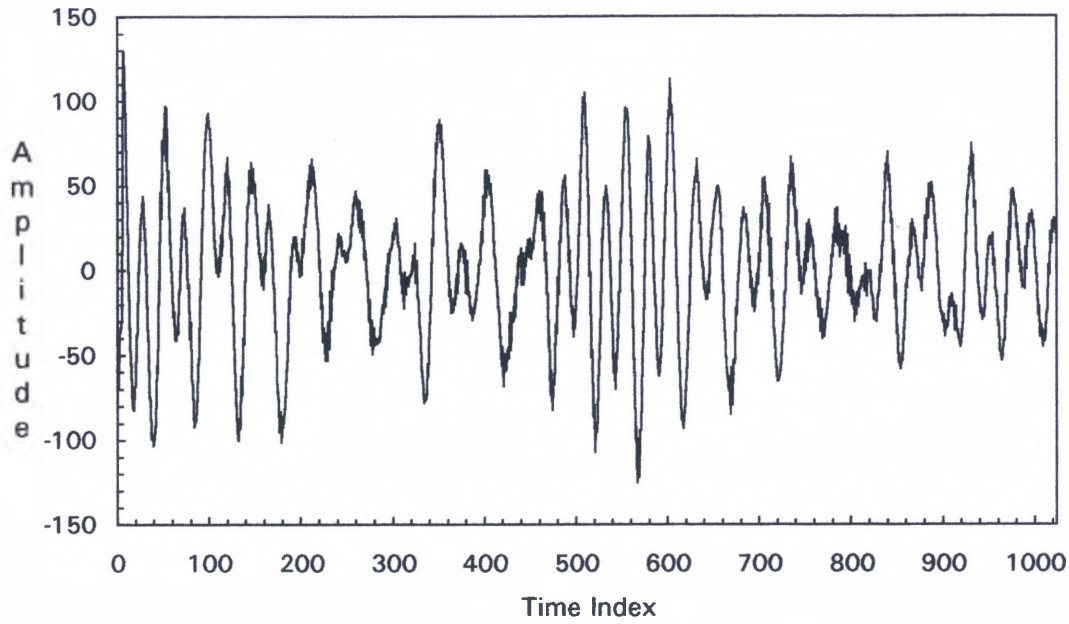

Fig. 1.2 Unprocessed Ultrasonic Signal.

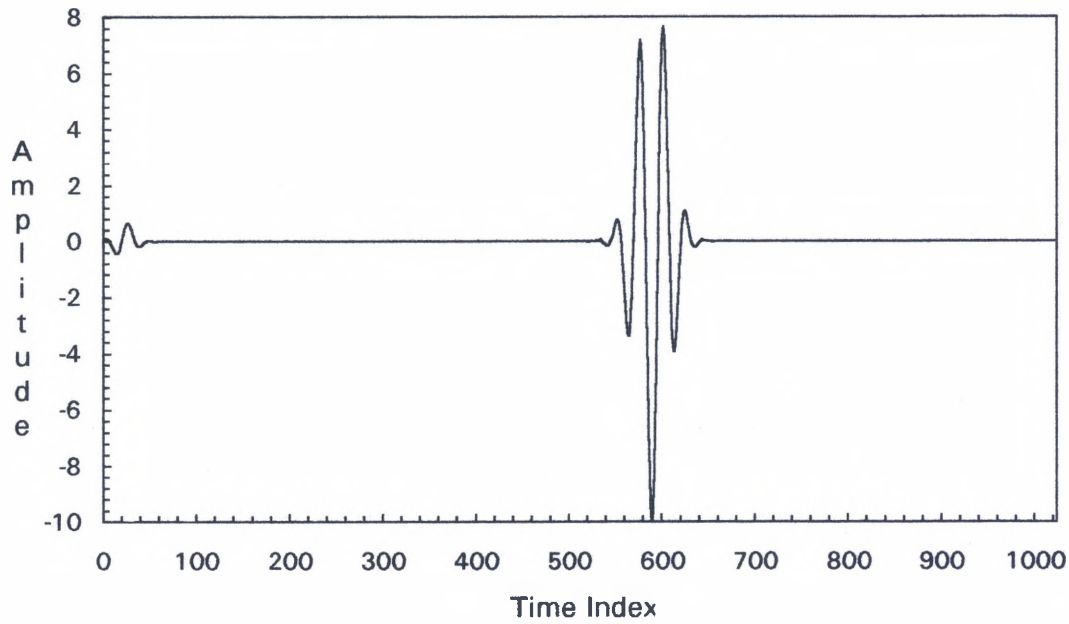

Fig. 1.3 Signal after Processing by SSP. A Target is Clearly Revealed.

1.2 Foundations of Split Spectrum Processing

Split spectrum processing is based on the physics of the interaction between ultrasonic waves and random scatterers of the material grain structure. Grain noise or clutter is an interference pattern produced when the ultrasonic signal is scattered by the randomly packed, unresolvable grains present in the material under test. Since it is an interference pattern, the clutter is dependent upon the relative spatial position of the transducer and the test material as well as on the frequency of the transmitted signal. Split spectrum processing makes use of the fact that the interference pattern is dependent on frequency.

A typical ultrasonic signal received from a material under test can be represented by a time limited signal

$$r(t) = f(t) + n(t) , \qquad 0 \leq t \leq T \qquad \textbf{(eq.1.1)}$$

where f(t) is the signal from a flaw or target and n(t) in the noise signal from the material grains. In SSP, the received signal is decomposed into a set of N narrow-band signals $r_i(t)$ of normalized amplitude by frequency-domain filtering, and the above equation becomes a set of N equations

$$r_i(t) = f_i(t) + n_i(t) , \quad i = 1, N \qquad \textbf{(eq.1.2)}$$

as shown in figure 1.4.

The narrow-band signals $f_i(t)$ have some invariable properties as they are produced by the same flaw or target; however, the noise frequency

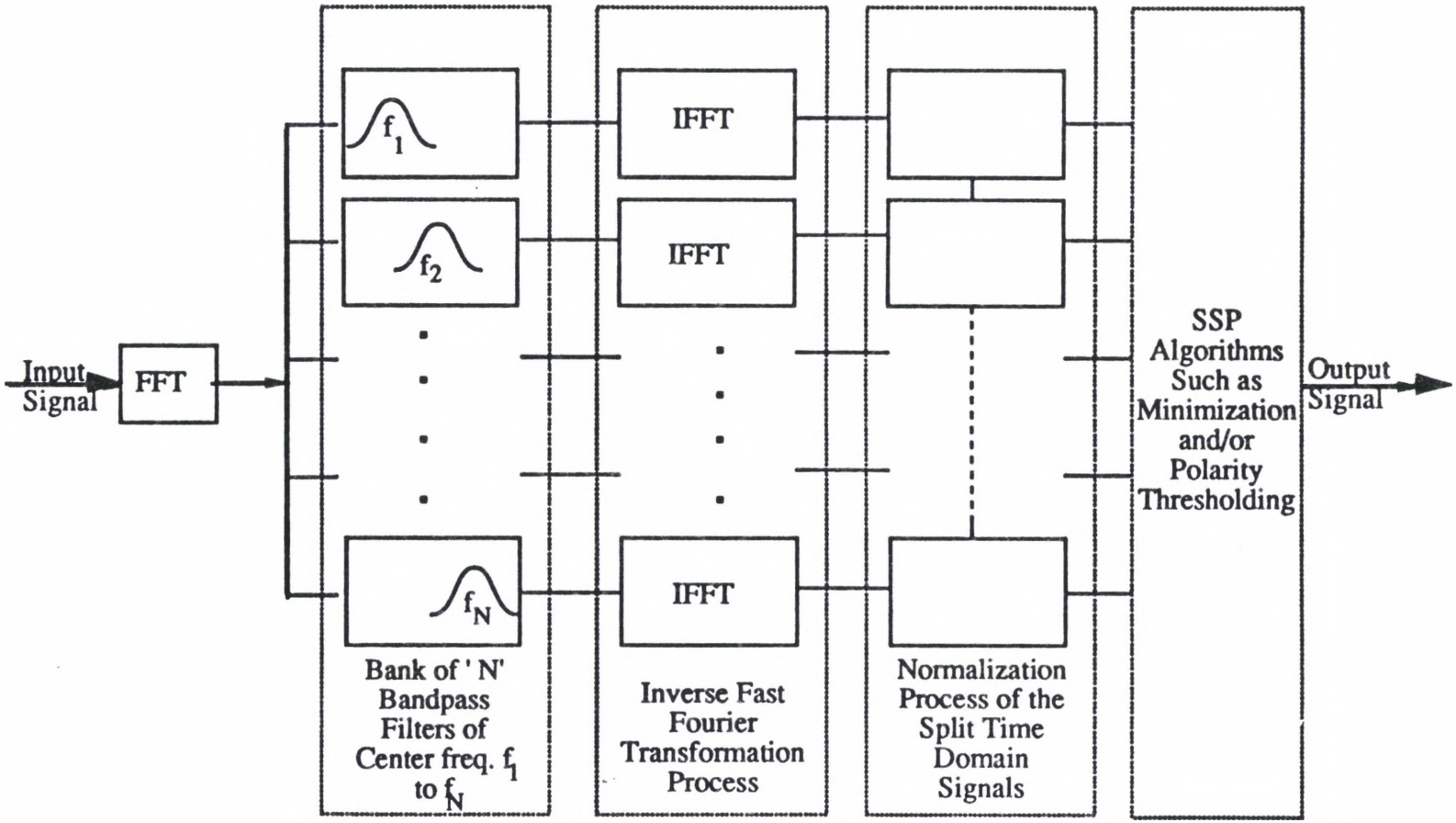

Fig. 1.4 SSP Implementation.

components $n_i(t)$ may exhibit variable properties since they are an interference pattern. This can be better understood by considering figure 1.5, where the principle of operation of the technique is illustrated in terms of phasors. The resultant phasor is a combination of both a phasor from a flaw or reflector and a set of randomly oriented phasors from random scatterers in the material. The SSP algorithms, in general, utilize the property that the energy from the specular reflector is distributed rather uniformly over the bandwidth of the receiver, whereas the backscatter is highly frequency dependent as depicted in figure 1.6. The split spectrum technique utilizes optimization algorithms which are applied to the set of signals in equation 1.2 in order to enhance the visibility of the flaw or target. As mentioned, these algorithms are based on the frequency properties of noise and target signals. The most effective algorithms reported to date are the **minimization algorithm** and the **polarity thresholding algorithm** or a combination of both.

The minimization algorithm uses the property that the target or flaw tends to distribute the received signal in a rather uniform fashion over the frequency bandwidth of the transducer; that is, the $f_i(t)$ have the same order of magnitude, whereas the interference pattern has a strong dependence on the frequency; meaning that the noise components $n_i(t)$ may have low or high levels in different frequency channels. The result from minimization is given by $s(t) = r_i(t)$, where $| r_i(t) | = \min\{|r_i(t)|\}$ for $i = 1, N$.

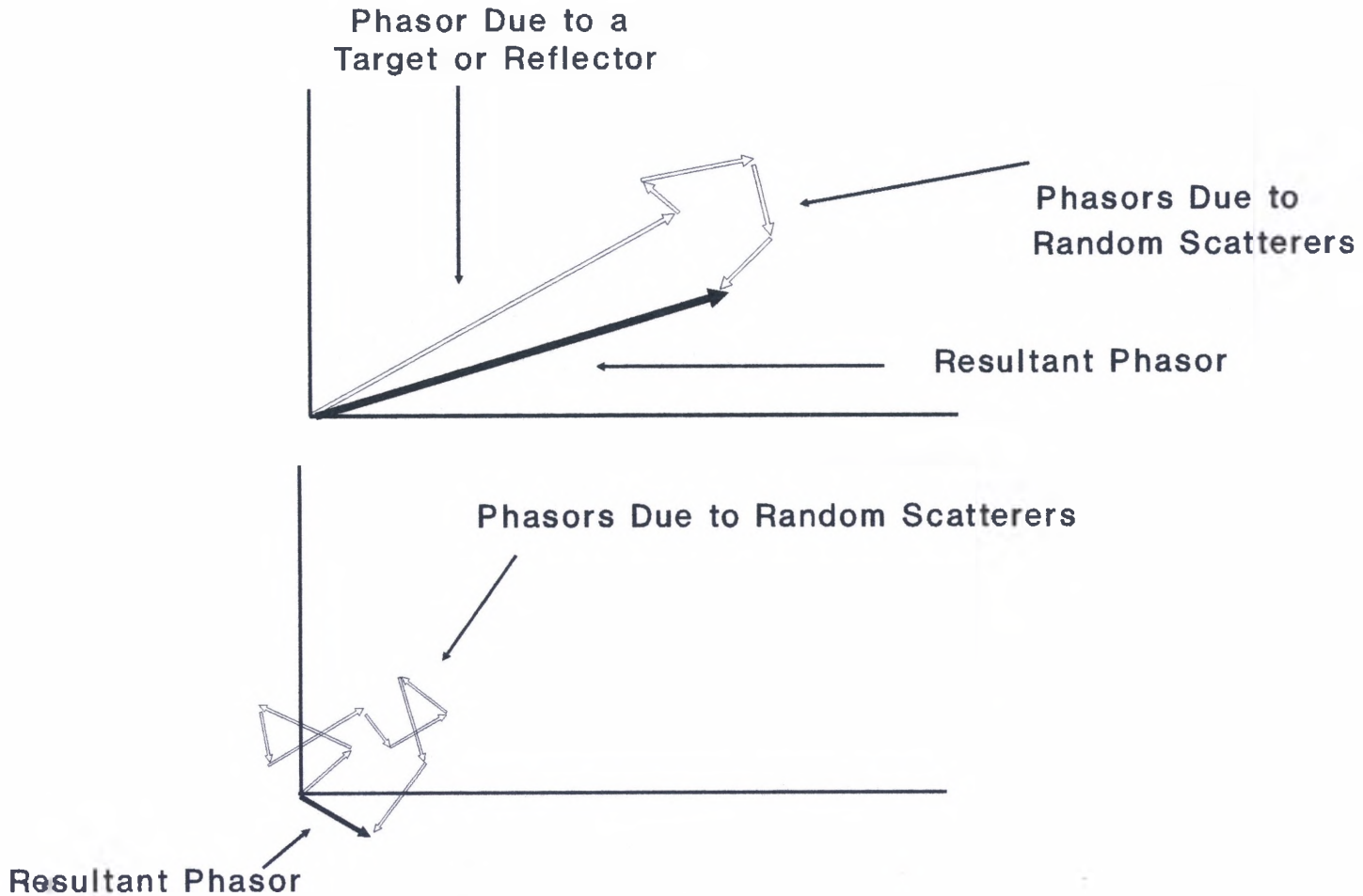

Fig. 1.5 Principle of Operation of SSP.

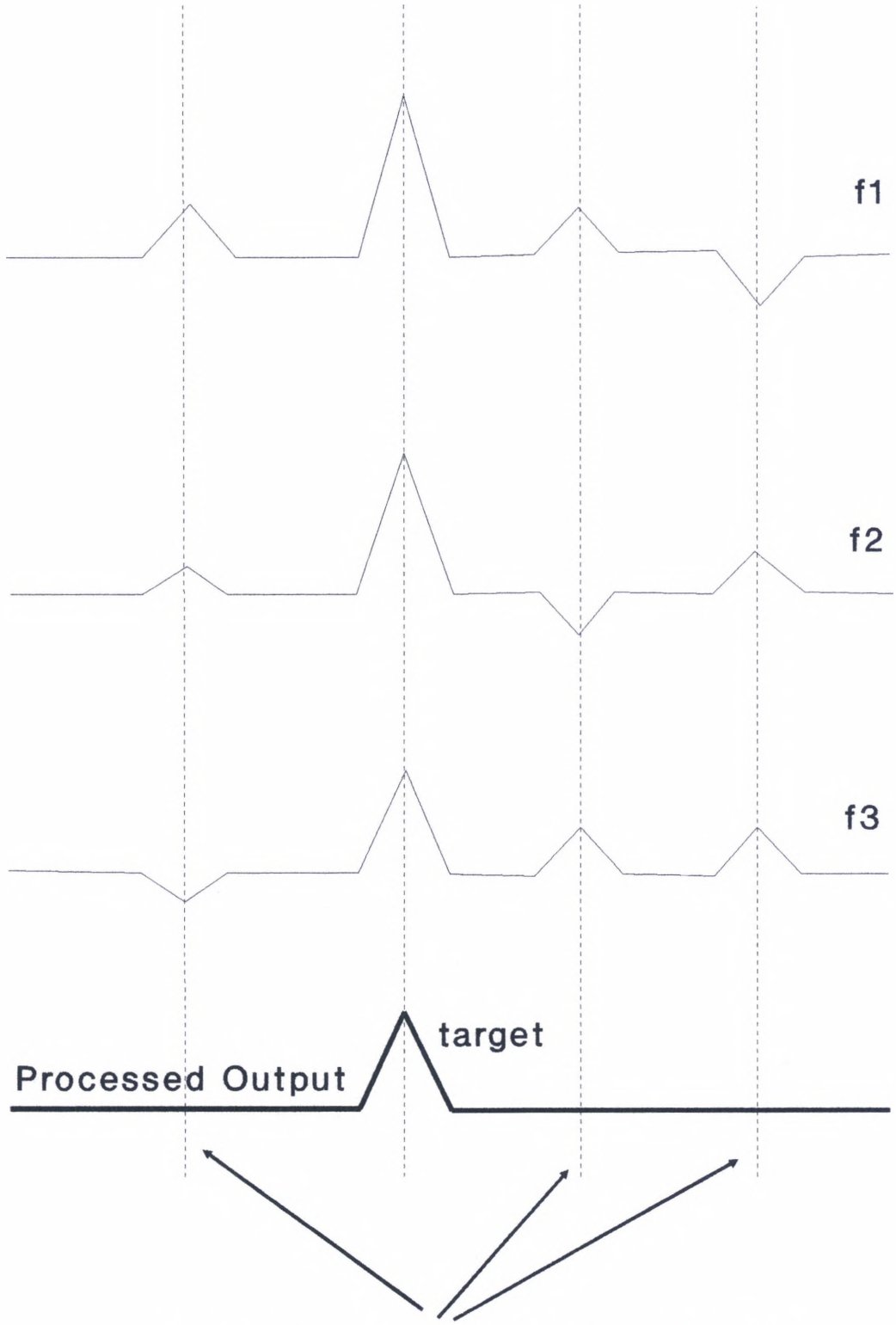

Fig. 1.6 Frequency Diverse Signals.

The polarity thresholding algorithm is based on the property that in the presence of a target, the probability that the components $f_i(t)$ all have the same sign is large, whereas, since the noise components $n_i(t)$ are independent the probability that they have the same sign decreases with the number of narrow-band signals N. The result of the polarity thresholding algorithm is $s(t) = r(t)$, if all decomposition components $f_i(t)$ have the same sign or $s(t) = 0$, otherwise. A combination of the two algorithms can also be applied for a further increase in performance and is given by $s(t) = r_i(t)$, where $|r_i(t)| = \min\{|r_i(t)|\}$, if no sign reversal occurs or $s(t) = 0$, otherwise. The signal-to-noise ratio enhancement and probabilities of detection of a target signal of these optimization procedures have been investigated as a function of the SNR and the number N of signals $r_i(t)$ from the decomposition of the input r(t) [4].

This spectral decomposition is a very critical step in SSP. In previous work, the decomposition of the input signal was carried out in the frequency domain with a bank of equally spaced Gaussian filters of constant bandwidth, as discussed in the next section.

1.3 Frequency Domain Constant Bandwidth Decomposition

The splitting of the spectrum of the received signal r(t) can be described as the multiplication of its Fourier Transform R(f) with a set of independent functions $H_k(f)$ in the following manner

$$R(f) = \sum_{k=-\infty}^{+\infty} H_k(f) = \sum_{k=-\infty}^{+\infty} R(f)\, H_k(f) \qquad \textbf{(eq.1.3)}$$

The set of functions $H_k(f)$ form an orthonormal basis and each $R_k(f)$ has an equivalent time domain representation $r_k(t)$. In practice, the receiving transducer's bandwidth places a limit on the number of orthonormal functions $H_k(f)$ that can be used for the decomposition. Theoretically, since the received ultrasonic signal is sampled within the time interval T, its frequency response is unlimited; however, the transducer's frequency response effectively bandlimits the ultrasonic signal. The spectral splitting process can be viewed as the sampling of the Fourier transform of the received pulse, and the frequency sampling theorem can then be invoked to express equation 1.3 in the following way

$$R(f) = \sum_{k=-\infty}^{\infty} R(\frac{k}{T})\ \mathrm{sinc}(f\pi T - k\pi) \qquad \textbf{(eq.1.4)}$$

where the functions $\mathrm{sinc}(x) = \frac{\sin(x)}{x}$ are an orthonormal set and equally spaced by a frequency interval $\delta f = \frac{1}{T}$. Equation 1.4 simply states that if a function r(t) is non-zero only in the time interval [0,T]; then its Fourier transform R(f) can be uniquely determined from its values $R(\frac{k}{T})$ at equally spaced points (distance δf). The sinc functions simply act as interpolators between adjacent samples to effectively generate the spectrum. Since the received ultrasonic signal is real, its spectrum exhibits complex conjugate symmetry ($R(f) = R^*(-f)$), and due to the transducer and instrumentation

ensemble frequency response, it has a lower and upper cut-off frequencies f_l and f_u. If for the sake of simplicity, it is assumed that the cut-off frequencies are integer multiples of the sampling frequency $\delta f = \frac{1}{T}$, such that $f_l = k_l \delta f$ and $f_u = k_u \delta f$; then eq. 1.4 reduces to

$$R(f) = \sum_{k=k_l}^{k_u} R(f_k)\,\mathrm{sinc}(\pi T(f - f_k)) + R^*(f_k)\,\mathrm{sinc}(\pi T(f + f_k)) \qquad \textbf{(eq.1.5)}$$

where $R(-f_k) = R^*(f_k)$ and $f_k = \frac{k}{T}$. The maximum number of orthonormal functions that can be used to decompose a signal of finite time duration T and bandwidth $BW = f_u - f_l$ is given by

$$N = k_u - k_l + 1 = T(f_u - f_l) + 1 = BW*T + 1 \qquad \textbf{(eq. 1.6)}$$

The frequency bands defined by the sinc functions spaced by $\frac{1}{T}$ and having a main lobe of width $\frac{2}{T}$ are perfectly uncorrelated with one another since the sinc functions form an orthogonal set. The resulting time-domain signals corresponding to each band are of a frequency diverse nature; and being uncorrelated, they could be compounded for an increased SNR. Equation 1.6 above gives the number of frequency bands the spectrum could be broken into, based on the spectral separation $\frac{1}{T}$ of the sinc functions. The decomposition expressed by the frequency sampling

theorem is not easily realizable by FFT filtering. Obviously, the sampling of such transfer function at $\delta f = \frac{1}{T}$, as required, would not allow enough resolution of this frequency response function for implementation. Therefore, as a matter of practicality, other frequency response functions suitable for this purpose must be employed. Frequency responses which may be amenable to perform the splitting of the spectrum of the ultrasonic signal are those with maximal time and frequency concentrations. Though correlated, a compromise can be reached between the number of filters and the bandwidths of the individual filters in order to achieve acceptable SNR levels.

If N_u uncorrelated frequency bands are used in SSP, the SNR enhancement is given by

$$SNR_e = \sqrt{N_u} \qquad \textbf{(eq.1.7)}$$

However, if there exists some measure ρ of correlation between the bands then the SNR enhancement is given by

$$SNR_e = \sqrt{\frac{(1-\rho)N_c}{1+\frac{2(N_c - 1)\rho^2}{N_c}}} \qquad \textbf{(eq.1.8)}$$

where N_c is the number of correlated bands. This equation reveals that small values of ρ are desirable in order to obtain better SNR performance. The effective number of uncorrelated bands can be estimated by

$$N_u^* = \frac{(1 - \rho)N_c}{1 + \frac{2(N_c - 1)\,\rho^2}{N_c}} \qquad \text{(eq.1.9)}$$

This equation may appear to indicate that by increasing the number of filters within the bandwidth of interest we ought to be able to increase the SNR correspondingly. However, the correlation factor ρ also increases due to greater overlap between filters and offsets the potential gains in performance. Experimental evidence to this effect has been provided by Karpur[4].

In current practice, the decomposition of the spectrum of the ultrasonic signal is carried out by using equally spaced Gaussian filters of constant bandwidth instead of sinc functions. The Gaussian filters are easy to implement digitally because of their maximal time and frequency concentration; that is, the time bandwidth product (TBP) is the smallest. The Fourier transform of the Gaussian filters can be described by

$$H_k(f) = e^{-(\frac{f - f_k}{0.85*\beta})^2} + e^{-(\frac{f + f_k}{0.85*\beta})^2} \qquad \text{(eq.1.10)}$$

where the standard deviation and the half-power bandwidth of the filter are related this way: $\sigma = 0.60043*\beta$ and f_k is the central frequency of the filter. The impulse response corresponding to this filter can be easily derived and is given by

$$h(t) = 1.7*\sqrt{\pi}\,\beta\, e^{-(0.85*\pi\beta t)^2} \cos(2\pi f_k t) \qquad \text{(eq.1.11)}$$

This expression is used to derive the coefficients of the digital Gaussian filters used in the simulations conducted here.

Karpur[4] established experimentally that, for the optimal separation $\delta f = \frac{1}{T}$ corresponding to the ideal interpolating sinc frequency responses, the Gaussian bandwidths must be about three to four times this separation: $\beta \approx [\frac{3}{T}, \frac{4}{T}]$. This is intuitively correct, since the energy concentrated within the half-power bandwidth of a sinc frequency response is only 50% of all its energy, whereas a Gaussian frequency response holds about 70%. This would lead us to suspect the need for smoother Gaussian responses to reduce the gaps that may exist between adjacent filters to prevent energy losses. Figure 1.4 is a representation of the conventional implementation of split spectrum processing based on frequency-domain FFT convolution.

1.4 Thesis Objectives

The main objective of this thesis is to investigate the efficient realization and implementation of the Split Spectrum Technique, whether based on FFT-convolution or tapped-delay lines, in order to advance forward towards a real time or near-real time implementation amenable to industrial inspection procedures. To achieve this basic goal, a modification to the conventional scheme of bandpass filtering has been introduced that, under certain circumstances, requires fewer filters in the splitting-filter bank for a desired SNR performance. This modification is introduced in chapter II

of this document, and experimental results are presented. Also, a more efficient implemention of the SSP technique with tapped-delay lines is introduced in chapter III, which may open the door to a real-time or near-real time implementation of the technique for industrial inspection procedures.

CHAPTER II

A NEW FILTERING SCHEME FOR SPLIT SPECTRUM PROCESSING IN ULTRASONIC NDE

2.1 Introduction

In the conventional approach to SSP, the filter bank utilized to perform the splitting of the spectrum of the signal is made up of equally spaced Gaussian filters of constant bandwidth. In the frequency domain, the processing time of the technique depends primarily on the number of filters in the bank required for a desired SNR performance. A feasible way to reduce the size of the filter bank (relative to the Gaussian filter bank) is to increase the energy confined within the half-power bandwidth (HPBW) of the filter without substantially increasing the correlation between adjacent or neighboring filters, that is to say, increase the number of effectively uncorrelated filters such that the corresponding increase in correlation is more than offset by the increase of target-signal energy. This chapter presents a new filtering scheme or rather a modification to the old scheme that may, under certain conditions, require fewer filters for a desired SNR enhancement performance than its Gaussian counterpart. The rationale for the selection of the processing parameters is established, and experimental results from computer-simulated signals as well as real ultrasonic signals are presented.

2.2 A New Filter Bank : Raised-Cosine Filters

As indicated in the literature[4], the splitting of the spectrum of a signal can be treated as the sampling of the Fourier transform of the signal. As such, the frequency sampling theorem can be used in analyzing the decomposition process and getting, at least, a rough idea as to the size of the filter bank and bandwidth of each individual filter. The frequency sampling theorem, as expressed by equation 1.4, indicates that the Fourier transform R(f) of a signal r(t) of duration T units of time can be reconstructed perfectly from samples $R(\frac{k}{T})$ of the transform taken $\frac{1}{T}$ Hz apart by interpolation with sinc functions. The set of interpolating sinc functions is given by

$$I_k(f) = \text{sinc}(f\pi T - k\pi) \qquad \textbf{(eq.2.1)}$$

which are separated by $\frac{1}{T}$. Figure 2.1 shows two sinc functions centered at $\frac{k}{T}$ and $(\frac{k+1}{T})$.

This figure depicts the main characteristics of the filters that perform the interpolation. The main lobe of the sinc function is of width $\frac{2}{T}$ or twice the spectral separation and contains most of the energy of the function. About 50% of the energy is contained within the half-power bandwidth. *However, it must be kept in mind that SSP is not an interpolation process intended to reconstruct the received noisy ultrasonic signal, but a technique meant to rid the signal of unwanted material-grain backscatter.*

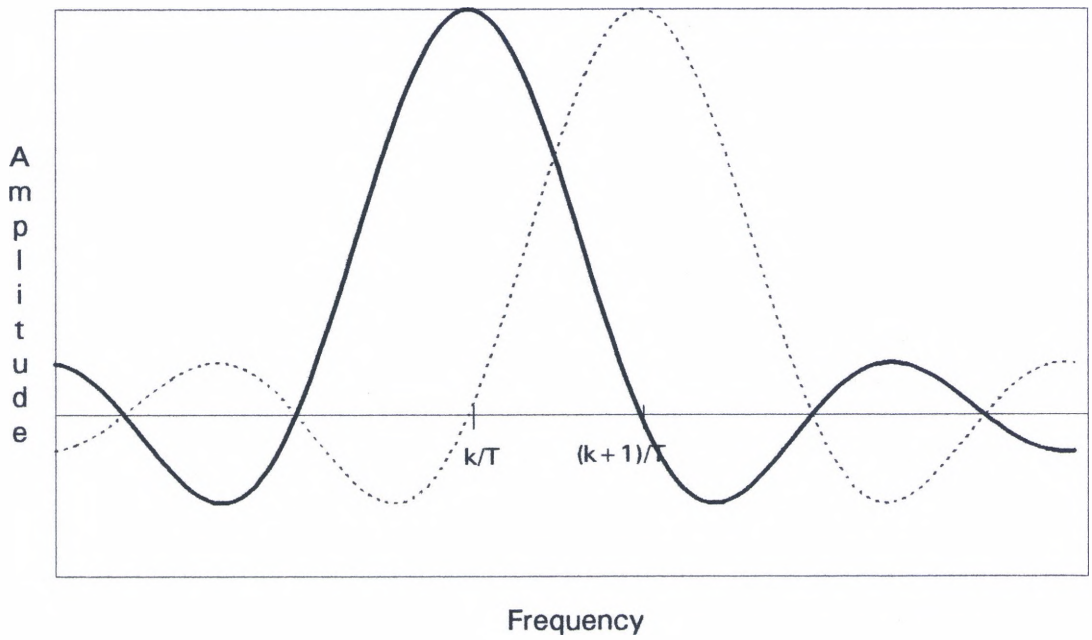

Fig. 2.1 Adjacent Sinc Functions of a Reconstruction Bank.

As a consequence, the use of sinc filters, as dictated by the frequency sampling theorem for signal reconstruction, might not yield good results in SSP even though these functions form an orthogonal set, this being due to the signal losses in the gaps between adjacent filters, not to mention the fact that sinc filters are rather hard to realize, as required, due to frequency resolution problems with the FFT. Such expectations have been borne out by experimental evidence. These considerations may lead to the conclusion that the best filter for SSP applications should preserve as much signal energy as possible within its passband and maintain its extension towards neighboring filters as small as possible, so as to keep the correlation between neighboring filters within reasonable bounds. This will ensure that signal energy is not lost and that the number of effectively uncorrelated

filters will be high enough to produce good SNR performance. However, this argument may not necessarily hold true for all signals and may, in some cases, be counterproductive depending on the noise levels present in the signal. More energy concentration within the passband of the spectrum-splitting filters means better detection or increased sensitivity of such filters, and if the noise levels are such that the SSP optimization algorithms will not perform very well or be ineffective, then the SNR performance could be degraded even more for filters with higher energy concentration within their half-power bandwidths.

Figure 2.2 depicts the possible shape of a transfer function which may afford better performance than the most conventional Gaussian-filter

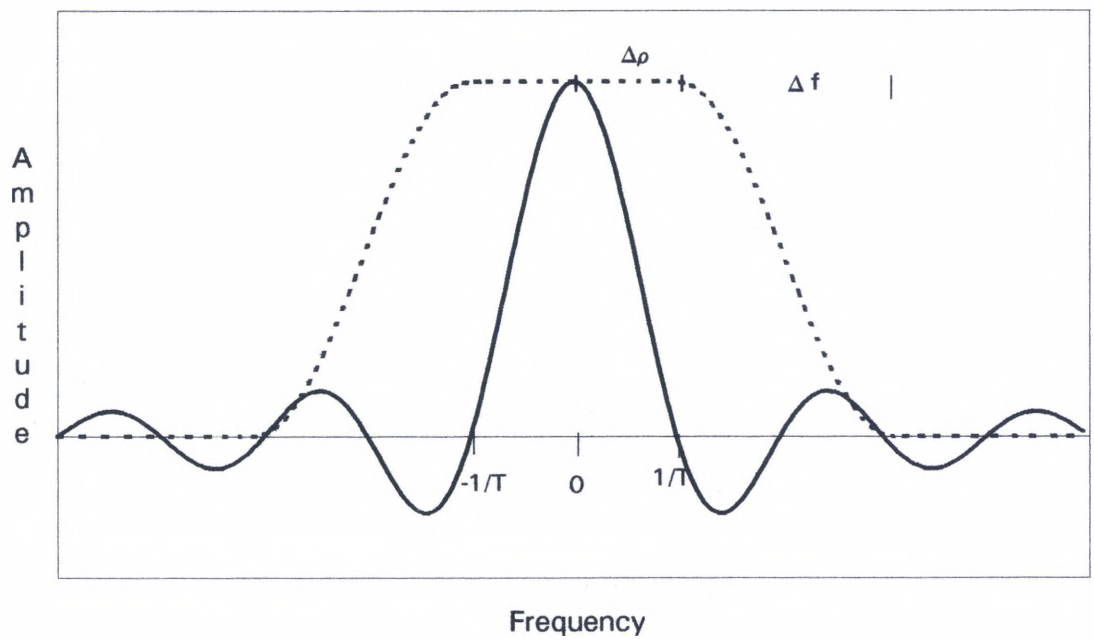

Fig. 2.2 A Filter with Flat-Top and Smooth Transition Band.

approach. The function exhibits a flat-top passband of width $\Delta\rho$ (half) and a transition bandwidth Δf of reasonably small extension. Theoretically, a perfectly rectangular window would be a better choice since it has no skirts, but it is impossible to realize since time aliasing problems arise due to the abrupt cut-offs, and its SNR performance would be impaired as reported by Draheim *et al.* [16]. Therefore, as a compromise, this work proposes a sinusoidal smooth transition bandwidth. A well known function that may serve as a prototype is the raised-cosine or Hanning window which, as its name suggests, is simply a frequency-selective filter whose skirts or transition bands make up a truncated full-cycle sine wave shifted upwards by unity and which may or not exhibit a flat top as shown in figure 2.3.

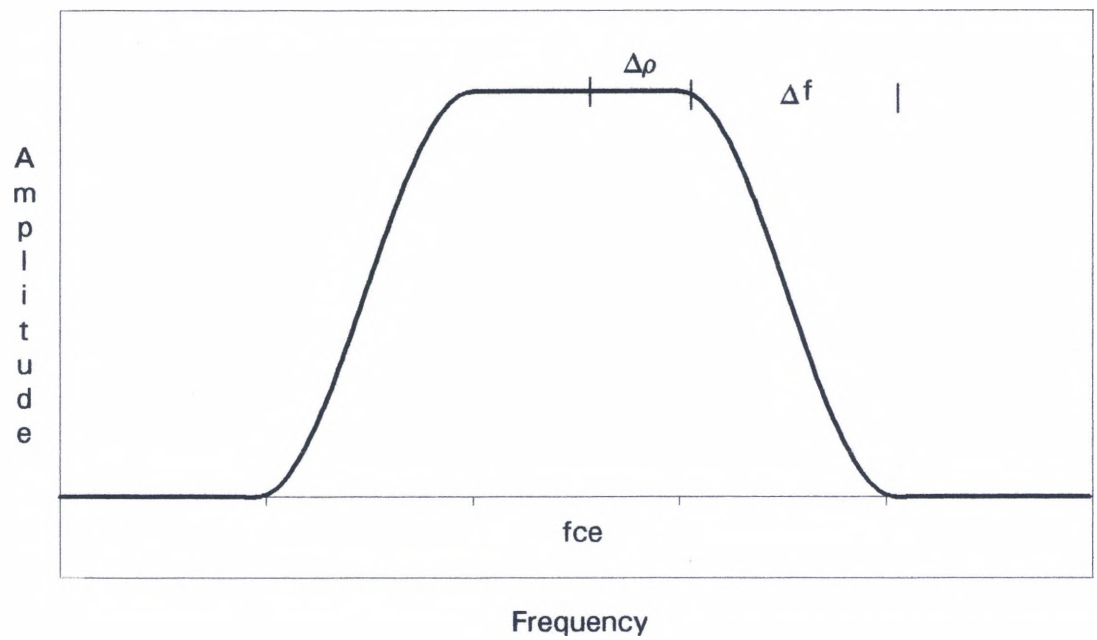

Fig. 2.3 Raised-Cosine Frequency Response.

It is to be noted here that it is also possible to fit a flat-top to a Gaussian filter, thereby generating a similar frequency selective filter with Gaussian skirts; however, the studies of this work have been conducted with raised-cosine (RAC) filters as a prelude to a real-time implementation with tapped-delay lines as well as a means of comparing relative performances of this filter shape and that of the Gaussian filters. The raised-cosine frequency response has extensive applications in the area of digital communications, and its impulse response can be approximated very efficiently with available filter design software. The frequency response of such a filter, as depicted in figure 2.3 is given by

$$H(f) = \begin{cases} \frac{1}{2}\{1 + \cos(\pi(\frac{f - f_{ce} - \Delta\rho}{\Delta f}))\}, & f_{ce} + \Delta\rho \le f \le f_{ce} + \Delta\rho + \Delta f \\ 1.0\ , & f_{ce} - \Delta\rho \le f \le f_{ce} + \Delta\rho \\ \frac{1}{2}\{1 + \cos(\pi(\frac{f - f_{ce} + \Delta\rho}{\Delta f}))\}, & f_{ce} - \Delta\rho - \Delta f \le f \le f_{ce} - \Delta\rho \end{cases} \qquad \text{(eq.2.2)}$$

where f_{ce} is the center frequency of the filter, and its impulse response is given by

$$h(t) = \frac{[\sin(2\pi(\Delta\rho + \Delta f)\, t) + \sin(2\pi\, \Delta\rho\, t)] \cos(2\pi f_{ce}\, t)}{\pi\, t\, [1 - (2\, \Delta f\, t)^2]} \qquad \text{(eq.2.3)}$$

when $t \neq \frac{1}{\Delta f}$ and

$$h(t) = \Delta f \cos(\frac{\Delta\rho\ \pi}{\Delta f}) \cos(\frac{\pi\ f_{ce}}{\Delta f}) \qquad \text{(eq.2.4)}$$

otherwise. These equations are used in the implementation of the raised-cosine digital filters used here as part of the simulations, where the digital impulse response of the filter can be readily obtained by appropriate sampling of eq. 2.3. As mentioned above, a similar expression can be derived for frequency-selective filters with Gaussian skirts

$$h(t) = 2\{\frac{\sin(2\pi\Delta\rho\ t)}{\pi t} + 0.85\sqrt{\pi}\beta \cos(2\pi\Delta\rho\ t)e^{-(0.85\pi\beta\ t)^2}$$

$$- 1.445\pi\beta^2 t \sin(2\pi\Delta\rho\ t) \sum_{k=-1}^{\infty} \frac{[-(1.2\pi\beta\ t)^2]^{k-1}}{(2k-1)!!} \}\cos(2\pi f_{ce} t)$$

where (2k-1)!! = 1x3x5...(2k-1) and β is the HPBW of the Gaussian filter that results when $\Delta\rho = 0$. The third term in this equation makes it rather ackward or hard to implement it for fast acquisition of filter coefficients. The appendix contains a FORTRAN 77 subroutine that returns the coefficients of a bandpass (or low, or highpass) RAC filter for a given set of specifications.

2.3 Selection of the Processing Parameters

The selection of the processing parameters, such as filter bandwidth and number of filters, is a critical step in SSP. The following comments

refer to the minimization algorithm since this algorithm exhibits an optimal bandwidth above or below which the performance drops below a peak value, and this optimal parameter can be ascertained in a reasonable manner. The polarity thresholding algorithm will show a SNR enhancement that starts to decline after a maximum which depends on the stochastic nature of the signal and noise; this makes it hard to establish any sort of criteria for optimal parameter selection. The frequency-sampling theorem gives an initial indication of what these parameters might be. If the sinc spectral separation $\frac{1}{T}$, where T is the duration of the signal, is the separation between adjacent filters in the spectral-splitting bank, then the maximum number of filters that can be used in an FFT implementation without zero padding is BW*T + 1, where BW is the available signal bandwidth. In current practice, Gaussian filters are utilized and Karpur[4] has established that a Gaussian bandwidth β of approximately $\frac{3}{T}$ to $\frac{4}{T}$ is required in order to obtain good SNR performance. This is intuitively satisfying since a wider bandwidth than that of the sinc functions should be required to provide sufficient overlap between adjacent filters in order to prevent signal-energy losses or leakage. The RAC filter can also be expected to require more bandwidth since more energy (80% or more) is contained within its half-power bandwidth; however, the raised-cosine window complicates matters somewhat since it becomes necessary to determine an optimal passband width $\Delta\rho$ and transition bandwidth Δf. An initial estimate concerning the best choice for the passband width is suggested in figure 2.2; that is, it is hinted that the passband be made at

least as wide as the width of the main lobe of the sinc functions since it is within this lobe that most of the signal energy in each frequency band is contained. The best choice of the width of the transition band Δf is not as clear, except that it is possible to expect that smaller transition bandwidths relative to the passband of the filter will produce better performances since smaller bandwidths imply more independence (less correlation) between neighboring filters in the bank which is a must for post-processors such as minimization and polarity thresholding. *However, a higher energy concentration within the half-power bandwidth (sharper filters) can lead to resolution problems with an FFT implementation or long impulse responses for a tapped-delay line implementation both of which will invariably lead to either degraded performance or increased computational loads or both.* When the energy concentrated within the filter's half-power bandwidth is varied, the optimal passband width can be expected to change in an inverse fashion to the choice of transition bandwidth, that is, smaller transition bandwidths will force the passband to widen to maintain or preserve the optimal half-power bandwidth, whereas wider transition bandwidths will force it to shrink. The percentage energy contained within the half-power bandwidth of a raised-cosine frequency response is given by

$$R_e = \left(\frac{\Delta\rho + 0.300\Delta f}{\Delta\rho + 0.375\Delta f} \right) \qquad \textbf{(eq.2.5)}$$

where it is clear that a 100% energy concentration can only be achieved with an abrupt transition bandwidth which would lead to the ideal rectangular window. Experiments were conducted to ascertain the best possible selection of these parameters, and certain guidelines have been established to aid in choosing near optimal values for such parameters. The experimentation was carried out in the time domain for the minimization processor and a combination of both minimization and polarity thresholding algorithms. Its implementation with FFT convolution is straightforward as long as resolution problems do not arise.

2.4 Signal-to-Noise Ratio Measurement and Ultrasonic Signal Simulation

In order to evaluate the SNR performance of the raised-cosine filter bank, as compared to that of Gaussian filters, an adequate simulation of the ultrasonic inspection process must be realized as well as an appropiate meausre of SNR performance. The unprocessed ultrasonic signals have been simulated by contaminating single-target signals obtained from the impulse responses of different transducers with digitally generated noise (though not perfectly random, computer simulations of random signals are suitable enough for this work) colored by the transducer's impulse response. These impulse responses exhibit a single well defined target region which is windowed out from the rest of the sequence, where the noise or erratic clutter shall be measured. The transducer (target) signal is fairly clean or free of noise outside the target region. A random noise signal (Gaussian or uniformly distributed noise) is generated with the FORTRAN

77 code in the appendix, and convolved with the clean target signal in order to generate the clutter, and this is then added to the transducer's impulse response to produce the unprocessed ultrasonic signal; that is, the noisy signal is generated as prescribed by the following equation

$$r(t) = n(t) \otimes f(t) + f(t) \qquad \textbf{(eq.2.6)}$$

where r(t) is the resulting unprocessed ultrasonic signal, n(t) is the random noise signal and f(t) is the transducer's impulse response. The signal is then processed using minimization alone and both minimization and polarity thresholding combined, and the signal-to-noise ratio is measured such that the fluctuations or erratic variations caused by the noise around the target, which tend to make detection hard, are measured outside the target region, as dictated by the following equation

$$SNR_{rms} = \frac{\text{Signal Peak-to-Peak Amplitude}}{\sigma_n} \qquad \textbf{(eq.2.7)}$$

where σ_n is the standard deviation of the sequence made up of all points in the processed signal outside the target region. This equation is useful and meaningful as a performance estimator only when a single target is present, since the variations or random fluctuations can be best observed in this fashion to ascertain the effectiveness of the filtering schemes used in the spectral splitting. When various targets are present, they will create significant amounts of fluctuations that will tend to decrease the SNR

sharply and obscure the relative performances of Gaussian filters and RAC filters.

The minimization and polarity thresholding with minimization algorithms have been used in order to establish a set of curves describing the SNR performance as a function of filter HPBW for different numbers of filters. For a particular number of filters, various bandwidths were tested and the peak values selected to generate SNR versus filter bank size for both Gaussian and RAC filters. A description of the experiments performed is given next.

Experiment I

This experiment is intended to establish the effect of a flat-top on the SNR performance of the SSP technique. The target signal of figure 2.4, which corresponds to the impulse response of a transducer with available bandwidth ranging from 1.36 MHz to 2.344 MHz, is used. The signal was sampled at the rate of 20 MHz and had a duration T of 25.6 microseconds, thereby generating 512 points or samples. The ideal sinc spectral separation $\delta f = \frac{1}{T} = 0.0390625$ MHz and the number of optimal filters can be estimated by $N = BW*T+1 = (2.344-1.36)*(25.6) + 1 = 26$. This equation gives the maximum number of filters that can be used with an FFT implementation without increasing the observation interval or zero padding, and sometimes more filters may be required to obtain an acceptable SNR level. The bandwidth at which the Gaussian filters are expected to show a peak performance is around 0.15625 MHz (4/T) and

the bandwidth of the RAC filters should be even wider. For this initial experiment, the full passband width $2\Delta\rho$ of the RAC filter has been made about half that of the transition band Δf. This concentrates roughly 87% of the energy of the RAC filter within its half-power bandwidth, and it is expected that $\Delta\rho \approx 0.039$ MHz and $\Delta f \approx 0.156$ MHz for a HPBW of 0.1915 MHz (see eq. 2.5). The half-power bandwidth of the RAC filter as a function of $\Delta\rho$ (half) and transition bandwidth Δf is given by

$$\beta_C = 2(\Delta\rho + 0.364\,\Delta f) \qquad \textbf{(eq.2.8)}$$

The target signal is used to generate the noisy signal as per equation 2.6, using randomly distributed noise, and the result is the signal of figure 2.5. This signal shows only moderate levels of noise and the target is still visually recognizable.

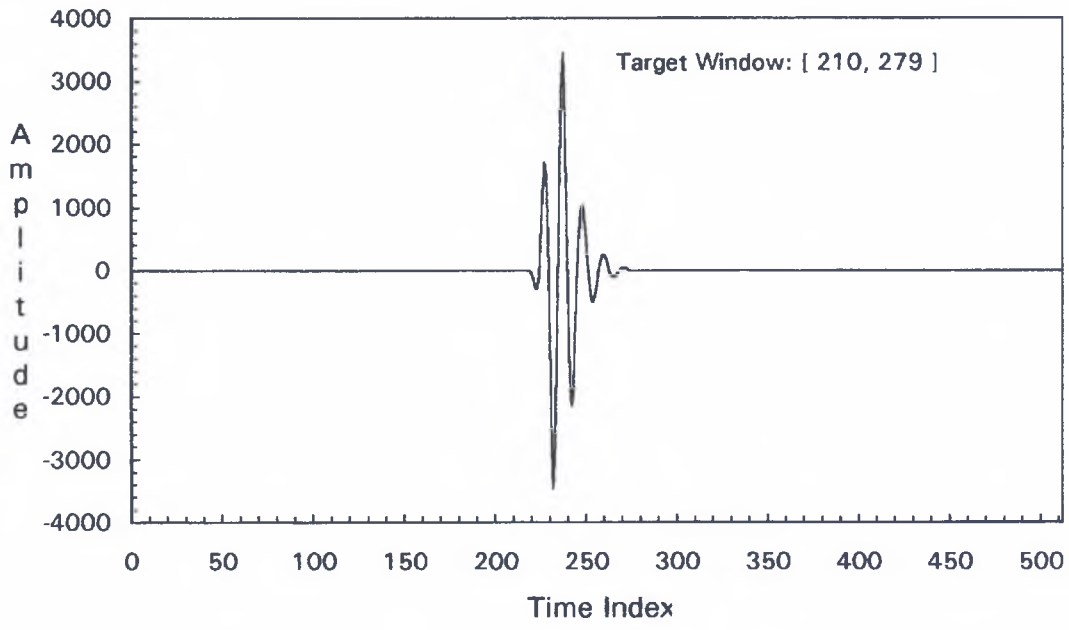

Fig. 2.4 Target Signal of Experiment I.

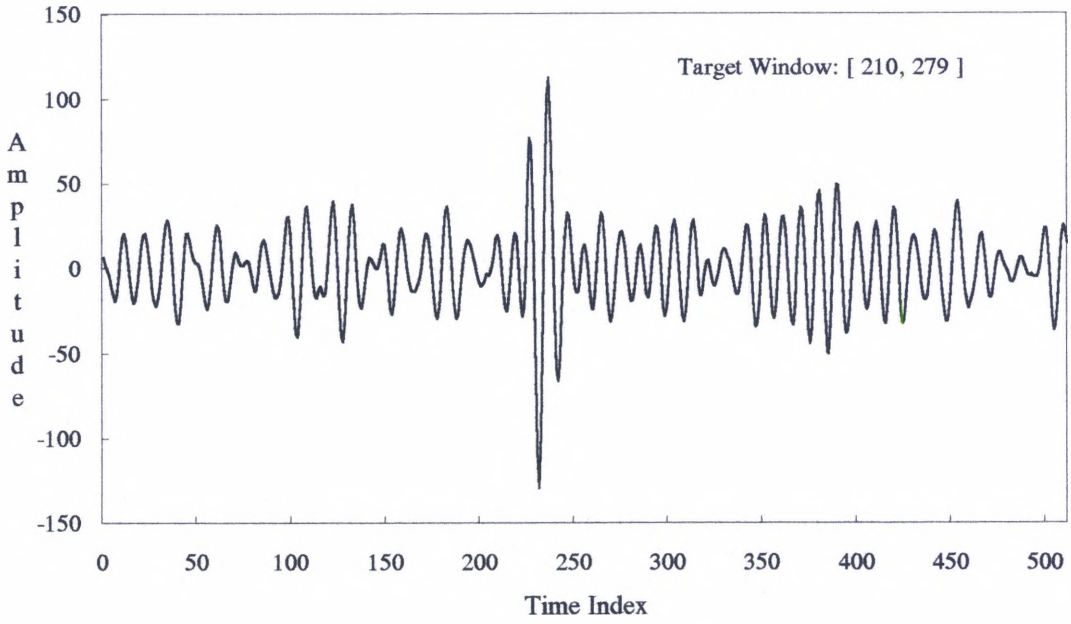

Fig. 2.5 Unprocessed Signal of Experiment I.

This signal was processed with filter banks of different lengths ranging from two to sixty filters using the minimization algorithm alone and both polarity thresholding and minimization combined for a range of bandwidths. The result of these experiments can be seen in figures 2.6 and 2.7 where the graphs of output SNR versus half-power bandwidth for different numbers of filters are shown. Figure 2.8 shows the output SNR versus the number of filters used and reflects the advantage, in this case, of the flat-top filter over that of the Gaussian. These curves were obtained by selecting the peaks in figures 2.6 and 2.7 for different numbers of filters. It can be seen that a given SNR can be achieved with a relatively smaller filter bank if flat-top filters are used. For instance, if 26 filters are

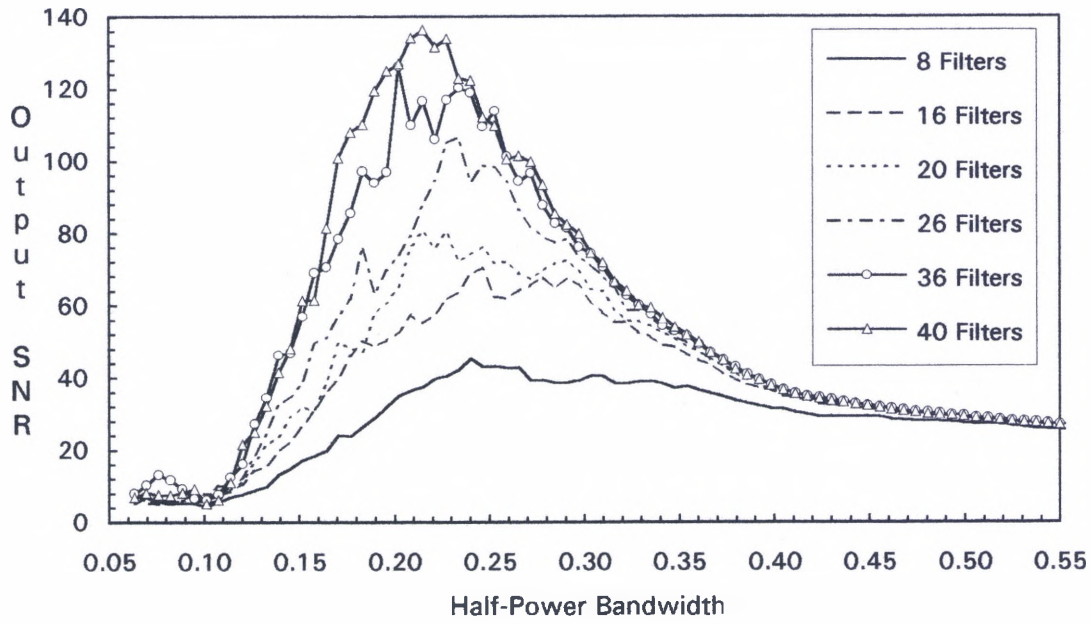

Fig. 2.6 SNR vs. Half-Power Bandwidth Curves for RAC Filters and Minimization.

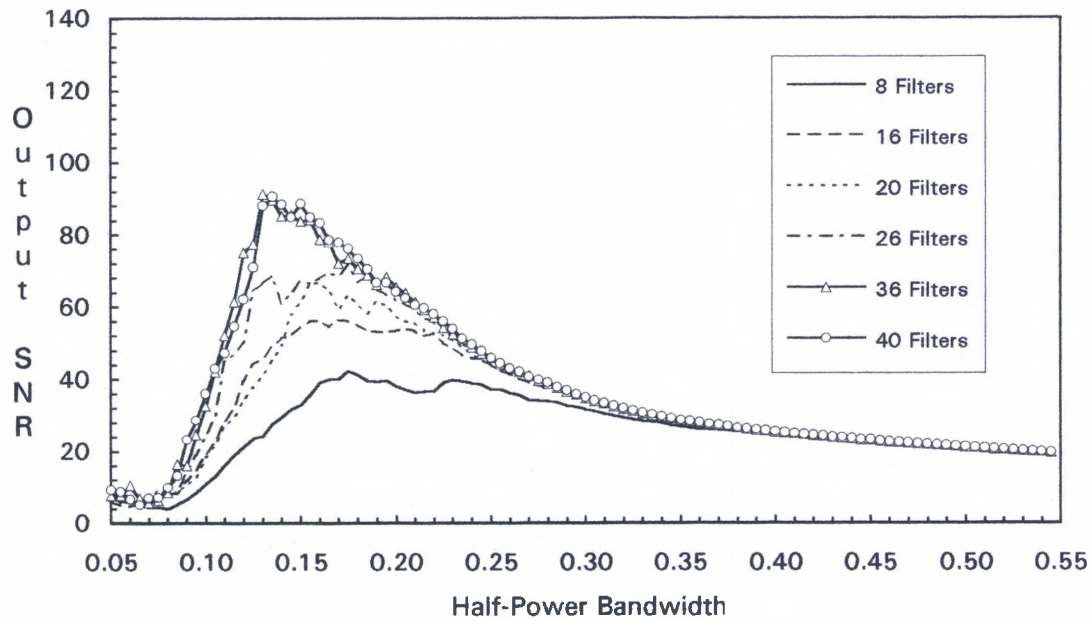

Fig. 2.7 SNR vs. Half-Power Bandwidth Curves for Gaussian Filters and Minimization.

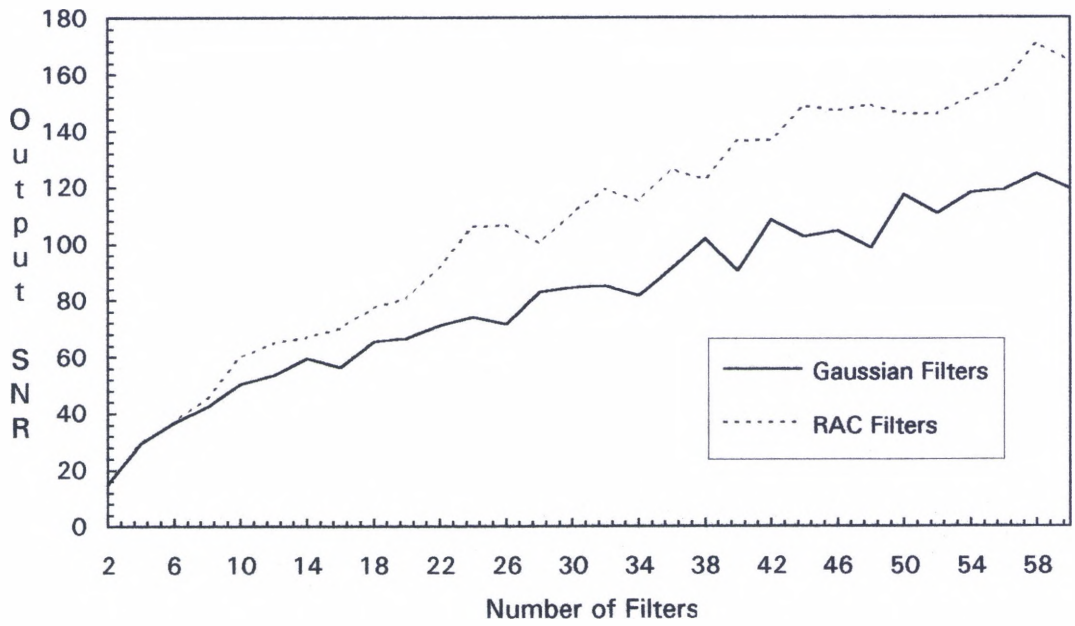

Fig. 2.8 Performance Levels vs. Number of Filters with Minimization.

selected for the filter bank for an SNR output of about 71 with Gaussian filters, a similar performance could be obtained with 18 flat-top RAC filters. This may appear to be a contradiction since the performance of the minimization algorithm depends only on the number of independent signals obtained by the decomposition and not on the decomposition itself[2]. However, this is not a new decomposition, but rather a modification to the conventional one which does not severely suppress signal frequencies within each band. Figure 2.9 shows the output of the minimization processor with 26 Gaussian filters at an optimal bandwidth of 0.175 MHz. The output SNR is about 71, which is lower, by far, than that of the flat-top filter, which was measured at 107 and whose output is seen in figure 2.10.

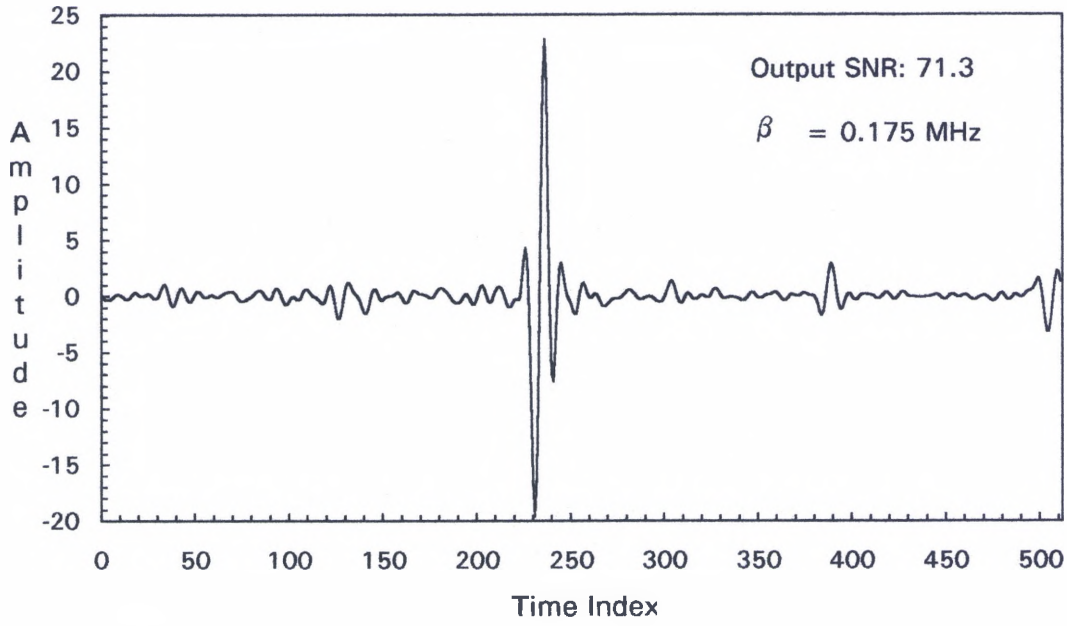

Fig. 2.9 Signal after Processing with 26 Gaussian Filters and Minimization.

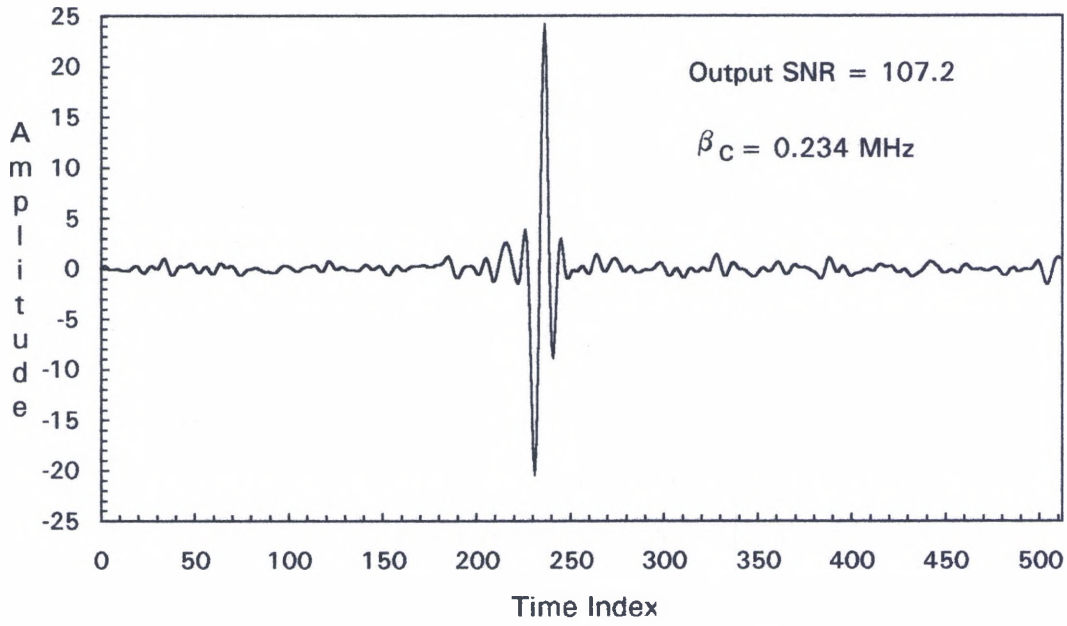

Fig. 2.10 Signal after Processing with 26 RAC Filters and Minimization.

Figure 2.11 shows the output of the minimization processor with 18 RAC filters at an optimal bandwidth of 0.2339 MHz. The width of the full passband is 0.0925 MHz (or $\Delta\rho$ = 0.04625 MHz). This value is only slightly greater than the optimal separation δf, and the transition bandwidth Δf is 0.19425 MHz, which is roughly five times as big as δf. This is in accordance with the initial theoretical estimates. A similar experiment was conducted with this transducer signal using zero-mean Gaussian noise, and even though the SNR levels achieved were lower than those achieved with uniformly distributed random noise, similar SNR versus half-power bandwidth and number of filters cuvers were obtained. Figures 2.12, 2. 13

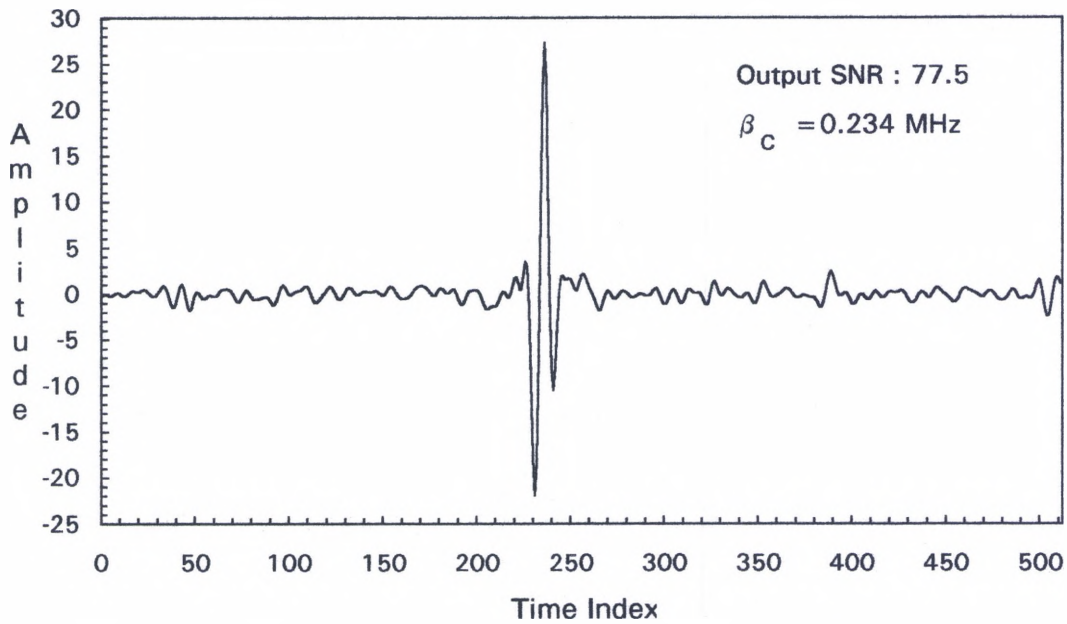

Fig. 2.11 Signal after Processing with 18 RAC Filters and Minimization.

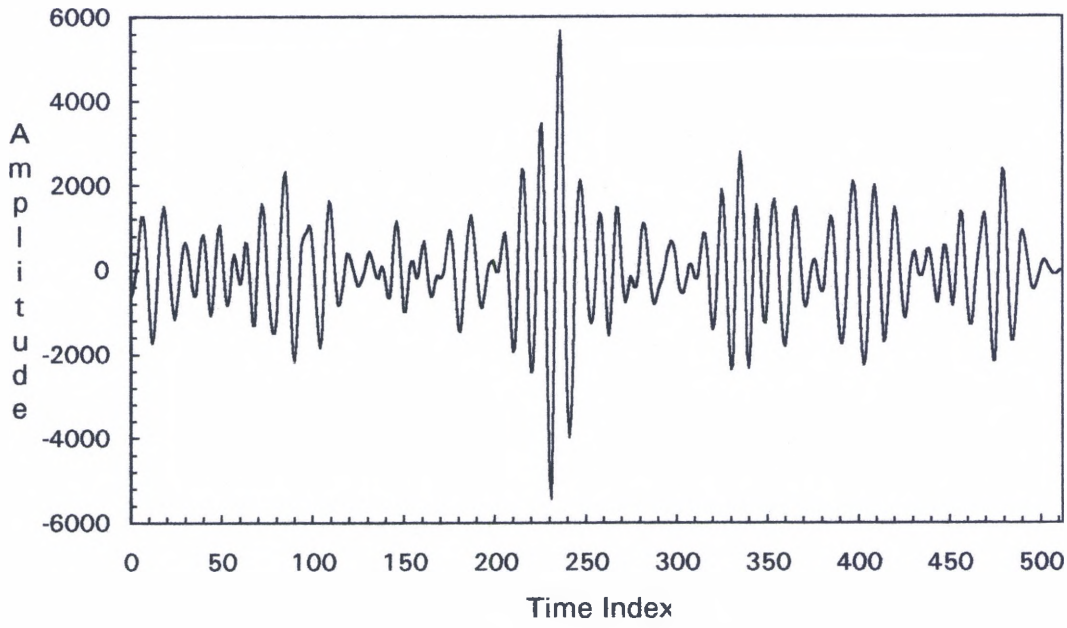

Fig. 2.12 Noisy Ultrasonic Signal Derived from the Signal in Fig.2.4 with Gaussian Noise.

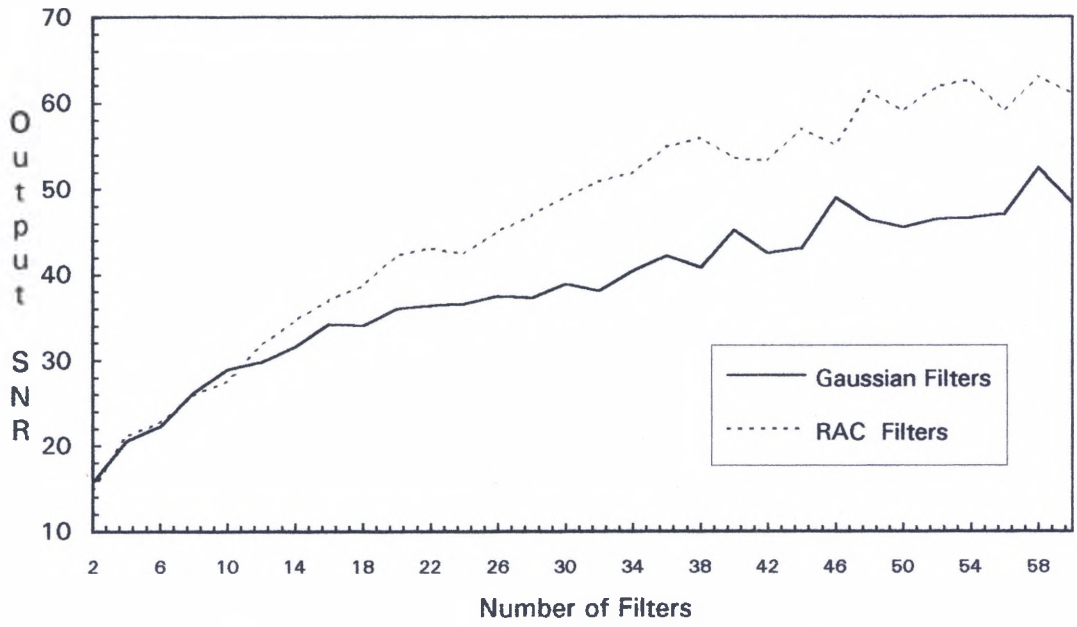

Fig. 2.13 Performance vs. Number of Filters for Signal of Fig. 2.12.

show the resulting simulated ultrasonic signal and a plot of output SNR versus number of filters respectively.

Experiment II

This experiment has the objective of showing the effect of increasing the energy concentrated within the half-power bandwidth of each filter. The unprocessed signal of figure 2.5 is used, and this time the energy concentrated within the passband of the RAC filters is about 91% (Δf is about 2 times $\Delta\rho$). The results of the experimentation are represented in figure 2.14, where the curves corresponding to SNR versus half-power bandwidth for 26 filters using minimization are shown for both 87% energy concentration and 91% energy concentration within the bandwidths of the

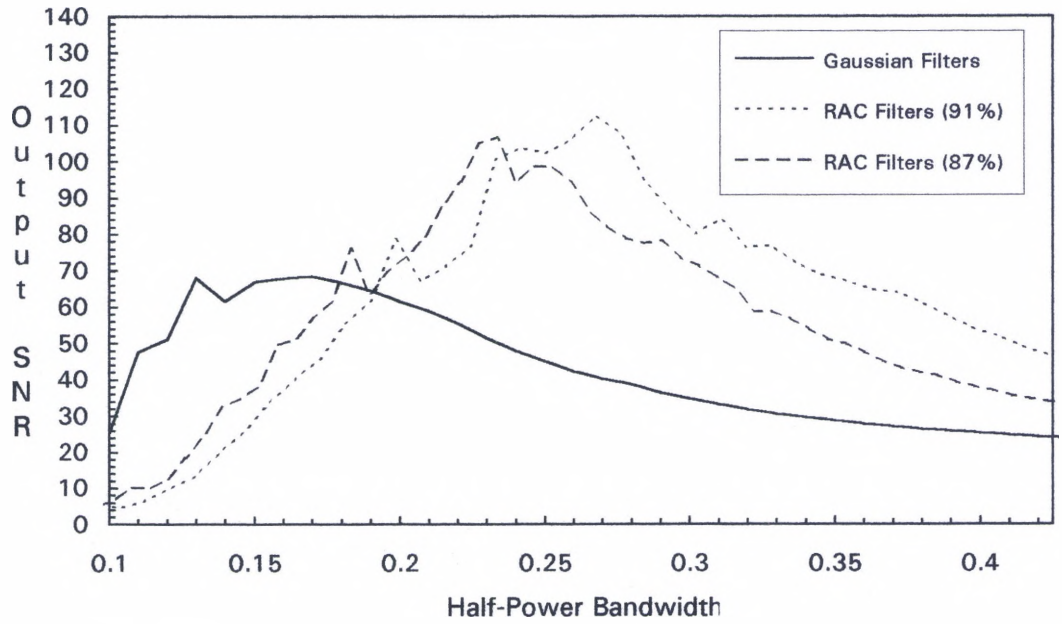

Fig. 2.14 Curves Depicting Effects of Energy Concentration on Output SNR.

filters. The curve corresponding to 26 Gaussian filters is also shown as a reference. This case reveals that a higher SNR can be obtained using a higher energy content. Note that the half-power bandwidth at which the peak occurs does not shift drastically.

Experiment III

This experiment makes use, once more, of the signal of figure 2.4 and has as an objective to highlight the possible perils that exist in using a flat-top filter when high levels of noise are present in the received signal. The signal to be processed is shown in figure 2.15. This signal exhibits considerably high levels of noise. It has been processed using 26 filters with flat tops and without flat tops for a range of bandwidths. The results are illustrated in figure 2.16, where it is evident that the field engineer

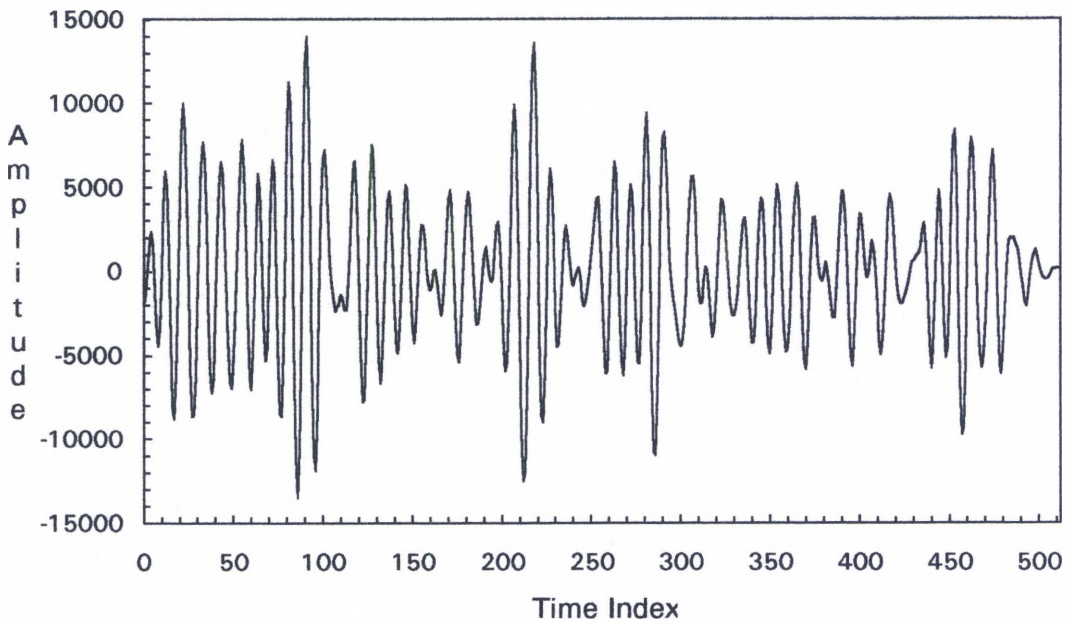

Fig. 2.15 Unprocessed Ultrasonic Signal of Experiment III.

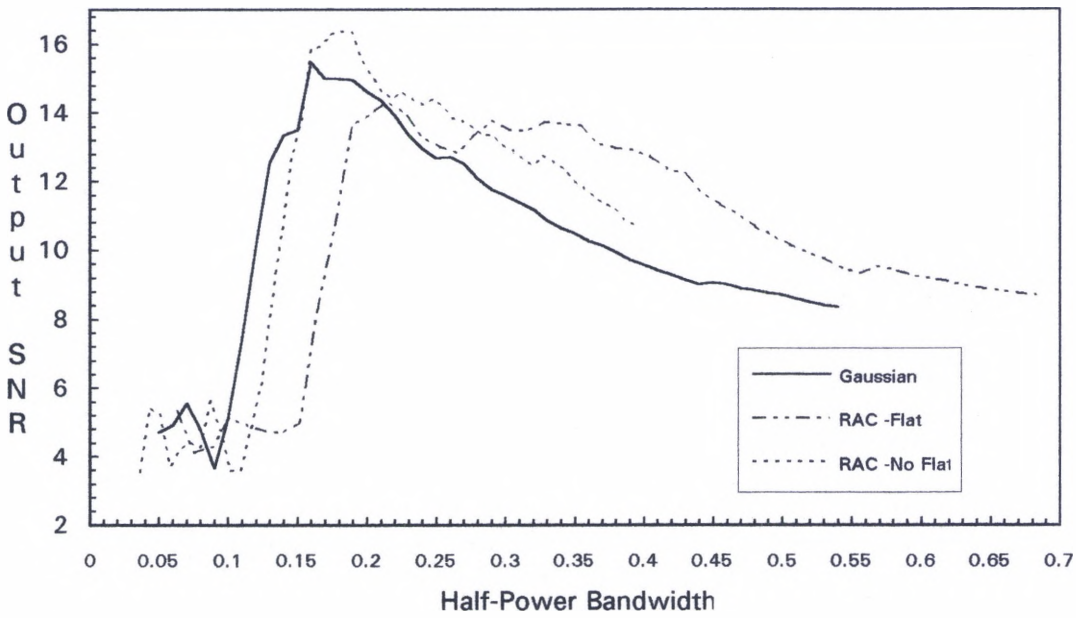

Fig. 2.16 Curves Depicting the Effect of the Flat-Top for very Noisy Signals.

must be cautious about using flat-tops. In general, flat-top filters should not be employed when high levels of noise are expected or observed on a sample signal.

Experiment IV

The transducer signal utilized in this experiment can be seen in figure 2.17. This signal had a duration of 2.56 microseconds and was contaminated with uniformly distributed noise, as explained, above with the resulting signal as depicted in figure 2.18. The available bandwidth ranges from 1.7578 MHz to 5.664 MHz, and the sampling rate was 100 MHz. The target region takes up a rather wide range within the 256-point signal [45,178]. The unprocessed or noisy signal exhibits rather moderate levels of distortion, and the target is still visible. The energy concentrated

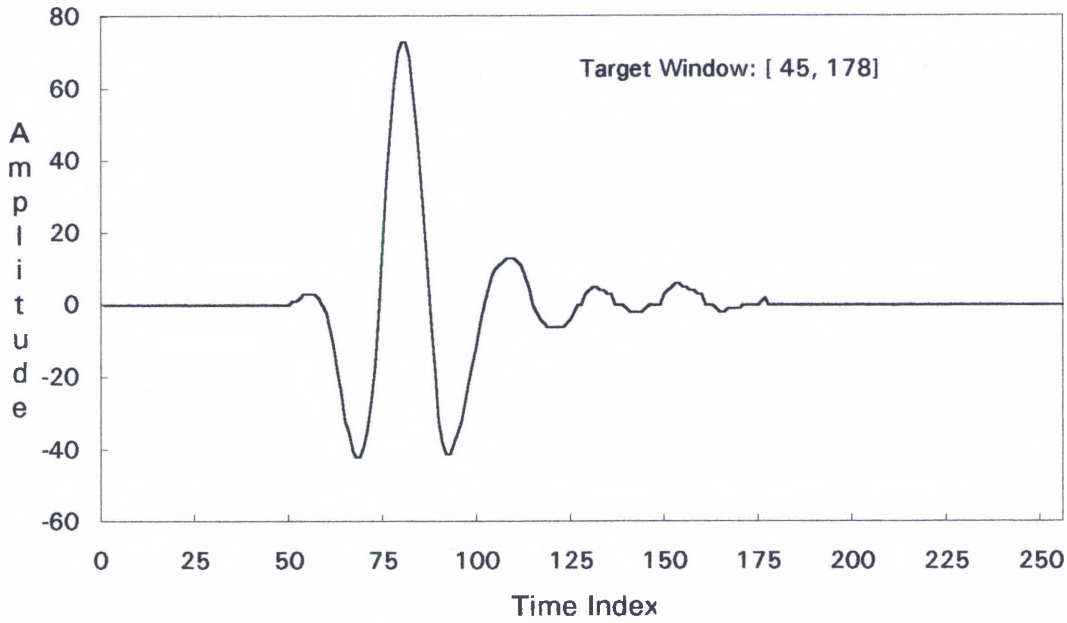

Fig. 2.17 Target Signal Corresponding to Experiment IV.

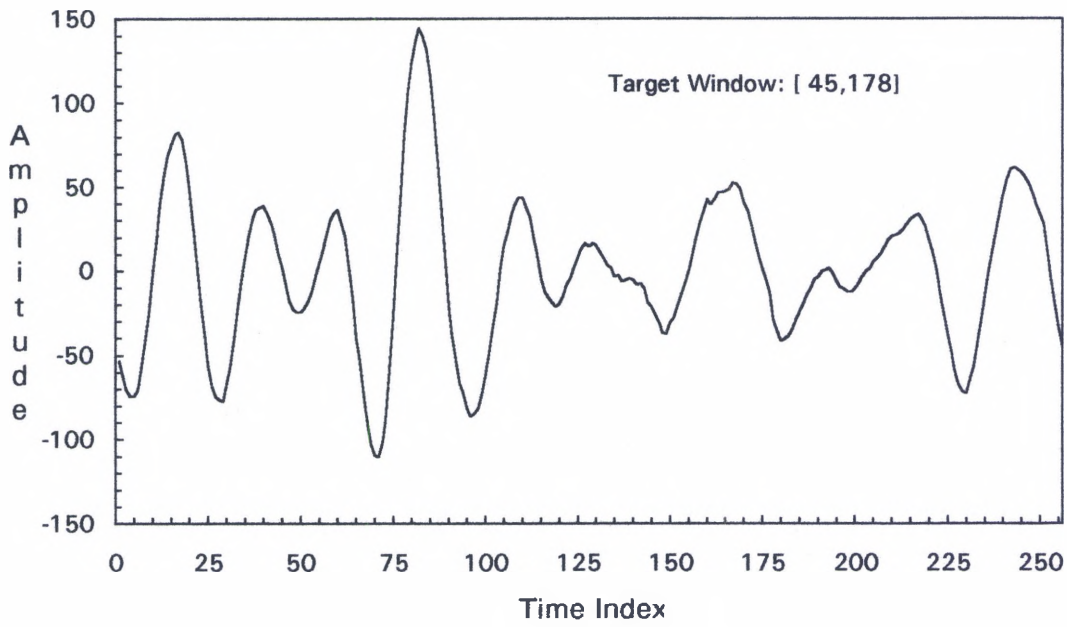

Fig. 2.18 Unprocessed Signal of Experiment IV.

within the half-power bandwidth of the RAC filters has been fixed roughly at 89.4% by choosing the transition bandwidth 1.5 times wider than the passband of the filters. The ideal spectral separation δf is 0.39 MHz and the Gaussian filters ought to show an optimal bandwidth between 1.17 MHz and 1.56 MHz. Based on the choice of energy concentration, $\Delta\rho \approx \delta f = 0.39$ MHz and Δf should be in the neighborhood of 1.17 MHz for a half-power bandwidth of about 1.632 MHz. The optimal number of filters is estimated at 11. A set of curves similar to those of experiment I were developed for this case, and from these, SNR versus number of filters curves were obtained, as shown in figures 2.19 and 2.20 for both minimization alone and polarity and minimization combined. These figures reveal that there appears to be no significant advantage to using more

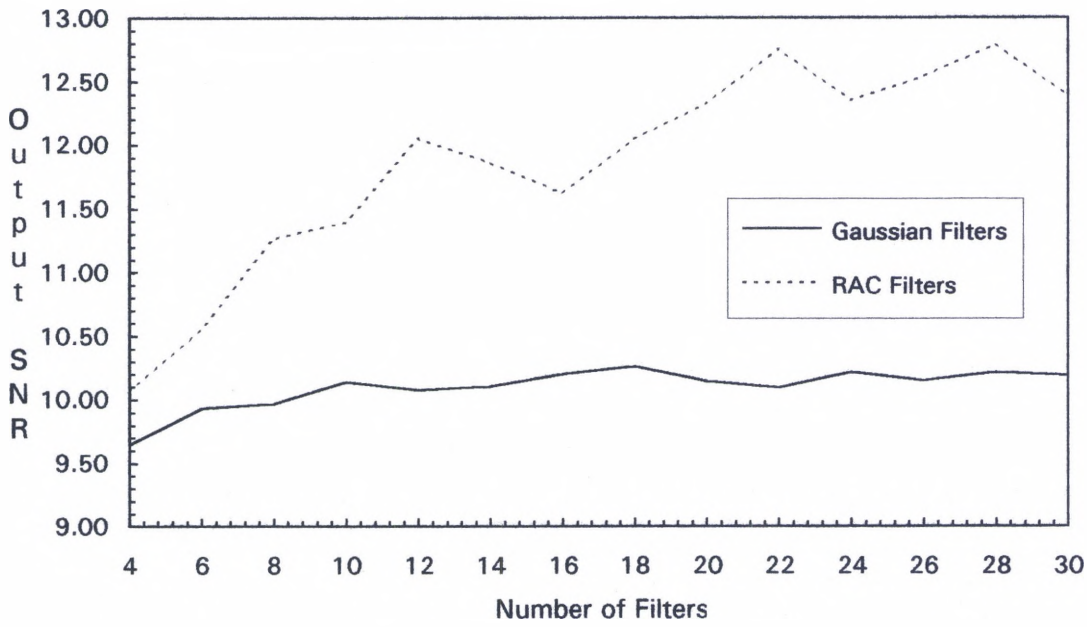

Fig. 2.19 SNR Performance vs. Number of Filters with Minimization Alone for the Signal of Experiment IV.

filters than the optimal number (11) for this case since both curves (Gaussian and raised-cosine) seem to saturate rather quickly. It is, however, clear that the flat-top filters give better performance for any particular number of filters and a certain number of such filters could be dropped with confidence without compromising performance. For instance, figures 2.21, 2.22 and 2.23 show the output signal after processing with 12 Gaussian, 12 RAC filters and finally with 8 RAC filters, respectively. It is obvious that the signal of figure 2.23 has roughly the same output SNR as that of figure 2.21 except that the signal in figure 2.21 was processed with a smaller bank. This could lead to great savings in processing time especially when thousands of signals like this have to be processed, as is the case in the processing of B and C scans. In this experiment, $\Delta\rho$ was found to be about 0.36 MHz and the transition bandwidth is about 1.0875

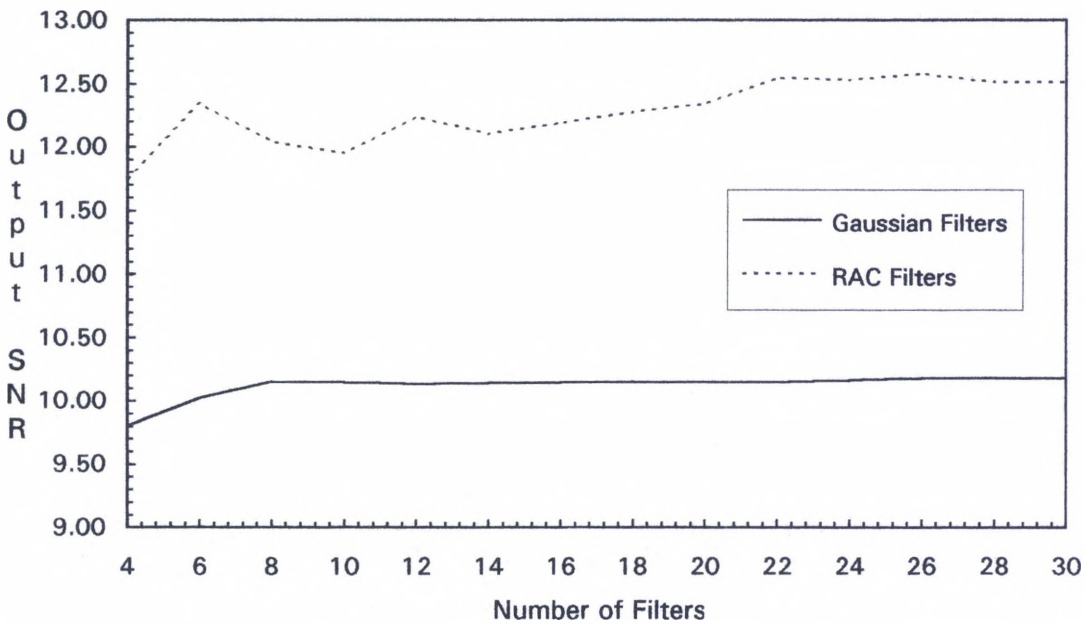

Fig. 2.20 SNR Performance vs. Number of Filters with Polarity/Minimization for the Signal of Experiment IV.

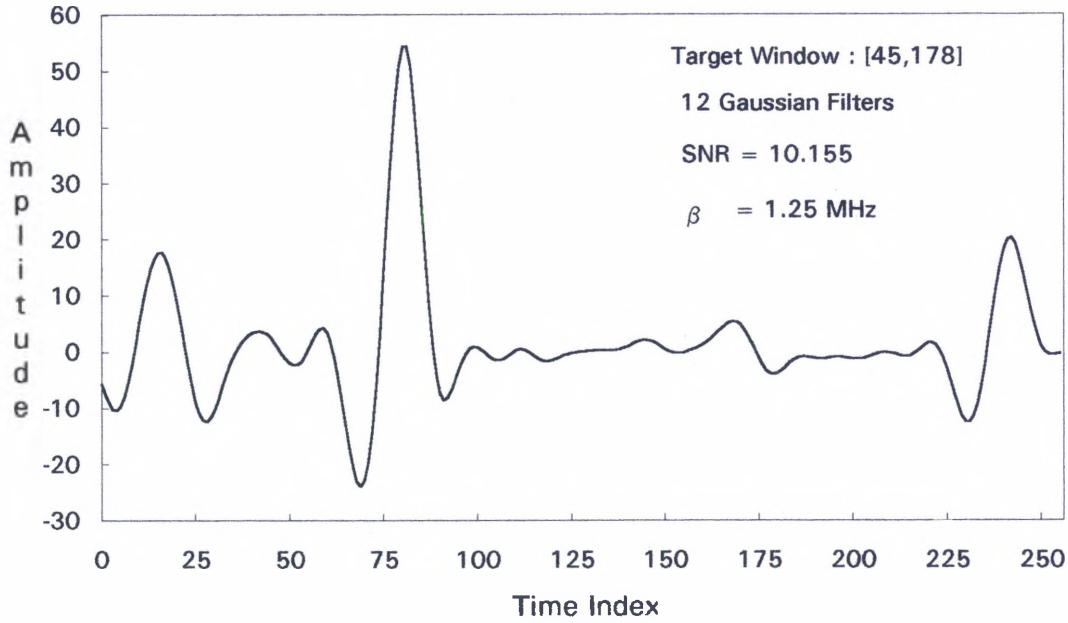

Fig. 2.21 Signal of Experiment IV after Minimization (12 Gaussian Filters).

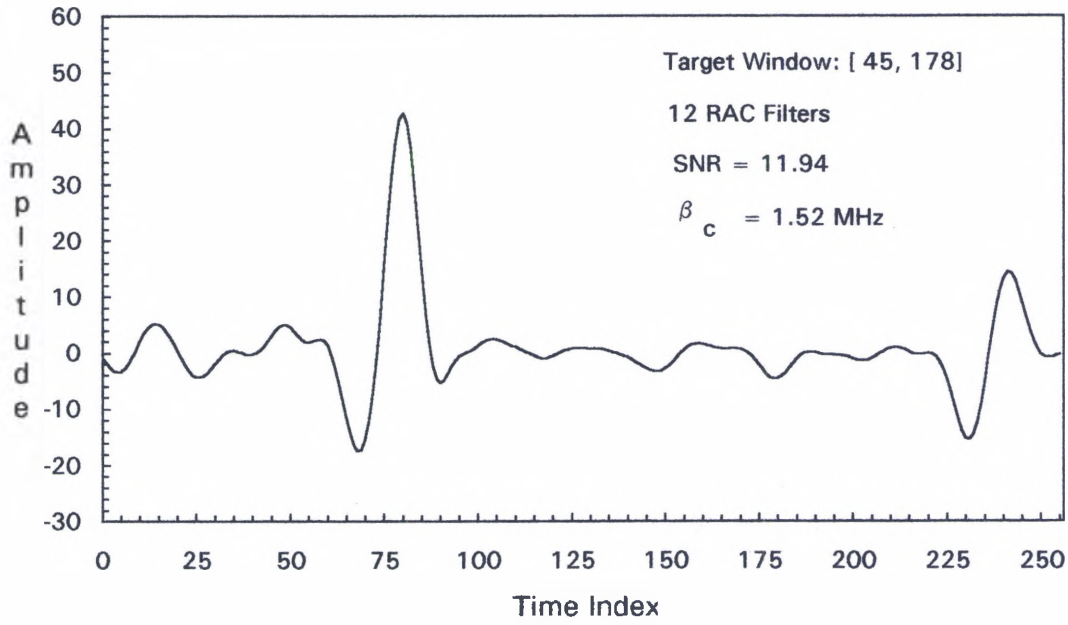

Fig. 2.22 Signal of Experiment IV after Minimization (12 RAC Filters).

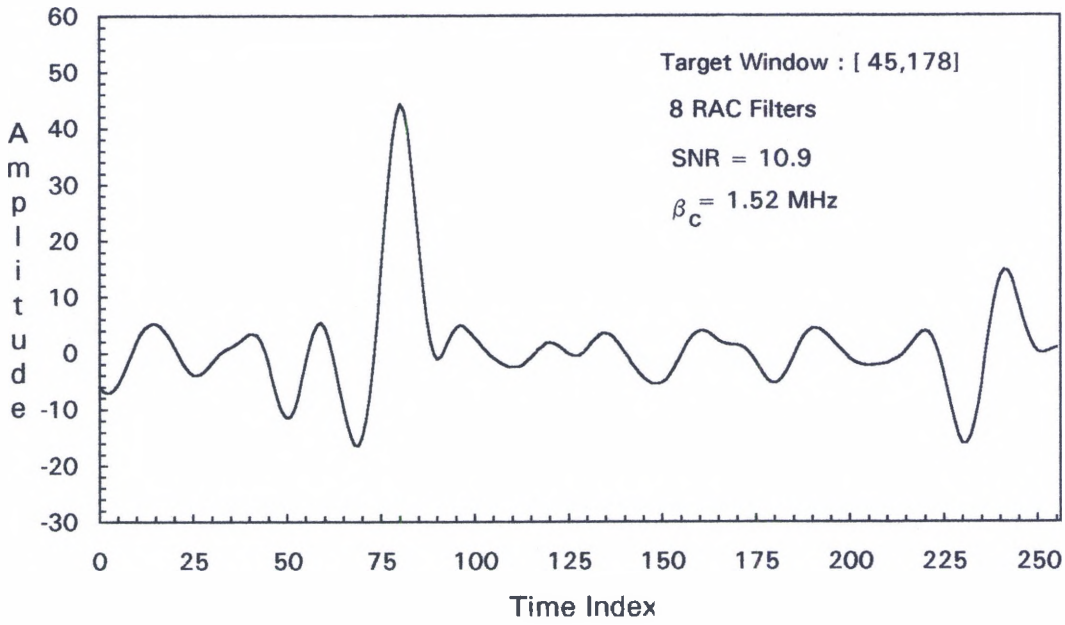

Fig. 2.23 Signal of Experiment IV after Minimization (8 RAC Filters).

MHz for the RAC filters, leading to a total half-power bandwidth of 1.52 MHz. These values are in close agreement with the theoretical estimates. The optimal Gaussian bandwidth was found to be about 1.25 MHz.

CHAPTER III

REALIZATION OF THE SPLIT SPECTRUM TECHNIQUE FOR ULTRASONIC NDE WITH TAPPED-DELAY LINES

3.1 Introduction

This chapter explores the implementation of the bandpass filtering phase of the split spectrum technique with tapped-delay lines thus departing from the more conventional FFT-based approach. Here, a filtering scheme based on a two-branch structure of cascaded subfilters of lower complexity is advanced towards the implementation of the very narrow-band bandpass filters which are typical of SSP. This approach is shown to exhibit a lower multiply count (up to 70%) than that of the direct approach with Parks/McClellan[14] at the expense of a somewhat longer network delay. In chapter II, it was shown that the bandpass filtering stage of the split spectrum technique can be implemented with flat-top filters and that it was possible to surpass the Gaussian-filter bank in SNR performance. The developments of this chapter are expressed in terms of generic flap-top filters of the type that is obtained with algorithms such as that in [14], but its validity extends to other shapes like raised-cosine (RAC) or Gaussian as well. It is shown that excellent SNRs and computational efficiency can be achieved. Experimental results from computer simulations are presented.

3.2 Linear Phase FIR Digital Filters and Computational Complexity Issues

Linear phase finite-impulse response (FIR) filters have very desirable properties such as guaranteed stability, no limit cycles problems, etc. However, their appeal is severely limited by the great lengths of the impulse responses needed in certain applications which may lead to very high computational loads. Usually, a filter is specified in the frequency domain analytically and an approximation process (analytical or numerical) is carried out in order to determine the impulse response coefficients, and the length of the impulse response bears a direct effect on the goodness of the approximation to the desired frequency response. Filter frequency responses with sharp transitions require long impulse response sequences. The most efficient known method of FIR linear-phase filter design is a numerical Chebyshev approximation technique based on the Remez exchange algorithm which is optimal in the minimax sense[14]; that is, it implements the filter with the least number of coefficients for a specific error in the approximation. Figure 3.1 shows the relationship of the impulse response length versus transition bandwidth (region between passband and stopband) of the filter for narrow-band filters with error $\delta = 0.01$(-40dB) in the stopband and passband, when using this algorithm. This graph reveals the reasons why very sharp filters are usually not implemented with tapped-delay lines.

Various authors have studied the problem of efficient FIR-filter implementation [9-13]. Most proposed implementations are particularly well

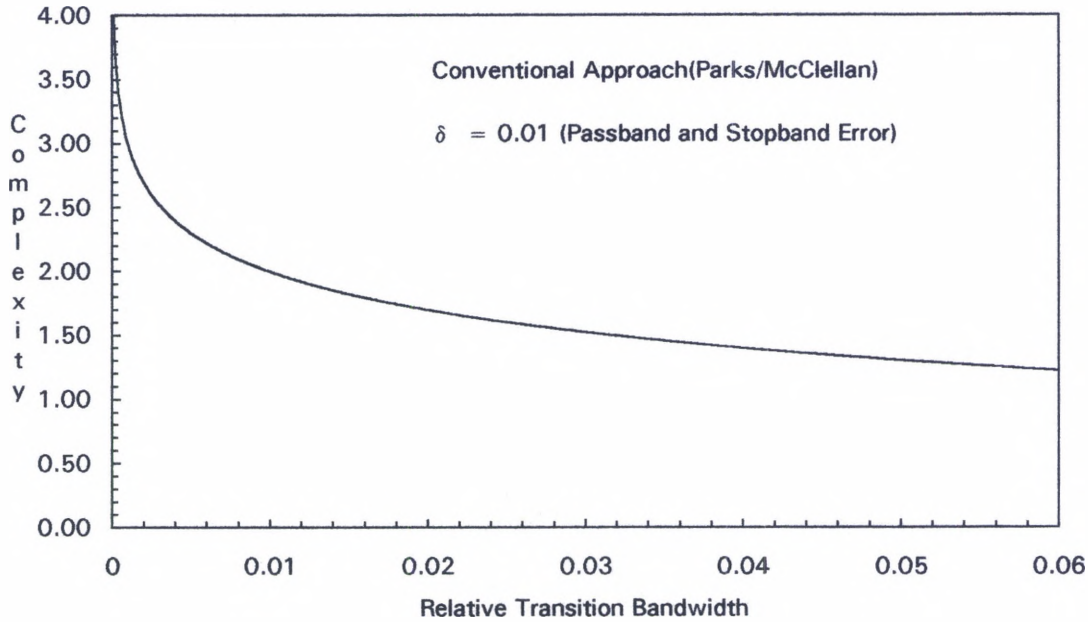

Fig. 3.1 Digital Filter Complexity by Numerical Approximation Approach (Parks/McClellan) for Narrow-Band Digital Filters.

suited for lowpass and highpass filters and, to a limited extent, for bandpass filters. In the bandpass cases, the most limiting factors are the center frequency and the width of the passband. In split spectrum processing, the bandpass filtering scheme must allow easy centering of the frequency response of the filter. The split spectrum technique requires, in most cases, very narrow-band filters that would demand rather long impulse responses making it prohibitive to implement the technique in the time domain. A *direct* implementation of SSP bandpass-filtering banks could be considered, possibly in cases in which the sampling frequency is very close to the Nyquist's sampling rate (roughly twice the maximum frequency component of the signal); however, even then, in many cases

the resulting impulse response may be too long, specially when very sharp filters and algorithms such as polarity thresholding are used.

3.3 Computationally Efficient Bandpass Filter Banks for Split Spectrum Processing

As indicated above, the main disadvantage of SSP lies in the very long processing times required by the technique. When the convolution process involved in the bandpass-filtering stage is performed in the frequency domain with the FFT, the processing time depends primarily on the number of filters used to split the spectrum, whereas, when convolution is performed in the time domain with tapped-delay lines, both the number of filters as well as the number of coefficients required to implement each filter become an issue. In the implementation of SSP, a time-domain filtering scheme must meet certain conditions. One of these is that the algorithm must be simple to make it suitable to VLSI implementation for real-time performance. This condition may appear superficial; however, DSP chips are becoming very pervasive and a low cost implementation (small program code) of this technique is appealing. Another condition is that it must allow easy tuning of the center frequency of the filter, that is, any filter in the bank must be easily produced once a center frequency has been specified; in this way there may be no need to load all filter coefficients initially. Finally, it must reduce the multiply count considerably. Current processor speeds could not support the bandwidths SSP requires for true real-time processing; however, in the near future

faster chips may be available that, when combined with highly efficient techniques of digital filter design may make true real-time SSP a reality.

Aussel [2] has proposed a method for the implementation of SSP with tapped-delay lines in which the filter bank is made up of unequally spaced Gaussian filters of different HPBWs. As the center frequency increases, so does the HPBW of the filter and the separation between adjacent filters. This makes the filters placed at the higher frequencies smoother and easier to implement. This approach may be very efficient for relatively wider filters; however, for very narrow-band filters, of the type used with polarity thresholding, this method may not be viable. Also, he finds that the number of filters needed is the same as with the conventional approach.

3.3.1 Graphical Development

The complexity or length of a digital FIR filter designed by the Parks/McClellan approach[14] in a *direct* manner can be estimated by

$$N \approx \frac{19 - 20\log \delta}{27\Delta f} \qquad \textbf{(eq.3.1)}$$

This equation holds true for very narrow-band filters where the stop band error δ and the relative (to the sampling rate) transition bandwidth Δf govern the length of the filter[16]. A graph of this equation is shown in figure 3.1. It is possible to design a digital filter in an *indirect* manner that would result in a filtering structure involving various filters of lower

complexity with a net lower-multiply count. This has been demonstrated by various authors[10-13] primarily for lowpass and highpass filters.

A similar approach can be taken towards the design of very-narrow bandpass filters that can achieve a net lower-multiply count of up to 70% compared to the direct approach. Consider, as a point of departure, the design of a bandpass filter centered at f_0 with transition bandwidth Δf and passband width $\Delta\rho$ as described in figure 3.2. All frequencies or frequency quantities shall be *relative* to the sampling frequency, that is, all quantities are normalized with respect to the sampling frequency. As presented, this filter has a very small Δf which would lead to a long impulse responses as per equation 3.1. The design of this bandpass filter can be started from a lowpass filter with a much smoother transition bandwidth as shown in figure 3.3. Since the design is based upon this filter, it shall be called the *base filter*. As shown in this picture, this lowpass filter has a transition bandwidth and passband width I times wider than that of the desired bandpass filter. Therefore, the length of the impulse response required to implement this filter is I times smaller, as indicated by equation 3.1. If the frequency response of this base lowpass filter were to be compressed or frequency scaled by a factor I, the frequency response of figure 3.4 would result. This response is that of a multiple-passband filter with the passbands being located at integer multiples of $\frac{1}{I}$,that is, at $\frac{k}{I}$ for $k = 0, \pm 1, \pm 2, \pm 3,...$ The effect of this operation on the impulse response of the filter is illustrated in figure 3.5. Here, figure 3.5a represents the impulse response of a sample base lowpass filter. Figure 3.5b shows the impulse

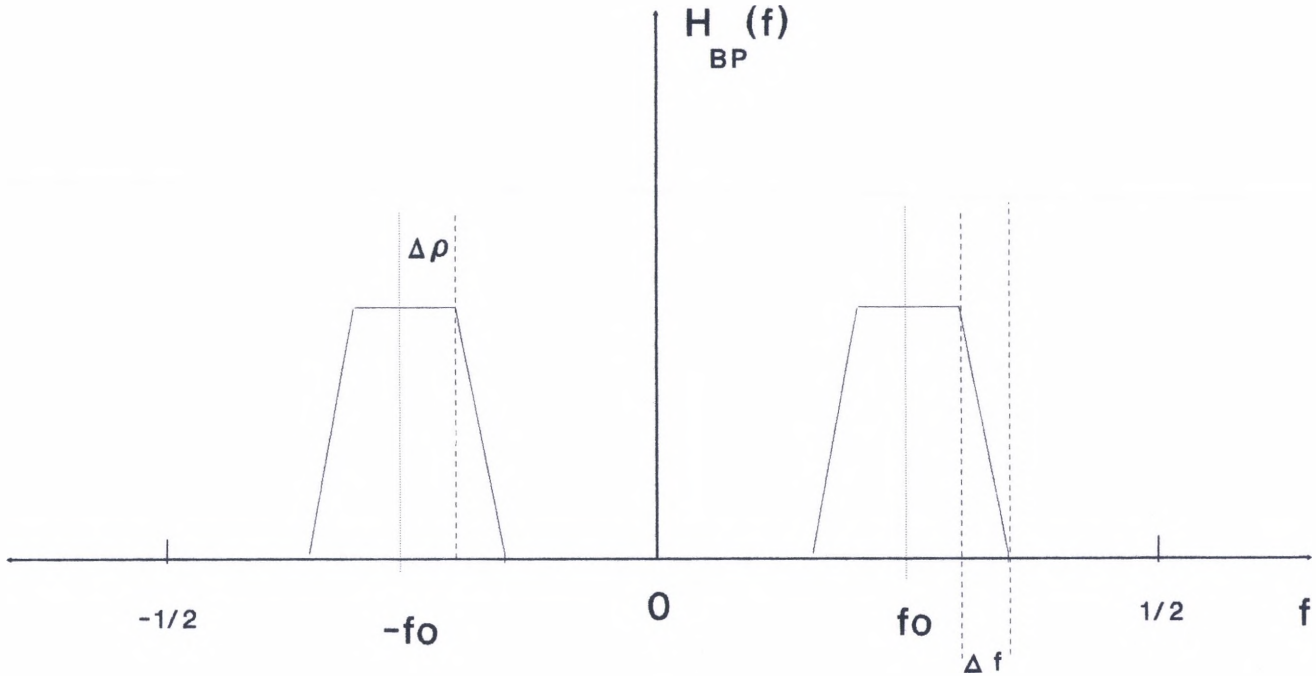

fo = center frequency
Δf = transition bandwidth
$\Delta \rho$ = passband width

Fig. 3.2 Narrow-Band Bandpass Filter.

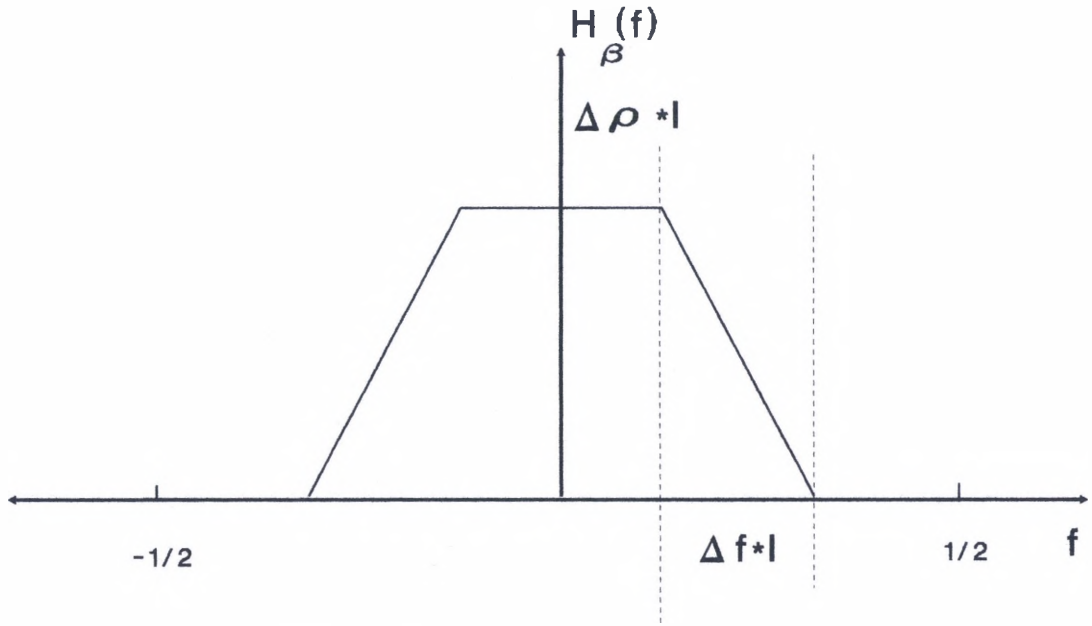

$$N_{\beta} \simeq \frac{19 - 20\log\delta}{27 * \Delta f * I}$$

Fig. 3.3 Base Lowpass Filter with Smoother Transition Bandwidth.

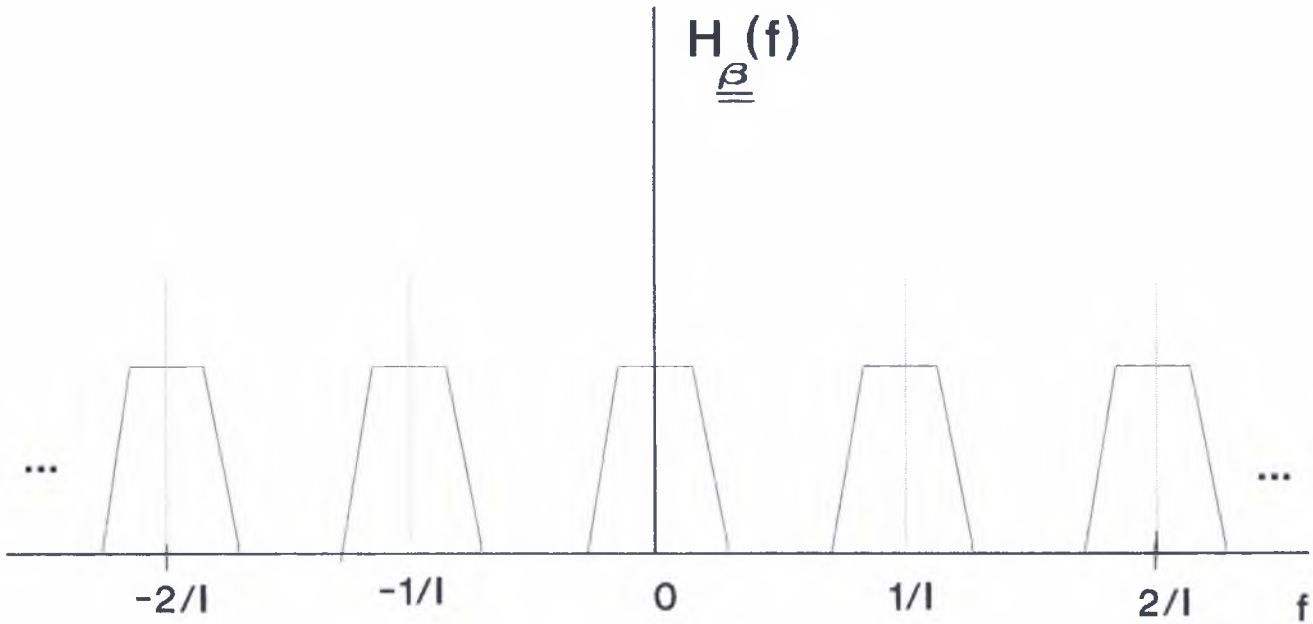

$$H_{\underline{\underline{\beta}}}(f) = H_{\beta}(f/I)$$

I = SCALING FACTOR (INTEGER)

ALL PASSBANDS ARE IDENTICAL TO THOSE OF THE DESIRED BP FILTER

Fig. 3.4 Frequency-Scaled Base Filter.

SAMPLE IMPULSE RESPONSES

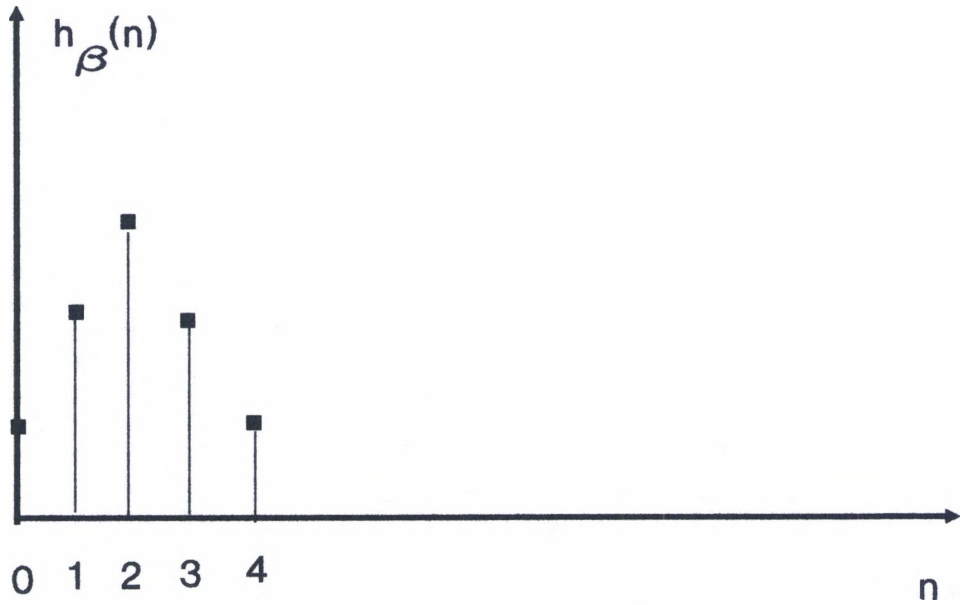

Fig. 3.5a Sample Impulse Response of Base Filter.

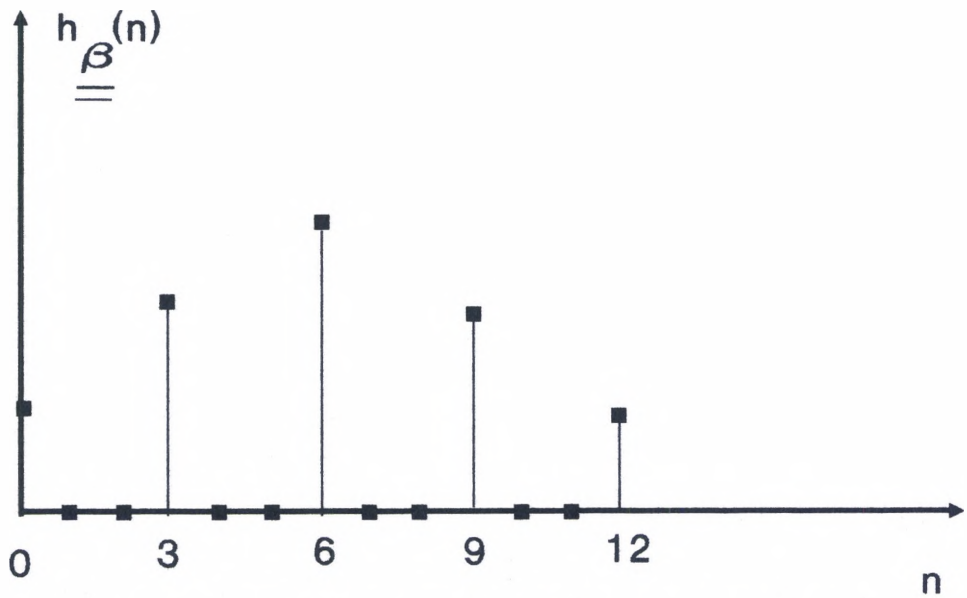

Fig. 3.5b Stretched Impulse Response for I = 3.

response of the base filter after it is been frequency scaled by a factor of I = 3. The effect is to simply stretch the impulse response by inserting I − 1 zero samples (in this case 2 zero samples) between all non-zero samples. This is a well known occurrence, compression in the frequency domain leads to expansion in the time domain; however, in the digital domain the stretching does not increase the number of non-zero samples, that is, the number of non-zero coefficients in the stretched impulse response is the same as that of the impulse response of the base filter. In the frequency-scaled base filter, all passbands are identical in shape to those of the desired bandpass filter. From this point, there is more than one way to arrive at the desired bandpass filter. One is to cascade a lowpass filter with the frequency-scaled base filter such that the center passband is retained and all others are *masked out,* as shown in figure 3.6, to produce the lowpass filter of figure 3.7. This filter's impulse response can then be modulated by a cosine sequence $\cos(2\pi f_0 n)$ to produce the desired bandpass filter. The modulation process is depicted in detail in figures 3.8a, 3.8b, where right and left shifted frequency responses are illustrated which are properly combined to yield the final bandpass filter of fig. 3.8c. However, it is obvious that this approach is equivalent to designing the filter in a direct fashion, and therefore the computational complexity would not be improved, and no effective advantage is achieved. This case does, however, serve as an illustration of the basic principle to be employed here in designing bandpass filters. This way to produce a bandpass filter from a lowpass one by frequency shifting or modulation with complex

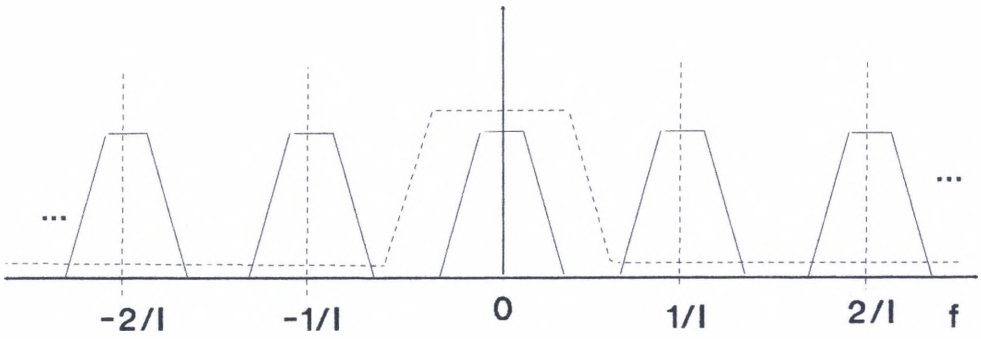

Fig. 3.6 Cascade of Lowpass Filter and Frequency Scaled Base Filter.

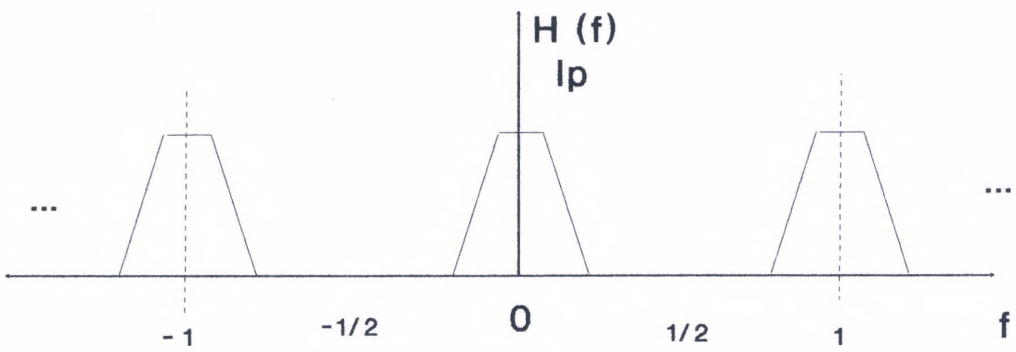

Fig. 3.7 Resulting Lowpass Filter.

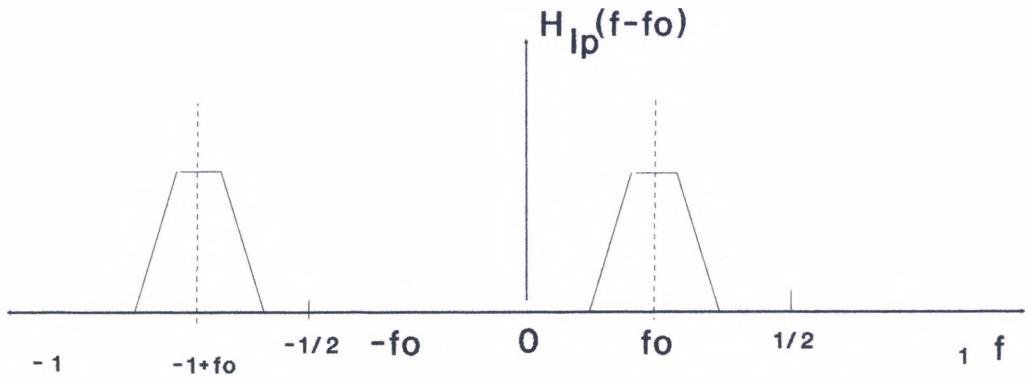

Fig. 3.8a Right-shifted Version of $H_{lp}(f)$ of Fig. 3.7

$$h_{lp}(n)e^{j2\pi nfo} \longleftrightarrow H_{lp}(f-fo)$$

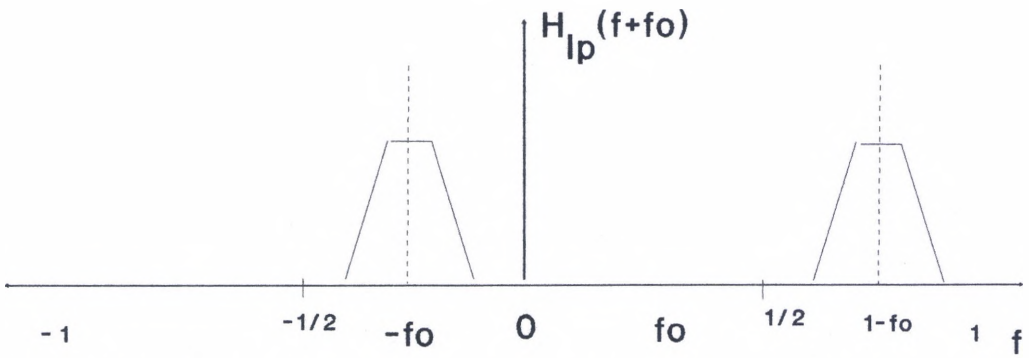

Fig. 3.8b Left-shifted Version of $H_{lp}(f)$ of Fig. 3.7

$$h_{lp}(n)e^{-j2\pi nfo} \longleftrightarrow H_{lp}(f+fo)$$

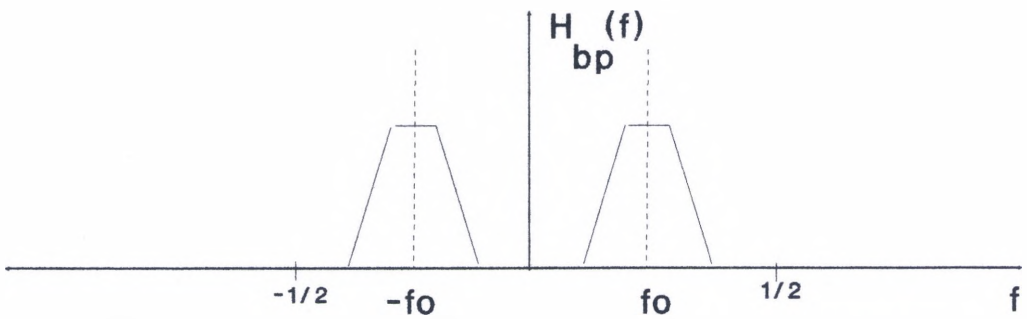

Fig. 3.8c Addition of Responses in a and b. Result is Equivalent to Modulation by $\cos(2\pi nfo)$.

exponentials is of central importance since it forms the basis for the formulation of the design procedure presented here. Fundamental to this is the *modulation* or *frequency shifting theorem* which simply states that, if

$$h(n) \Leftrightarrow H(f)$$

then

$$h(n)e^{j2\pi f_o n} \Leftrightarrow H(f - f_o)$$

that is, multiplication or modulation of the impulse response h(n) of a filter by a complex exponential $e^{j2\pi f_o n}$ simply shifts the frequency response by f_o. An application of this theorem has already been seen and detailed in figure 3.8. This theorem is now used to formulate an efficient procedure to design a bandpass filter departing from the filter of figure 3.4 or frequency-scaled base filter.

3.3.2 Two-Branch Cascaded Filter Structure

A bandpass filter can be easily designed from the *frequency-scaled base filter* in figure 3.4. A right and a left shifted frequency-response versions of this filter can be obtained by modulating its impulse response by the appropriate complex exponentials. Figures 3.9a and 3.9b show both frequency-shifted versions. These frequency responses correspond to those of filters which are complex conjugates of one another and which are asymmetric about zero. If a lowpass filter is designed with a passband wide enough to encompass the entire center passband of the frequency-scaled base filter and *mask out* all other passbands, as shown in figure

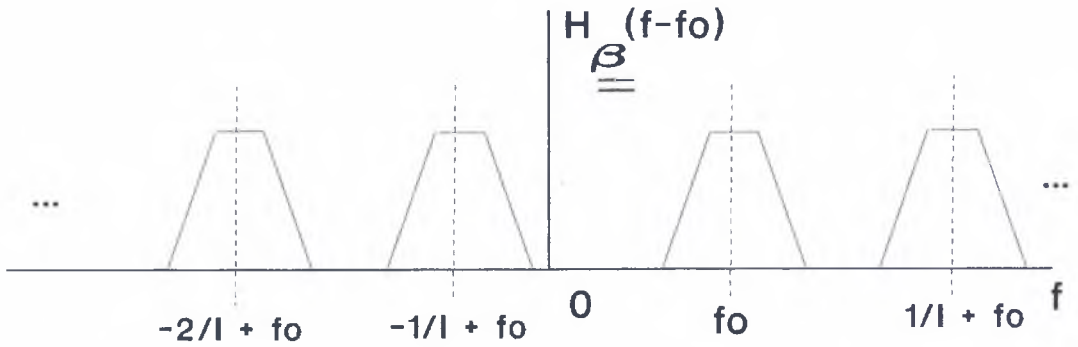

Fig. 3.9a Right-shifted Frequency-Scaled Base Filter.

$$h_{\underline{\beta}}(n)e^{j2\pi fo(n-N)I} \longleftrightarrow H_{\underline{\beta}}(f-fo)$$

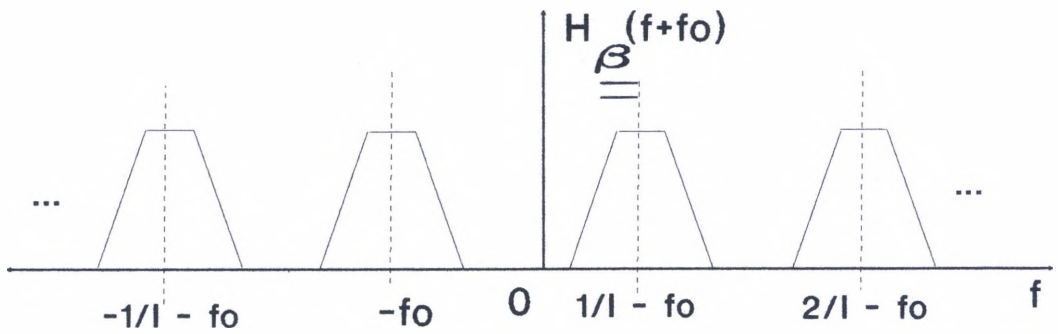

Fig. 3.9b Left-shifted Frequency-Scaled Base Filter.

$$h_{\underline{\beta}}(n)e^{-j2\pi fo(n-N)I} \longleftrightarrow H_{\underline{\beta}}(f+fo)$$

3.10a, and its impulse response modulated or shifted in the same fashion as that of the frequency-scaled base filter then the filters of figures 3.10b and 3.10c will result. The filters of figures 3.9a and 3.10b can be cascaded together to generate the filter of figure 3.11a. That is to say, the frequency right-shifted version of the frequency-scaled base filter is cascaded with the frequency right-shifted version of the lowpass filter or *masking filter* of figure 3.10b. The result is the right-shifted frequency response of figure 3.11a, which simply represents an asymmetric bandpass complex filter with a passband centered at fo. A similar filter results by cascading the frequency left-shifted versions of the frequency-scaled base filter and the masking filter as shown in figure 3.11b . These two cascades of filters can be combined or added together to yield the desired bandpass filter of figure 3.2. The total process to design the bandpass filter is then condensed into a filtering structure composed of two branches and four subfilters as shown in figure 3.12. The top branch would correspond to the net filter of figure 3.11a and the bottom branch to the net filter of figure 3.11b. This overall filter structure generates the desired bandpass filter. A more formal presentation of this implementation is now given such that the design can be readily undertaken.

3.3.3 Formalization of the Design Procedure

The design procedure described above in a graphical fashion, indicates that the design involves two basic lowpass filters. One is a lowpass filter that have been called the *base filter* and from which the desired shape is derived by frequency-scaling or compression. This filter is

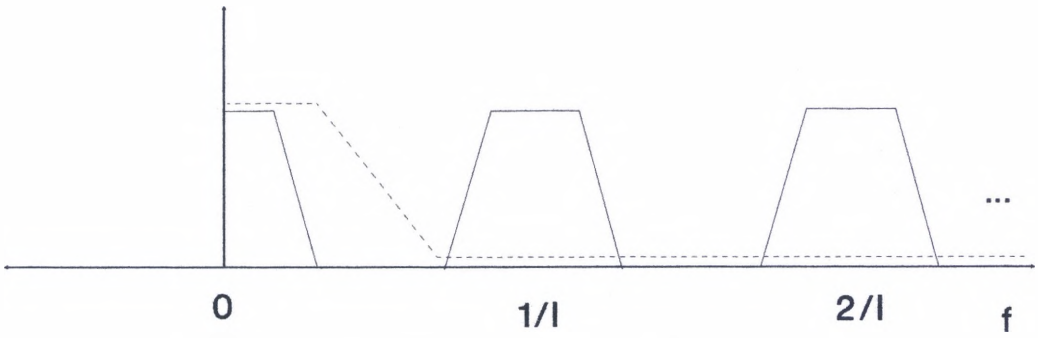

Fig. 3.10a Frequency-Scaled Base Filter and Masking Filter (Dashed Line).

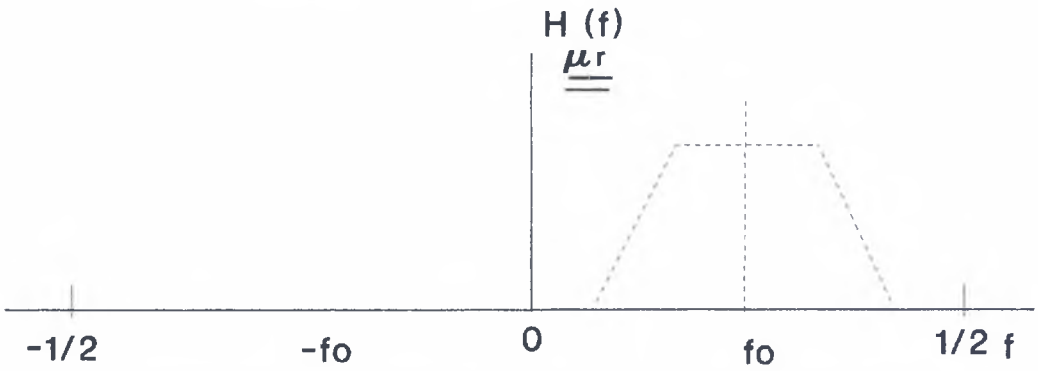

Fig. 3.10b Right-shifted Version of Masking Filter.

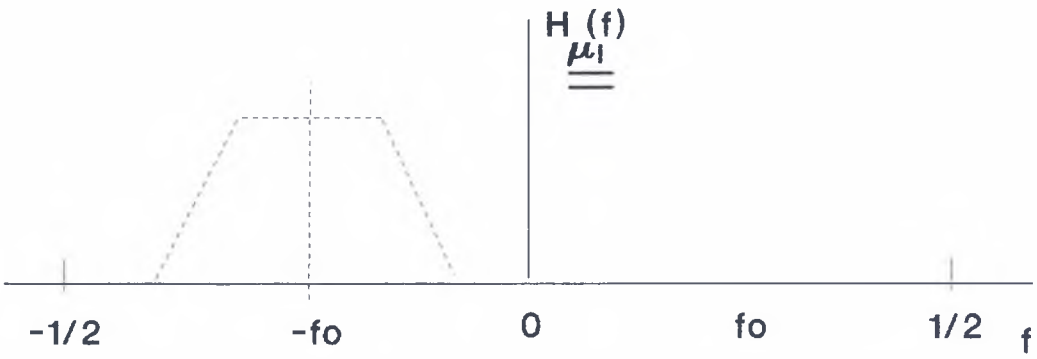

Fig. 3.10c Left-shifted Version of Masking Filter.

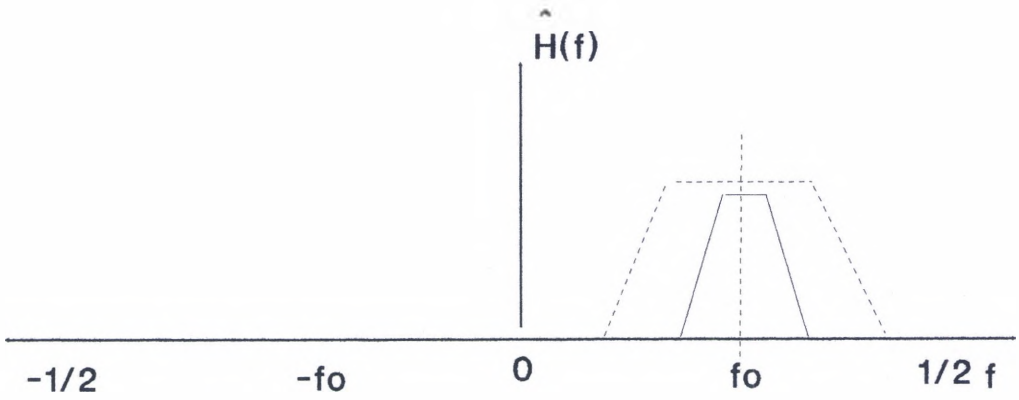

Fig. 3.11a Result of Cascade of Filters in Figures 3.9a and 3.10b. This is one of the Branches.

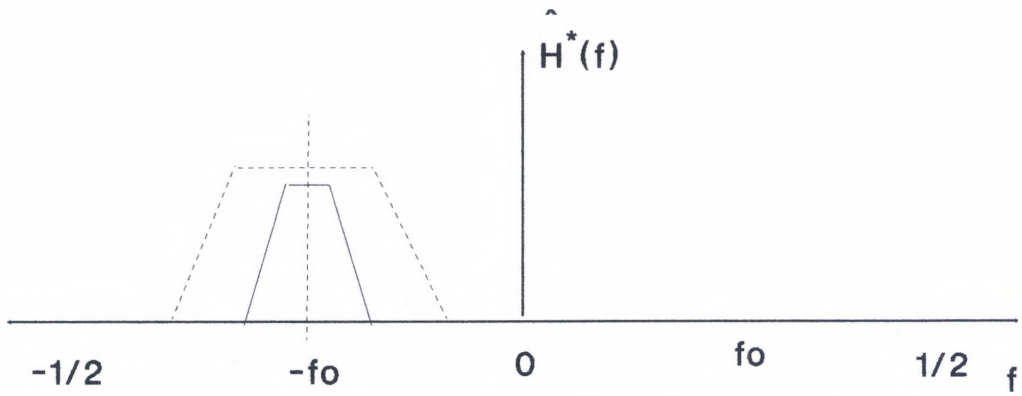

Fig. 3.11b Result of Cascade of Filters in Figures 3.9b and 3.10c. This is the other Branch.

Fig. 3.11 The Result from Adding the above Responses is the desired Bandpass Filter shown in Fig. 3.8c.

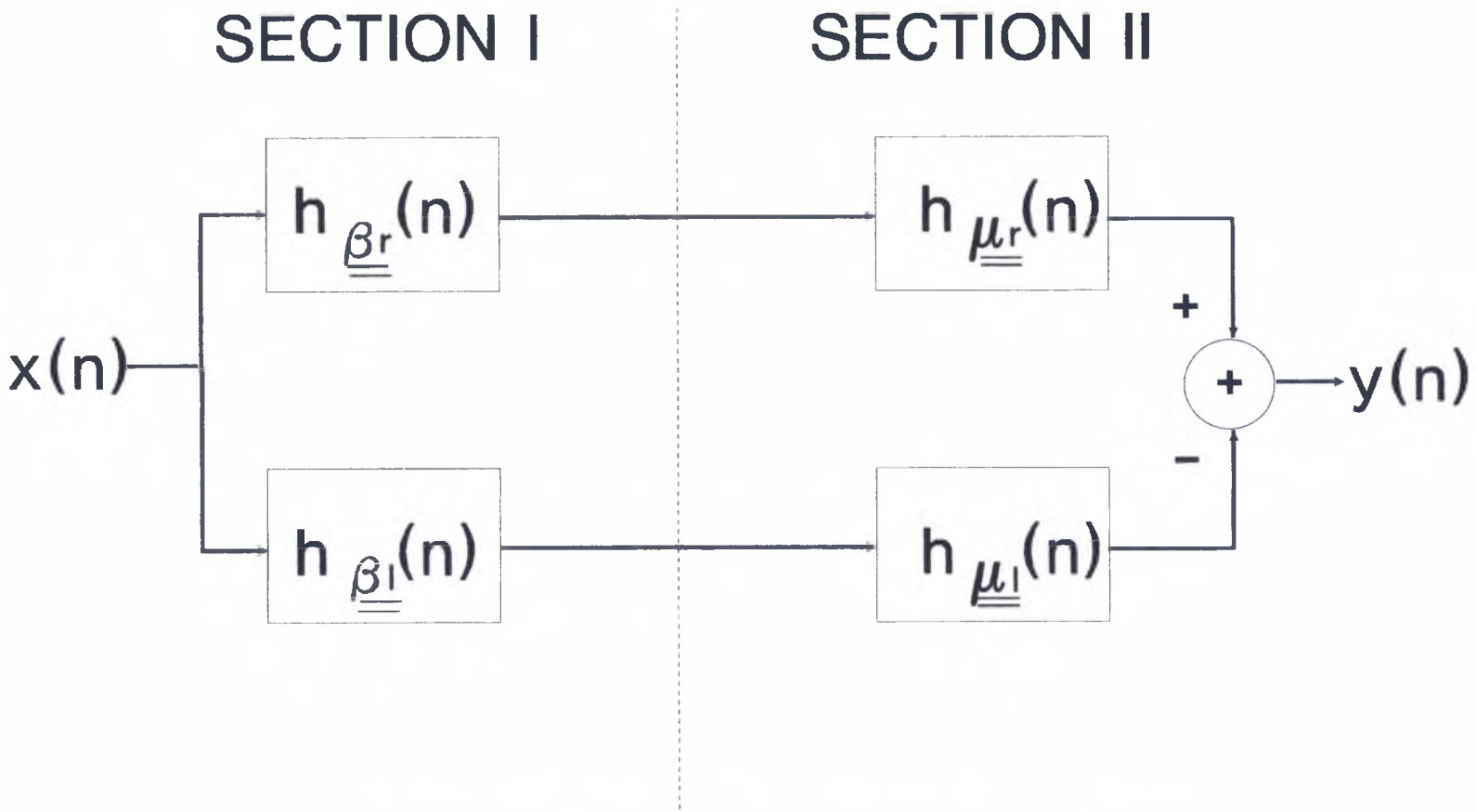

Fig 3.12 Overall Filtering Structure. The Filter Coefficients are Complex.

described as having a much smoother transition bandwidth than that of the desired bandpass filter and therefore as requiring a much shorter impulse response for its implementation. Upon being frequency compressed, the shape of each passband is identical to the shape of the passband of the desired bandpass filter, except that this frequency-scaled filter is a multiple-band filter. Two complex conjugate filters are derived from this frequency-scaled base filter, one is frequency right-shifted and the other left shifted to f_o and $-f_o$ respectively. The other basic lowpass filter required here is a *masking filter* from which two complex conjugate filters are also derived, one has a right-shifted frequency response and the other a left-shifted one to f_o and $-f_o$ respectively. It is seen here that the function of the masking filter is to remove or mask out all extra passbands and to retain only those centered at f_o. Two series connections are then formed, one is a cascade of the right-shifted frequency-response filters and the other one the left-shifted frequency-response filters corresponding to the base and masking filters and then these two branches are added to form the desired bandpass filter. The net result is shown in figure 3.12.

If $h_\beta(n)$ represents the impulse response of the base filter of figure 3.3, then the impulse response $h_{\underline{\beta}}(n)$ of the frequency-scaled base filter in figure 3.4 is given by

$$h_{\underline{\beta}}(n) = \begin{cases} h_\beta(\frac{n}{I}) & \text{for} \quad n = 0, I, 2I, 3I, \ldots, (N_\beta - 1) \\ 0, & \text{otherwise} \end{cases} \qquad \textbf{(eq.3.2)}$$

where I is the scaling factor and N_β is the length of the impulse response of the base filter. This expression indicates that the number of *non-zero* coefficients in the frequency-scaled base filter is the same as that of the impulse response of the original base filter. The Z-transform is the mathematical tool commonly used to describe digital filters, and it shall be used here for such purpose. The Z-transform expression corresponding to the base filter is

$$H_\beta(z) = \sum_{n=0}^{N_\beta - 1} h_\beta(n) z^{-n} \qquad \textbf{(eq.3.3)}$$

and that of the frequency-scaled base filter is given by

$$H_{\underline{\beta}}(z) = \sum_{n=0}^{N_\beta - 1} h_\beta(n) z^{-nI} \qquad \textbf{(eq.3.4)}$$

The Z-transforms of the right-shifted and left-shifted frequency-response frequency-scaled base filters are given by the two expressions

$$H_{\underline{\beta r}}(z) = \sum_{n=0}^{N_\beta - 1} h_\beta(n) e^{j\,[2\pi(n - N)If_o]} z^{-nI} \qquad \textbf{(eq.3.5a)}$$

and

$$H_{\beta l}(z) = \sum_{n=0}^{N_\beta - 1} h_\beta(n) e^{-j\,[2\pi(n - N)lf_o]z - nl} \qquad \textbf{(eq.3.5b)}$$

respectively. N is equal to $(\frac{N_\beta - 1}{2})$ and not necessarily an integer. Likewise, similar expressions can be obtained for the masking filter as follows

$$H_{\mu r}(z) = \sum_{n=0}^{N_\mu - 1} h_\mu(n) e^{j\,[2\pi(n - M)f_o]z - n} \qquad \textbf{(eq.3.6a)}$$

and

$$H_{\mu l}(z) = \sum_{n=0}^{N_\mu - 1} h_\mu(n) e^{-j\,[2\pi(n - M)f_o]z - n} \qquad \textbf{(eq.3.6b)}$$

for the right-shifted and left-shifted frequency-response filters respectively. $h_\mu(n)$ is the impulse response of the masking filter and N_μ is its length and M is equal to $(\frac{N_\mu - 1}{2})$. N and M are simply the points about which $h_\beta(n)$ and $h_\mu(n)$ are symmetric. Figure 3.13 summarizes the transform pairs for all four subfilters involved. The transfer function of the overall structure can be found as follows

$$H(f) = (H_{\beta rl} + j\,H_{\beta i})(H_{\mu rl} + j\,H_{\mu i}) + (H_{\beta rl} - j\,H_{\beta i})(H_{\mu rl} - j\,H_{\mu i})$$

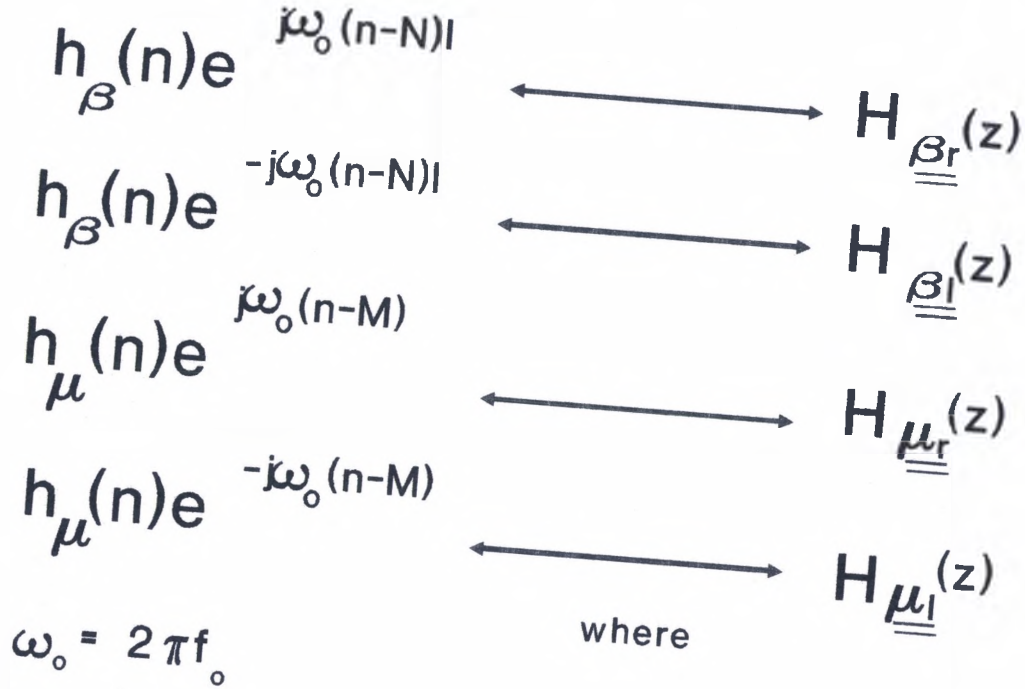

Fig. 3.13 Complex-valued Impulse Responses of Subfilters.

which reduces to

$$H(f) = 2*(H_{\beta rl}*H_{\mu rl} - H_{\beta i}*H_{\mu i})$$

This last expression allows the realization of the filtering structure with purely real arithmetic. Here, $H_{\beta rl}$ and $H_{\mu rl}$ are the real parts, and $H_{\beta i}$ and $H_{\mu i}$ are the imaginary parts corresponding to $H_{\underline{\beta r}}(z)$ ($H_{\underline{\beta l}}(z)$) and $H_{\underline{\mu r}}(z)$ ($H_{\underline{\mu l}}(z)$) described in equations 3.5 and 3.6 respectively (it should be obvious that the right and left-shifted versions of the filters are complex conjugates of each other). These real-valued impulse responses are all summarized in figure 3.14 and the corresponding Z-transform expressions are

$$H_{\underline{\beta rl}}(z) = \sum_{n=0}^{N_\beta - 1} h_\beta(n) \cos[2\pi f_o(n - N)l]\, z^{-nl} \qquad \textbf{(eq.3.7a)}$$

$$H_{\underline{\beta i}}(z) = \sum_{n=0}^{N_\beta - 1} h_\beta(n) \sin[2\pi f_o(n - N)l]\, z^{-nl} \qquad \textbf{(eq.3.7b)}$$

$$H_{\underline{\mu rl}}(z) = \sum_{n=0}^{N_\mu - 1} h_\mu(n) \cos[2\pi f_o(n - M)]\, z^{-n} \qquad \textbf{(eq.3.7c)}$$

and

$$H_{\underline{\mu i}}(z) = \sum_{n=0}^{N_\mu - 1} h_\mu(n) \sin[2\pi f_o(n - M)]\, z^{-n} \qquad \textbf{(eq.3.7d)}$$

$$h_{\beta}(n)\cos[\omega_o(n-N)I] \longleftrightarrow H_{\underline{\underline{\beta_{rl}}}}(z)$$

$$h_{\beta}(n)\sin[\omega_o(n-N)I] \longleftrightarrow H_{\underline{\underline{\beta_{i}}}}(z)$$

$$h_{\mu}(n)\cos[\omega_o(n-M)] \longleftrightarrow H_{\underline{\underline{\mu_{rl}}}}(z)$$

$$h_{\mu}(n)\sin[\omega_o(n-M)] \longleftrightarrow H_{\underline{\underline{\mu_{i}}}}(z)$$

where

$$\omega_o = 2\pi fo$$

Fig. 3.14 Center Frequency Tuning.

These equations, in essence, lead to the implementation of the structure of figure 3.12 in a very straightforward manner. This is discussed next.

3.3.4 Implementation of the Two-Branch Filtering Structure

The equation that defines convolution with tapped-delay lines is given by

$$y(n) = \sum_{k=0}^{N-1} h(k)\, x(n-k) \qquad \textbf{(eq.3.8)}$$

where h(n) is the impulse response of the filter, x(n) is the input to the filter and y(n) is the output sequence and N is the length of the impulse response. If a filter is of the linear-phase type, h(n) is symmetric about $M = (\frac{N-1}{2})$. A practical implementation of equation 3.8 is shown in figure 3.15 for a linear-phase filter with five samples. Advantage can be taken of the symmetry of the impulse response, as shown in figure 3.16, to reduce the multiply count by roughly 50 percent. The structure in figure 3.12 can be implemented in two sections with each section mechanized in a combined-delay network in which top and bottom branches are integrated to expedite the processing. The first section is implemented as shown in figure 3.17 in a direct fashion using the same scheme as that of figure 3.16, except that, the two filters at the input of the system are implemented simultaneously or made to share the same set of delay elements. The second section is implemented in a somewhat different manner out of convenience. This section has two different input streams and one output stream. For this, a different implementation of equation 3.8

FIR CONVOLUTION

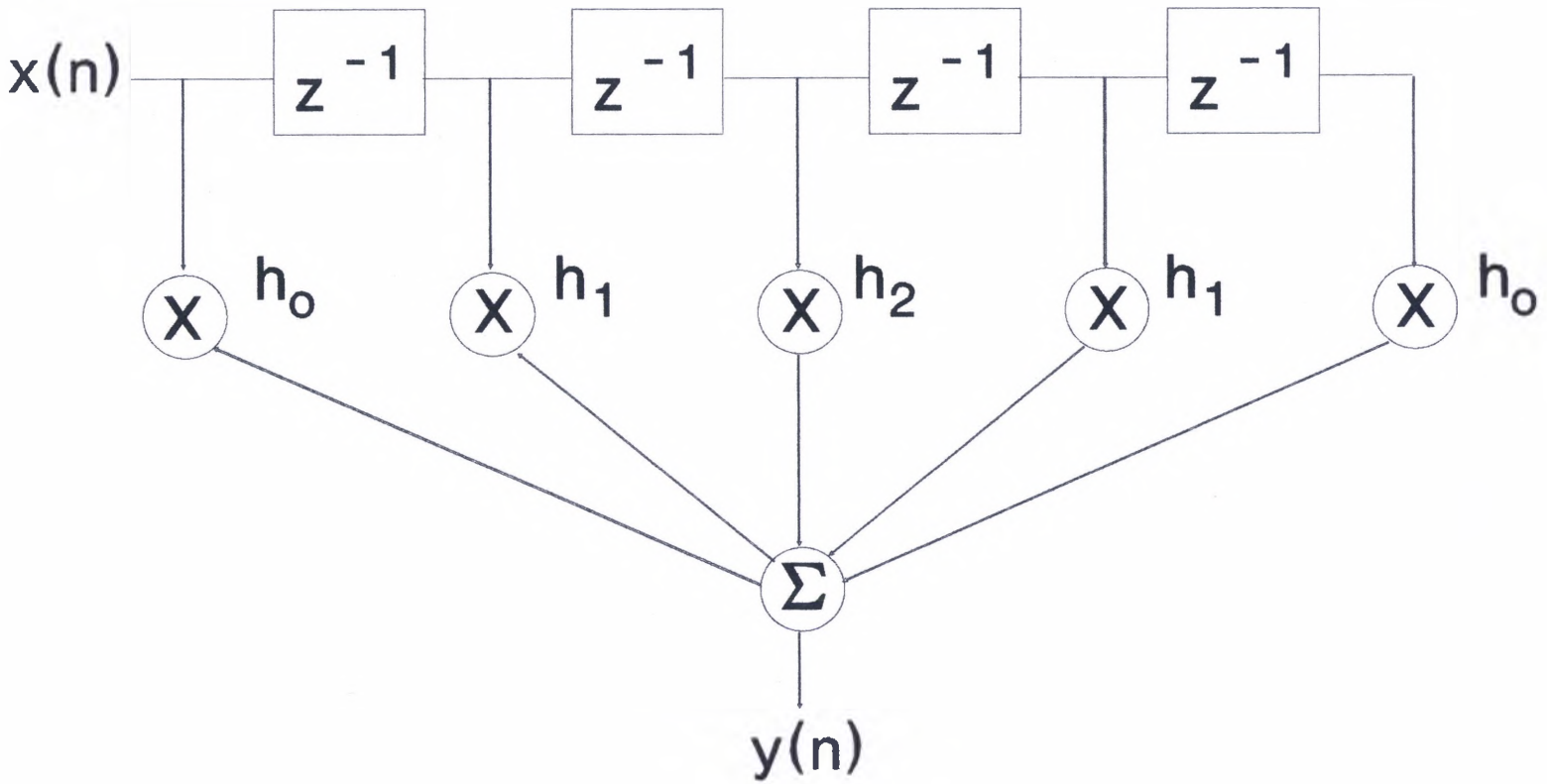

Fig. 3.15 Tapped-Delay Line.

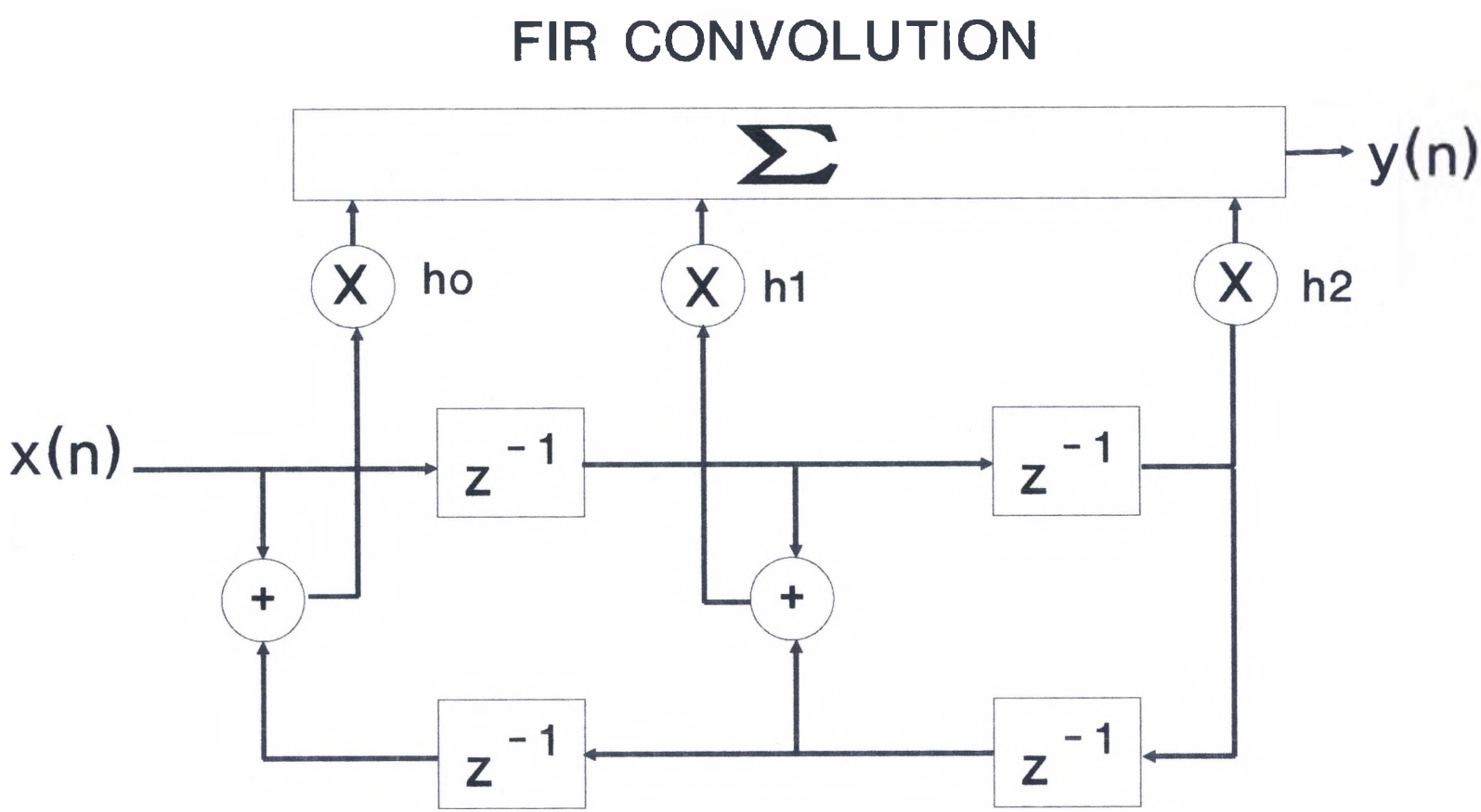

Fig. 3.16 Direct Form Implementation.

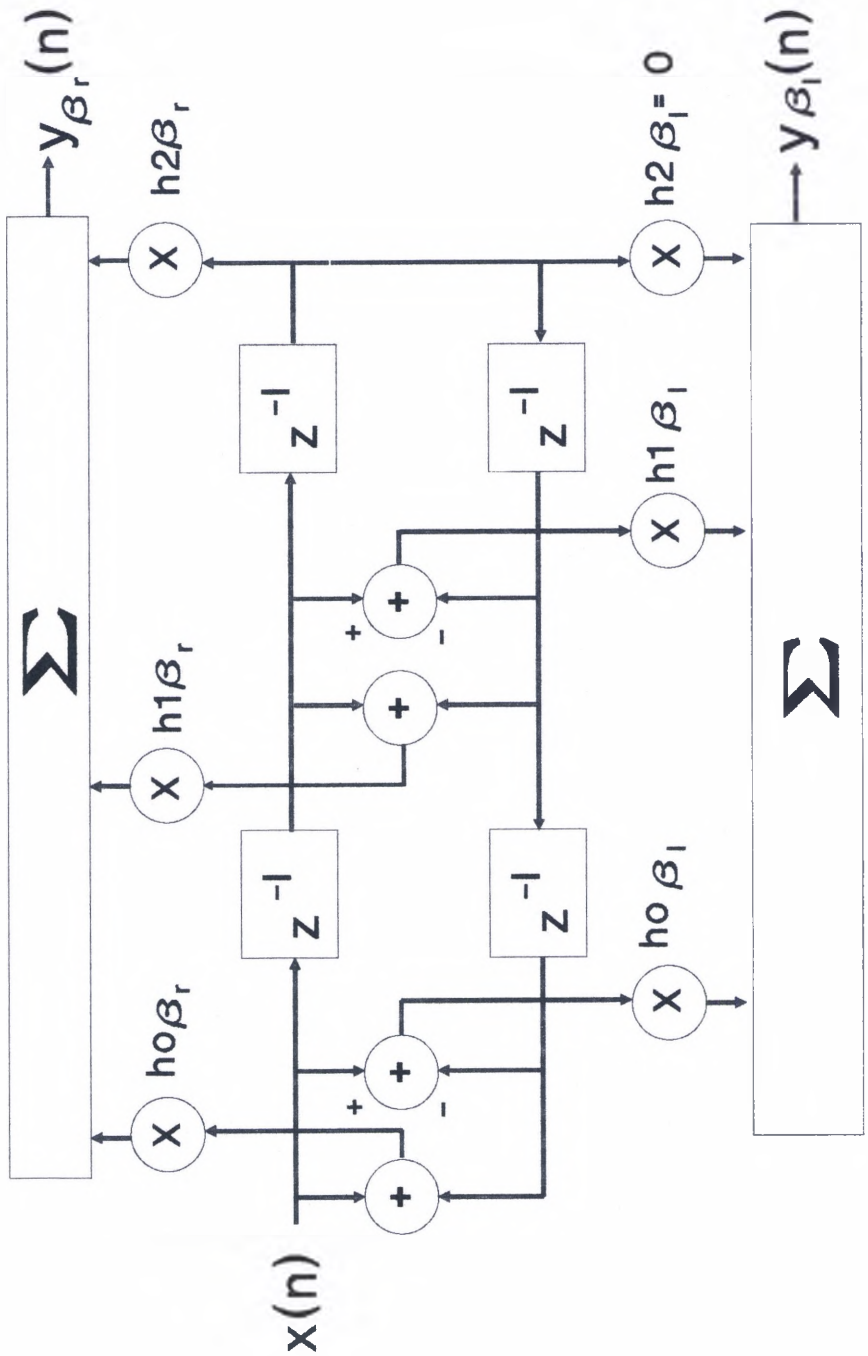

Fig. 3.17 Implementation of Section I.

is considered which is equivalent to that of figure 3.15, and which can be better understood by looking at the way each individual output sample is computed from equation 3.8 :

$$y(0) = h(0)x(0)$$

$$y(1) = h(0)x(1) + h(1)x(0)$$

$$y(2) = h(0)x(2) + h(1)x(1) + h(2)x(0)$$

$$y(3) = h(0)x(3) + h(1)x(2) + h(2)x(1) + h(3)x(0)$$

$$y(4) = h(0)x(4) + h(1)x(3) + h(2)x(2) + h(3)x(1) + h(4)x(0)$$

$$\vdots$$

The mechanization of the process represented in the above equations results in the structure of figure 3.18. Figure 3.19 shows the implementation of one the filters and figure 3.20 shows the implementation of both using the same set of delays. It is important to note that this implementation is adopted for the second section of the structure in order to combine the two branches and make them share the same set of delays; in this fashion, the entire structure is a combined-delay structure which roughly halves the delay of the signal through the net filter. These two sections can be easily translated into a very simple program. The appendix

FIR CONVOLUTION

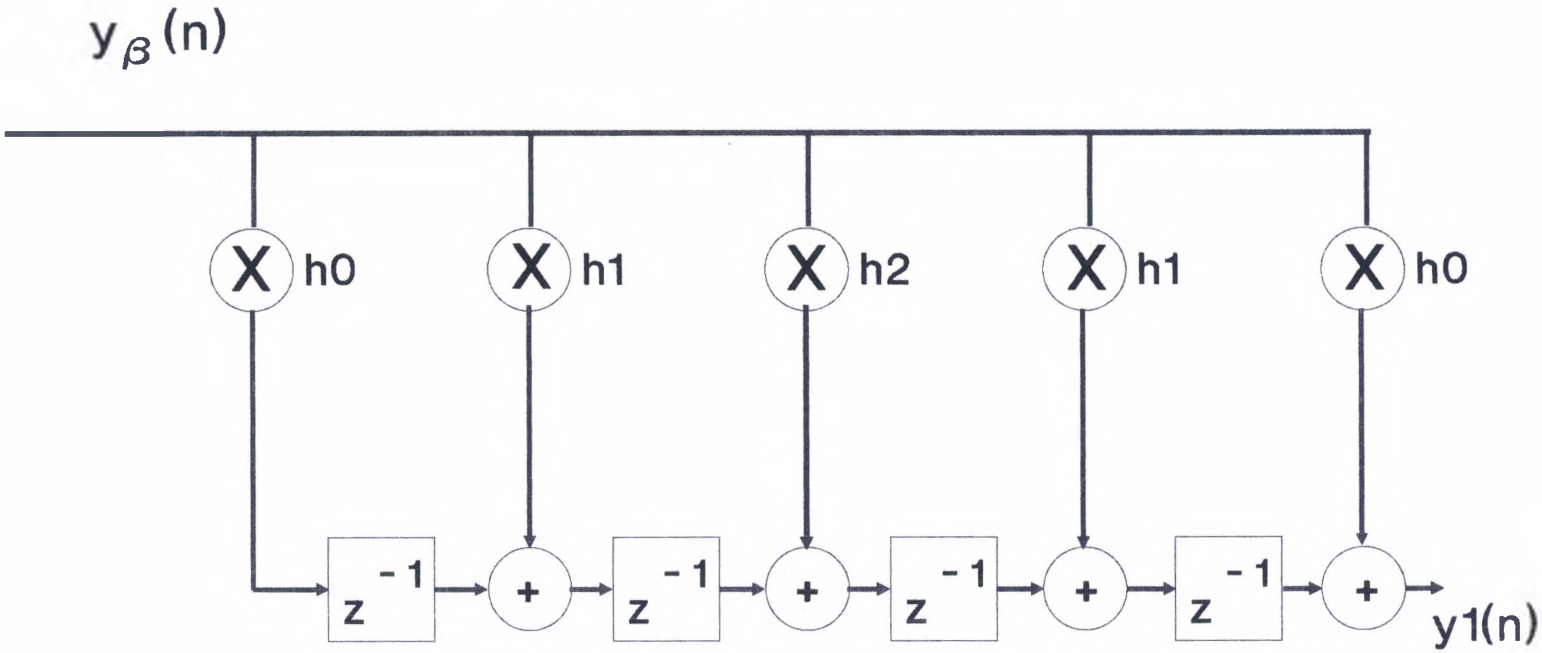

Fig 3.18 Another Implementation of FIR Convolution.

FIR CONVOLUTION

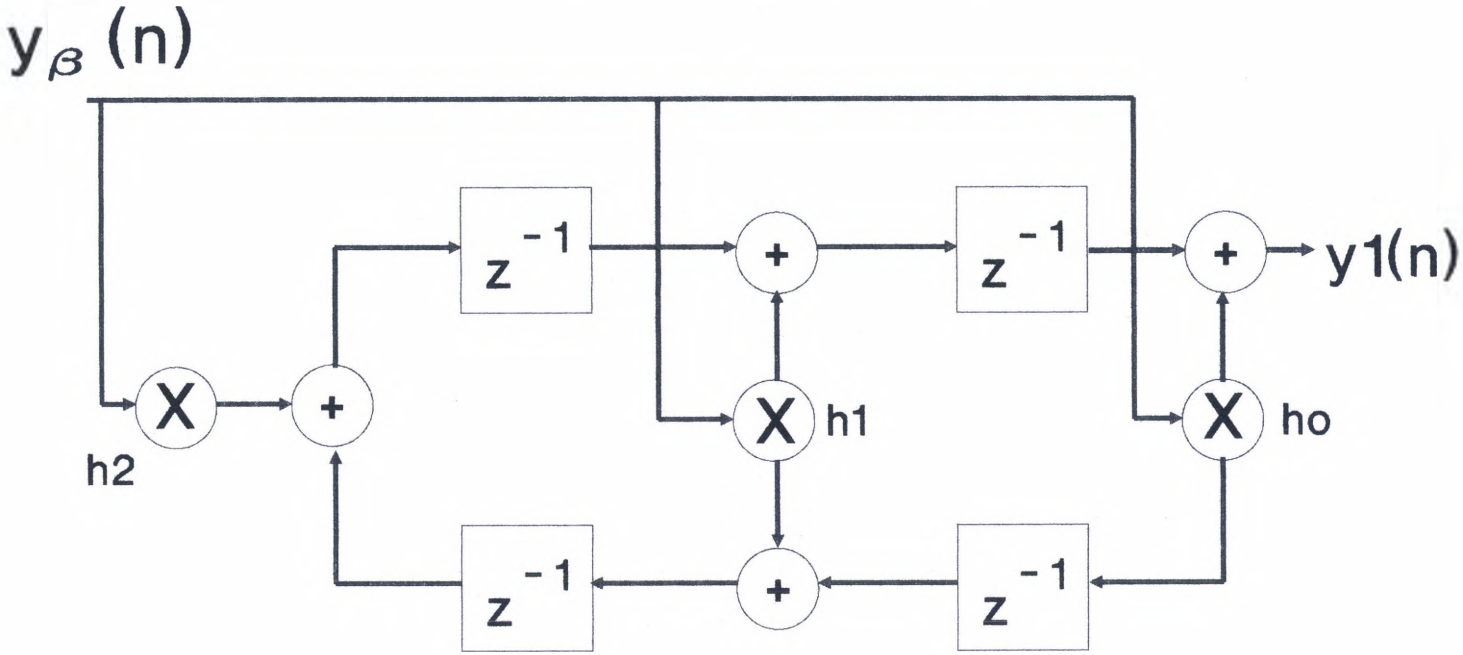

Fig. 3.19 Direct Form Implementation.

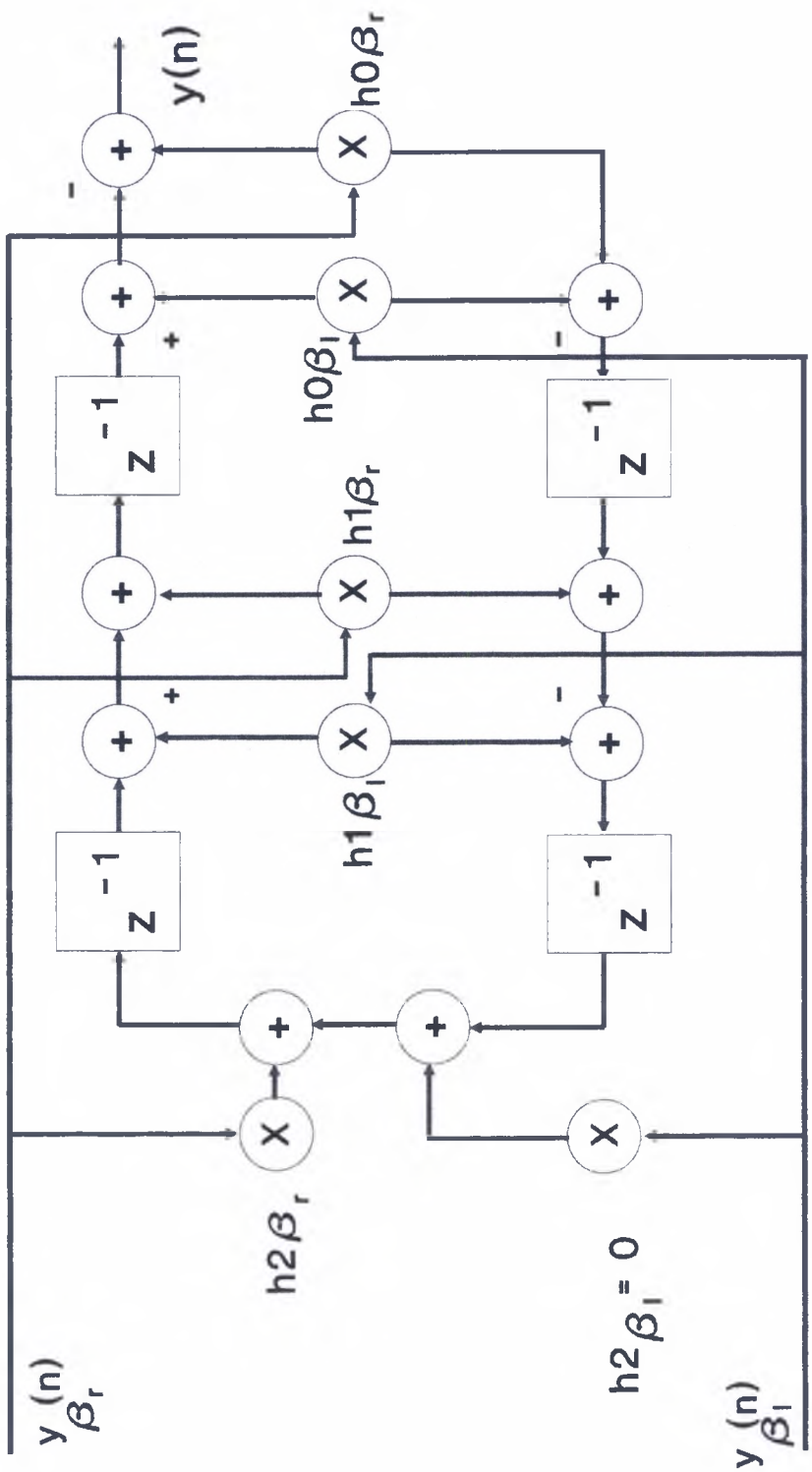

Fig 3.20 Implementation of Section II.

shows the FORTRAN-77 code that implements the bandpass filter structure of figure 3.12.

3.3.5 Approximation Error Considerations

If $\delta_{\mu p}$ and $\delta_{\beta p}$ are the passband approximation errors of the masking and base filters respectively and $\delta_{\mu s}$ and $\delta_{\beta s}$ the corresponding errors in the stopbands of these filters, then the worst case error the designer must face is given by

$$\varepsilon = \delta_{\beta p} + \delta_{\mu p} + \delta_{\beta p} * \delta_{\mu p} + \delta_{\mu s} + \delta_{\mu s} * \delta_{\beta p}$$

or desregarding the smallest or product terms

$$\varepsilon = \delta_{\beta p} + \delta_{\mu p} + \delta_{\mu s} \qquad \textbf{(eq. 3.9)}$$

where the absence of the error in the stopband of the base filter is noted. This error can be made as high as the desired error, whereas all the other error specifications in equation 3.9 could be made approximately half the desired errors to roughly achieve the needed specifications; that is, if δ is the desired error in the approximation, then the subfilter errors are selected such that $\delta_{\beta p} = \delta_{\mu p} = \delta_{\mu s} = \delta/2$ and $\delta_{\beta s} = \delta$. As shown in the sample designs to be considered ahead, this basic rule of thumb shall almost always work very well.

3.3.6 Computational Complexity Considerations

It is quite evident from the presentation above that the computational complexity of the two-branch filtering structure (fig. 3.12)

depends on the complexity of the two lowpass filters: the base filter and the masking filter, that is, the length of the impulse responses of these filters. The total number of multiplies per output sample for this structure is roughly given by

$$TM = N_\beta + N_\mu \qquad \textbf{(eq. 3.10)}$$

and by using equation 3.1, this expression can be written as

$$TM = \frac{\alpha}{\Delta f * I} + \frac{\alpha I}{1 - 2*(\Delta f + \Delta\rho)*I} \qquad \textbf{(eq.3.11)}$$

where α is given by $(\frac{19 - 20\log\delta}{27})$, and the transition bandwidth of the masking filter as indicated in the second term of the above equation is

$$\Delta\mu = \frac{1 - 2*(\Delta f + \Delta\rho)*I}{I} \qquad \textbf{(eq.3.12)}$$

It is important to select the scaling factor I such that the number of multiplies in equation 3.11 is reduced or minimized. This optimization leads to

$$I = \frac{\sqrt{\Delta f} - 2*(\Delta\rho + \Delta f)}{\Delta f - 4*(\Delta\rho + \Delta f)^2} \qquad \textbf{(eq.3.13)}$$

and for very narrow-band filters with no flat top ($\Delta\rho = 0$), this equation reduces to

$$\frac{1}{\sqrt{\Delta f}} - 2 \qquad \textbf{(eq. 3.14)}$$

This equation allows to estimate the interpolating factor, which can then be used to design the base lowpass filter. Figure 3.21a shows a graph of equation 3.1 and equation 3.11, with I given by equation 3.13; or number of unique impulse response samples versus width of transition band for a stopband error $\delta = 0.01$ and $\Delta\rho = 0$. Figure 3.21b depicts the scaling factor as a function of the relative transition bandwidth and it shows that the experimental data is in close agreement with the theory. It is apparent that this design approach is well suited to the implementation of very narrow-band bandpass filters, specially those whose relative transition

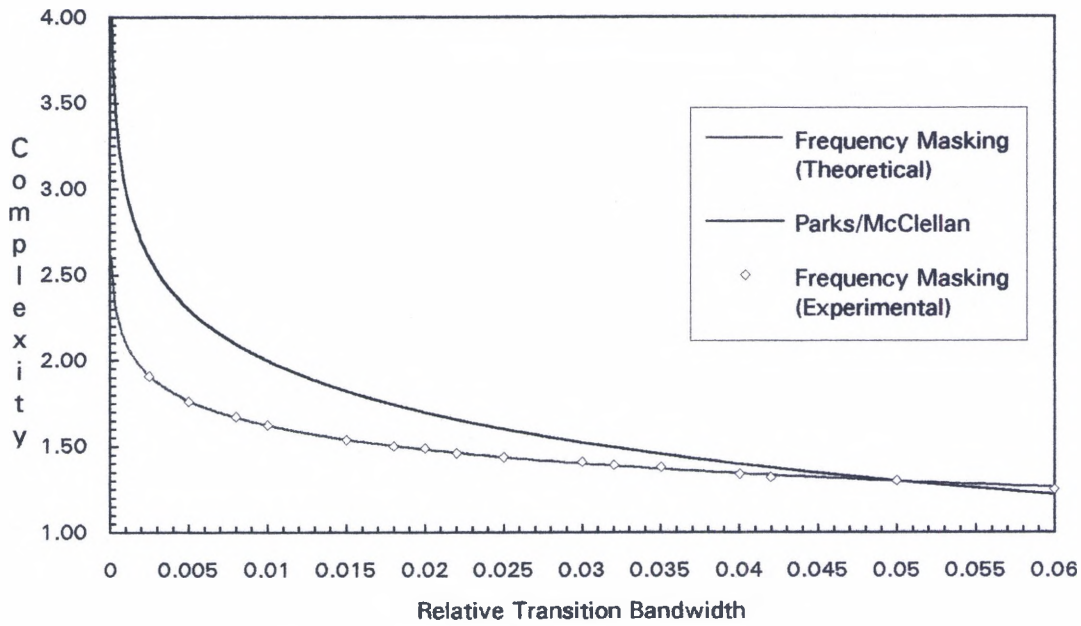

Fig. 3.21a Filter Complexity Curves for Direct and Indirect Methods.

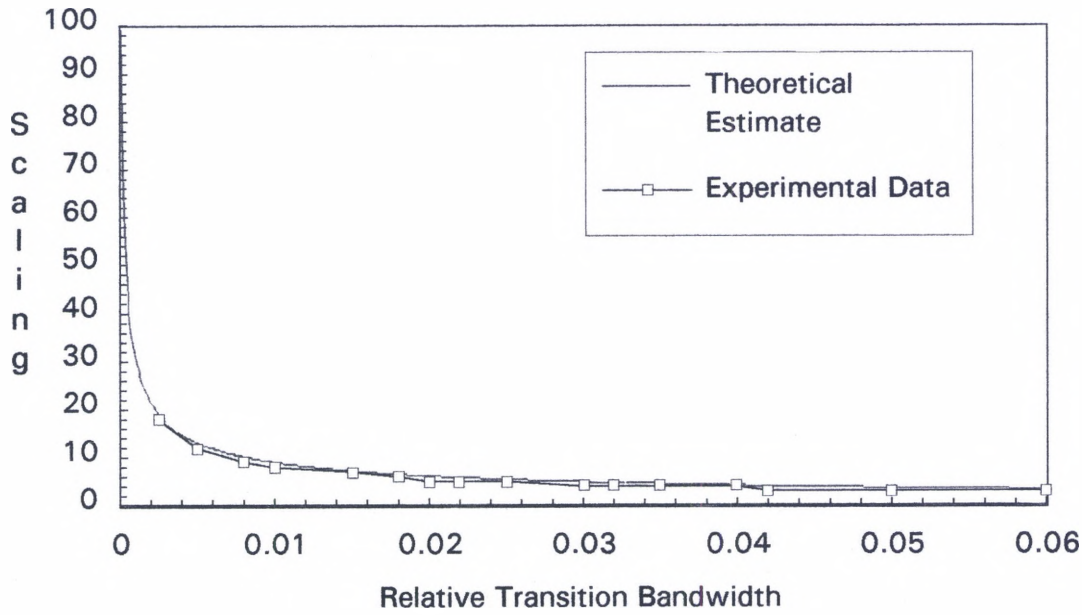

Fig. 3.21b Scaling Factor vs. Relative Transition Bandwidth.

bandwidths are such that $\Delta f << 0.04$, which are very typical of split spectrum processing with polarity thresholding. For transition bandwidths wider than this, the direct application of Parks/McClellan to the design of the band pass filter may be preferable.

3.3.7 The Design Procedure

The steps towards the design of the bandpass filter by the two-branch structure is very simple and can be summarized as follows:

I. From the given specifications ($\Delta\rho$ and Δf), the scaling or interpolating factor is determined by equation 3.13 or 3.14.

II. The Base Filter is designed with a transition bandwidth of $I*\Delta f$ and a passband width of $I*\Delta\rho$.

III. The Masking Filter is designed with passband cut-off at $f_p = \Delta\rho + \Delta f$ and a stopband cut-off at $f_{stp} = \frac{1 - I*(\Delta\rho + \Delta f)}{I}$. The width of the transition band of this filter is $\Delta\mu = \frac{1}{I - 2*(\Delta\rho + \Delta f)}$. Note that the passband of this filter can be made zero for the design of a very narrow-band filter. The basic filters can be efficiently designed with the program in [14]. The specifications for the errors can be given following the guidelines of equation 3.9. This very simple procedure is used next to experimentally study the numerical complexity of the structure of figure 3.12.

3.3.8 Experimental Verification

Following are a set of sample designs intended to show the application of the above design procedure and to demonstrate the advantages or gains of this method over the direct application of the Parks/McClellan program in [14].

Sample Design I

The specifications for this filter are as follows : the center frequency of the filter is 0.25. The width of the passband $\Delta\rho = 0.0$, and the transition bandwidth $\Delta f = 0.005$. The desired passband and stopband error is $\delta = 0.01$ (-40dB). From equation 3.14, the optimal scaling factor can be estimated and is found to be 12. The stopband cut-off frequency of the base filter is then 0.06 or 12 times 0.005, and the passband and stopband

cut-off frequencies of the masking filter 0.005 and 0.078 respectively. The error in the stopband of the base filter is set to 0.01 and the remaining errors are set to 0.005 to design this bandpass filter. The program in [14] is used in the design of these filters. Figures 3.22a and 3.22b show the resulting frequency response of the filter. The masking filter required 30 taps or multipliers for its implementation, whereas the base filter needed 29 leading to roughly 59 multiplies per output sample. The direct approach would have required about 160 multiplies per output sample. This represents a savings of about 63%. The specifications are met or surpassed by following this approach; however, it may be necessary to play with the errors in the approximation to get the best possible or lowest complexity filter.

Sample Design II

This time a bandpass filter with a transition bandwidth Δf of 0.02 and a passband width of $\Delta\rho = 0.0$ and desired approximation error of 0.01 in both passband and stopband is desired. The optimal scaling factor is readily estimated at $I = 5.5$ by equation 3.13 and is rounded up to 6. The stopband cut-off frequency of the base filter is then 6 times 0.02 or 0.12 and the passband and stopband cut-off frequencies of the masking filter are 0.02 and 0.146. The errors of the individual filters are selected as before to meet the given specifications. This gives a base filter requiring 15 multipliers and a masking filter of 20 multipliers for a total multiply count of 35 per output sample. The resulting filter is shown in figures 3.23a and 3.23b. If the scaling factor had been selected to be 5, the

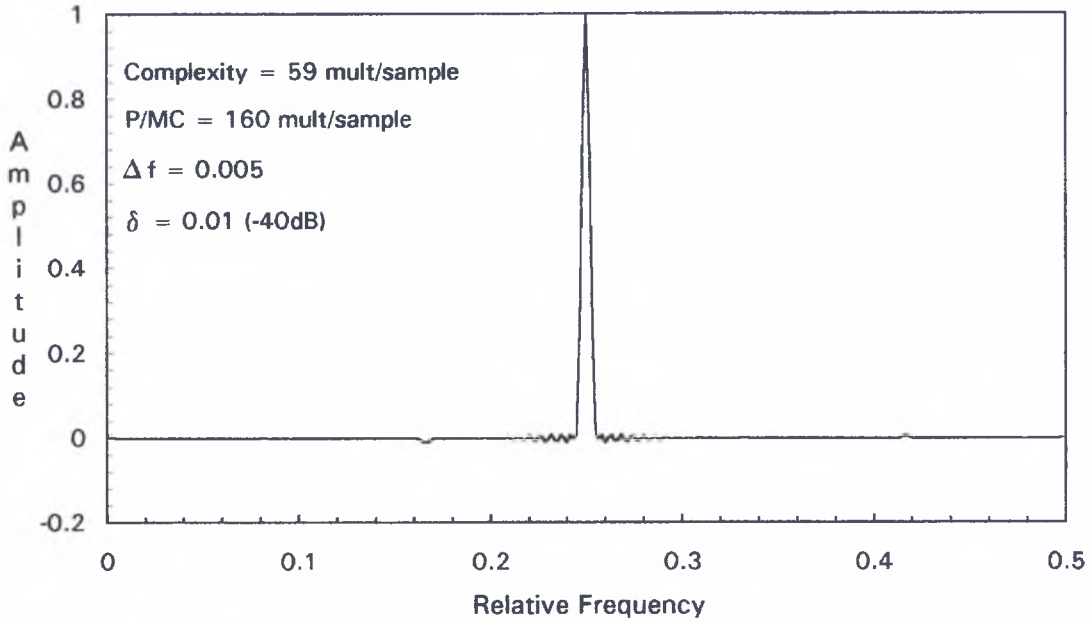

Fig. 3.22a Frequency Response for Very Narrow BP Filter. Sample Design I.

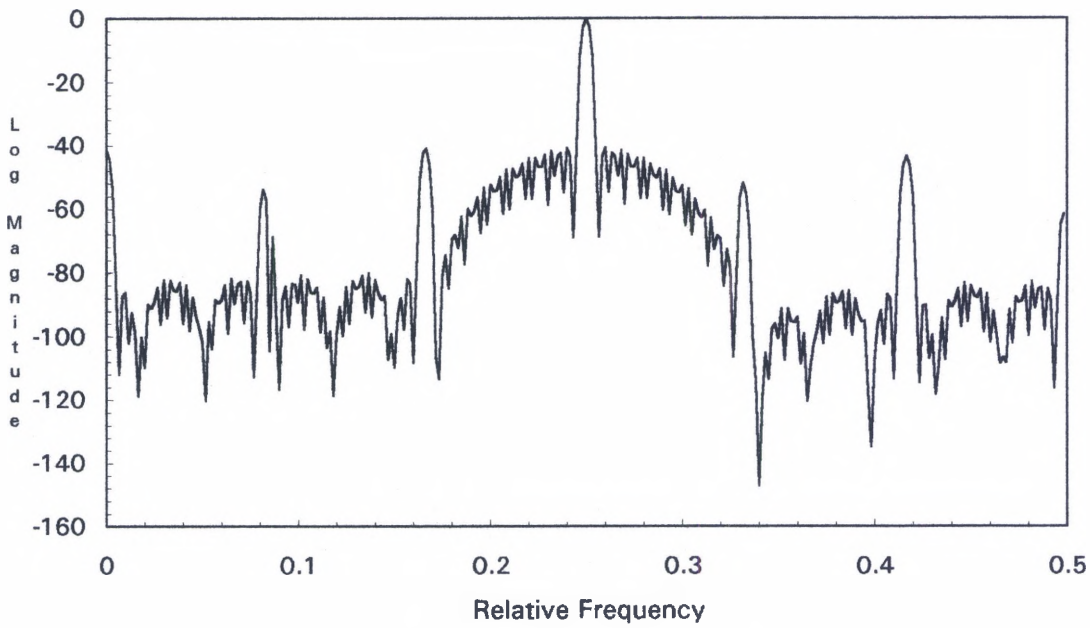

Fig. 3.22b Log Magnitude Frequency Response of Filter. Sample Design I.

overall multiply count would have been only 31. This shows that the equations above only give approximate optimal values and that some trail and error work may be needed. The direct approach would need 43 multiplies per output sample or 28% more.

Sample Design III

For this particular design, a transition bandwidth $\Delta f = 0.04$, very close to the crossover frequency in figure 3.21, has been selected. As before, the passband has been set to zero ($\Delta\rho = 0.0$) and the approximation error δ is set to 0.01(-40dB). With these specifications, the interpolating factor turns out to be 4 and the base and masking filters have lengths of 11 and 10 respectively, for a net filter of 21 multiplies per output sample. The direct approach would have required 22 multiplies per output sample which makes the two approaches roughly the same. This filter's amplitude and log magnitude frequency responses are shown in figure 3.24. Other sample designs are shown in figures 3.25, 3.26 and 3.27. These filters are rather sharp; the one in figure 3.25 requires about 76% more multiplication per output sample than the indirect approach, the one in figure 3.26 requires 62.5% more and the one in figure 3.27 42% more. These last three filters are the same, though they may appear different, only the sampling rates differ. The filter of fig. 3.26 has a sampling rate half as high as that of the filter of fig. 3.25, and the filter of fig. 3.27 has a sampling rate one fourth as high. Note that the complexities of the filters are not in inverse proportion to the sampling rates.

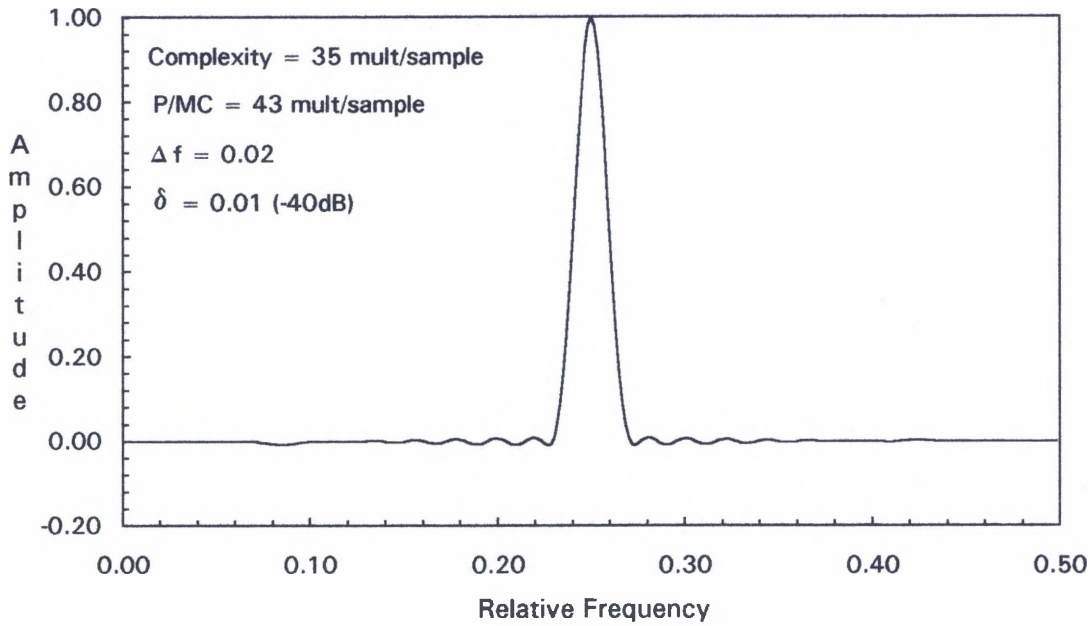

Fig. 3.23a Amplitude Frequency Response of Filter of Sample Design II.

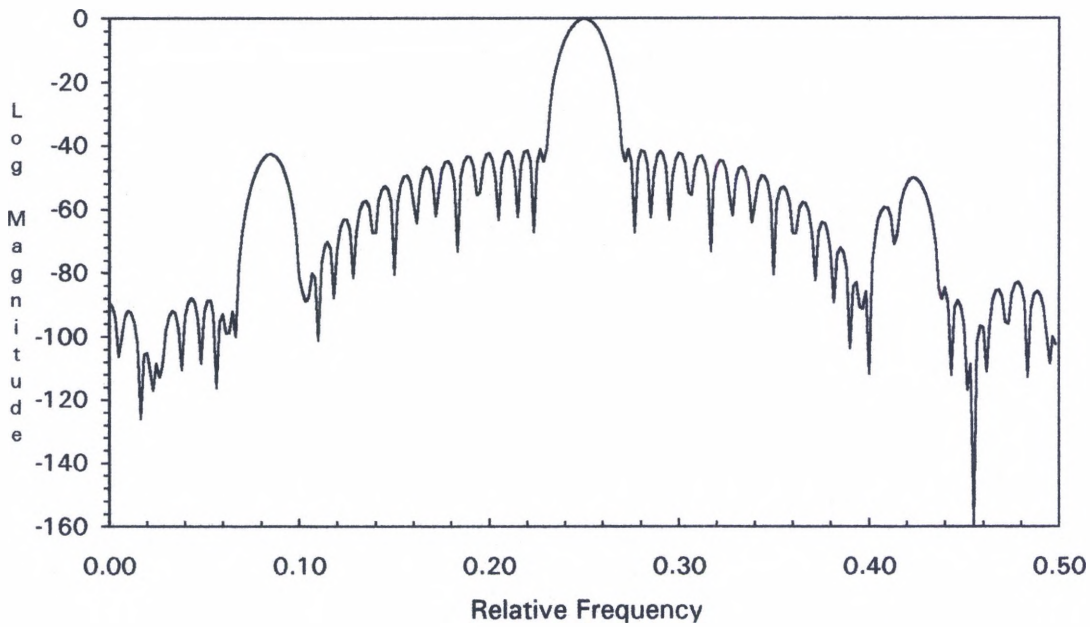

Fig. 3.23b Log Magnitude Response of Filter of Sample Design II.

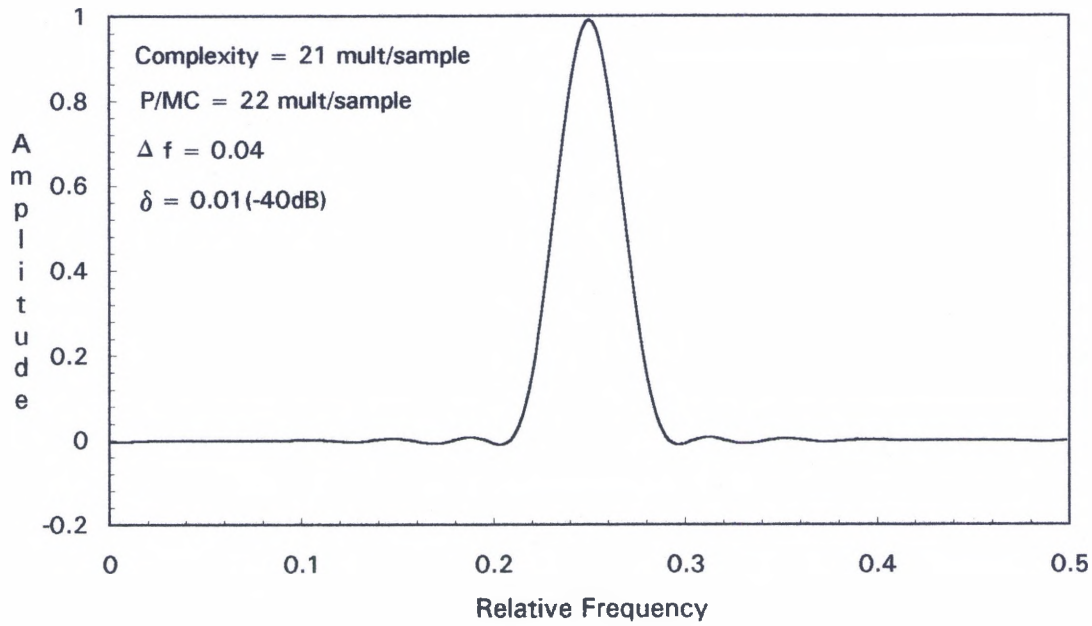

Figure 3.24a Amplitude Frequency Response of Filter of Sample Design III.

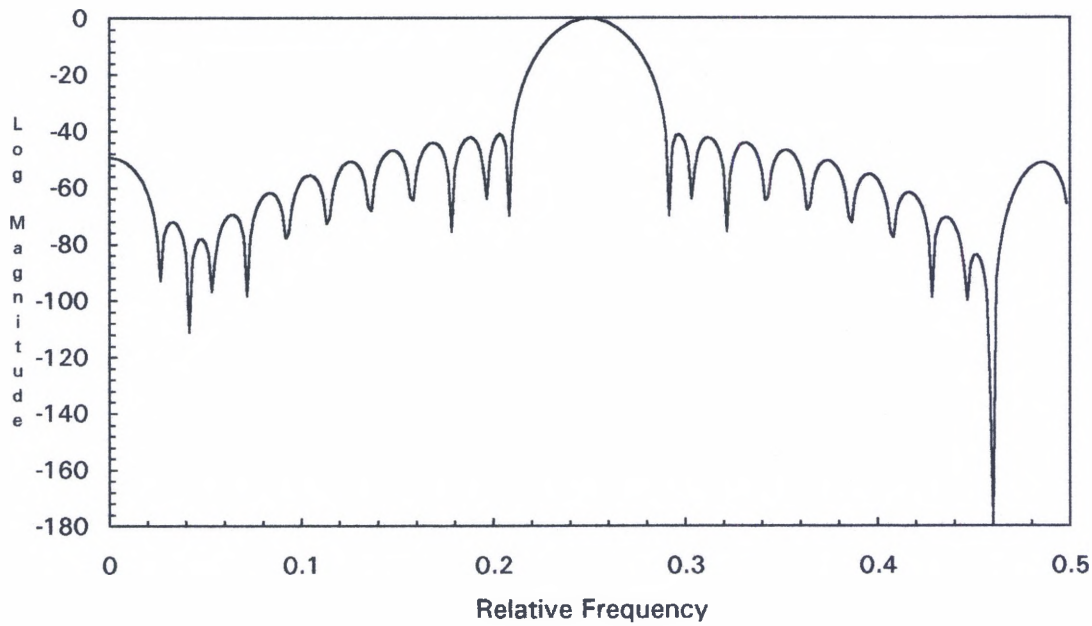

Figure 3.24b Log Magnitude Response of Filter of Sample Design III.

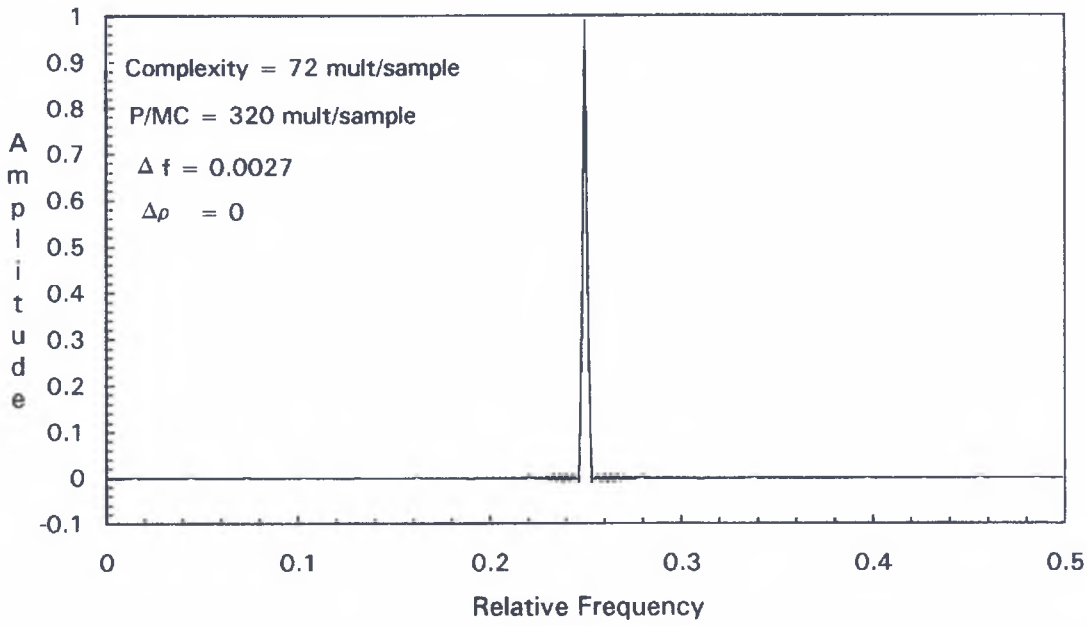

Fig. 3.25a Amplitude Frequency Response of a Sample Filter.

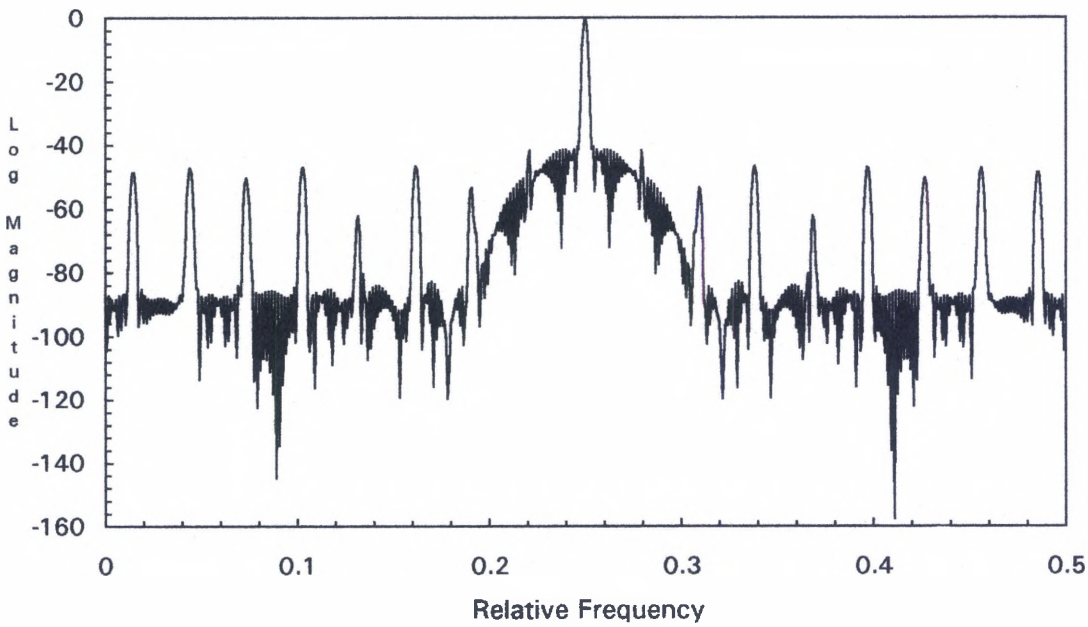

Fig. 3.25b Log Magnitude Frequency Response of a Sample Filter.

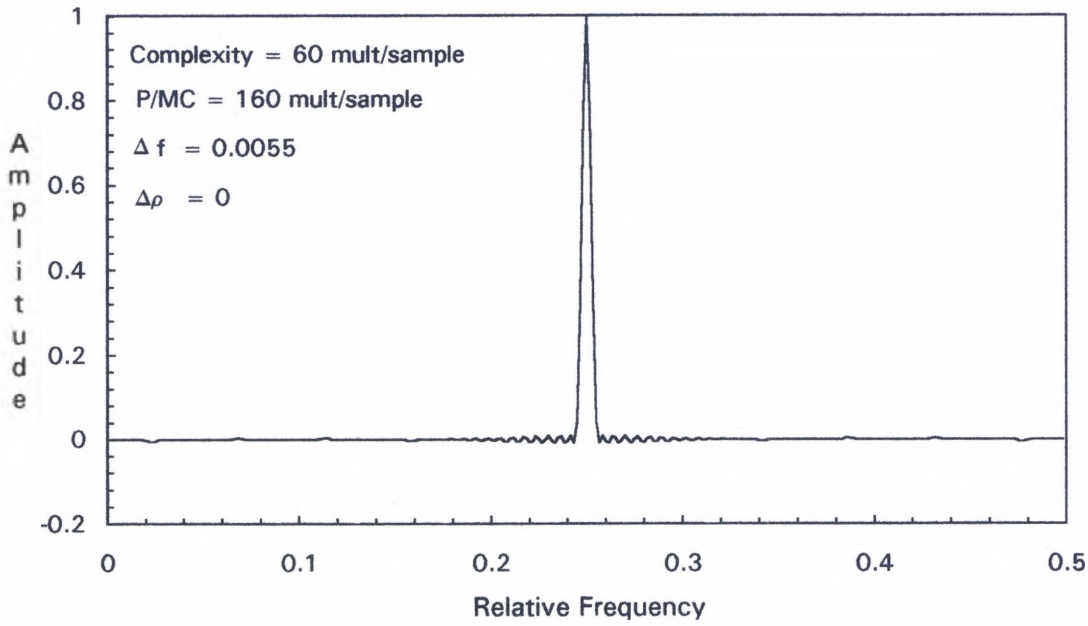

Fig. 3.26a Amplitude Frequency Response of a Sample Filter.

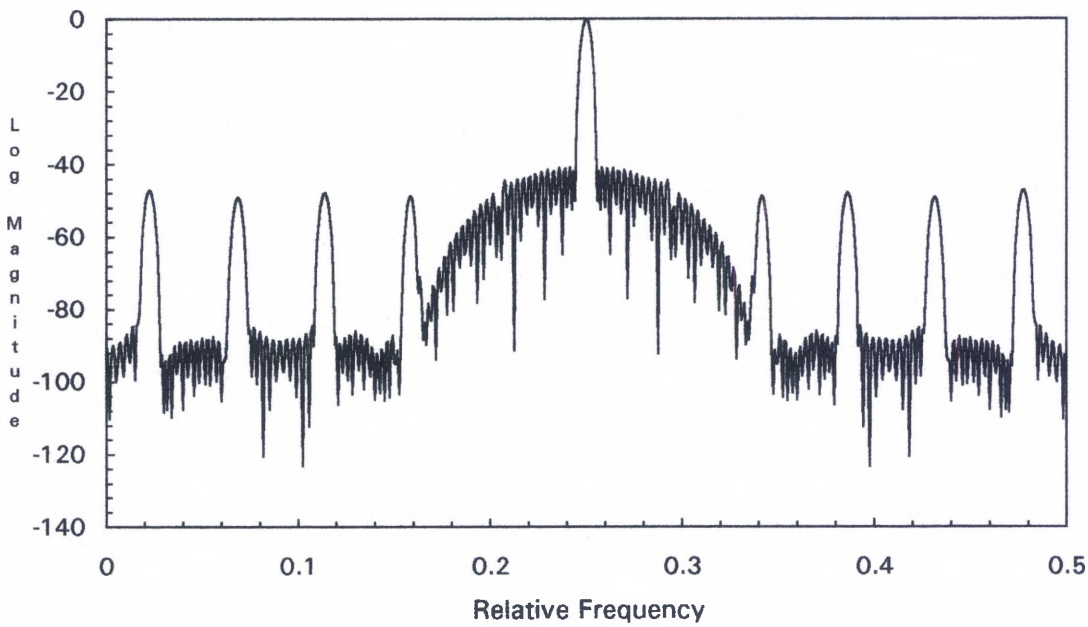

Fig. 3.26b Log Magnitude Frequency Response of a Sample Filter.

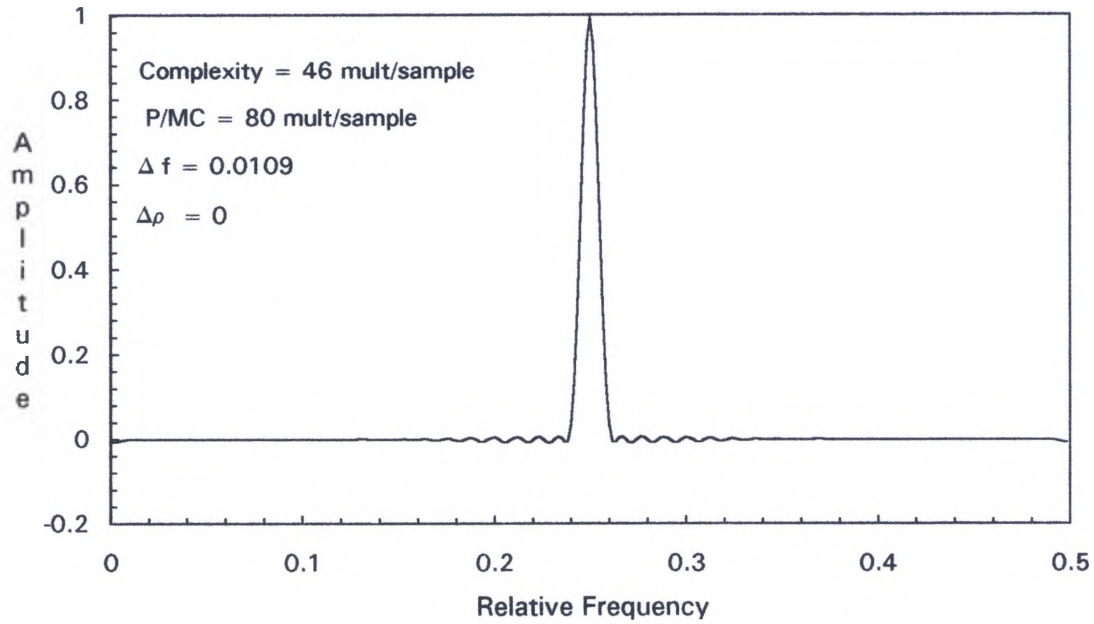

Fig. 3.27a Amplitude Frequency Response of a Sample Filter.

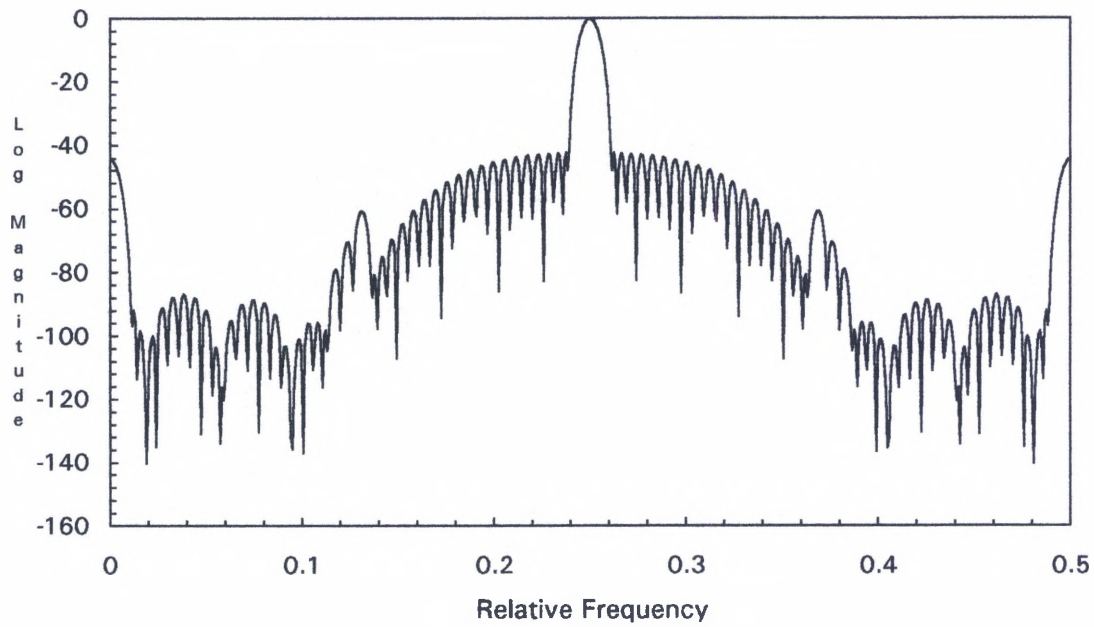

Fig. 3.27b Log Magnitude Frequency Response of a Sample Filter.

Designing filters with relative transition bandwidths greater than 0.04 in the indirect fashion presented here will not provide a computational advantage over the direct approach. For instance, a filter with a relative transition bandwidth of 0.06 shall require only 15 multiplies per output sample with the Parks/McClellan program[14], whereas a similar filter designed with the structure above would require 18. In the design examples above, the filters exhibited no flat tops ($\Delta\rho = 0$), as in the conventional SSP Gaussian filters. Increasing the size of the passband (assuming a fixed sharp Δf) will simply make the net filter computationally more complex since a non-zero passband will take up some of the space available to the relative transition bandwidths of the base and masking filters; that is, as the filter becomes wider, its complexity approaches that of the direct approach filter. However, as long as the relative transition bandwidth of the desired bandpass filter remains below 0.04, as shown in figure 3.21, and its passband width is small enough, the bandpass filter design approach of the previous section shall provide a simpler filter. To estimate the narrowness of the desired filter, compute the scaling or interpolating factor and make sure that it is, at least, as great as four. Consider now the design of other filters which exhibit a flat-top passband.

Sample Design IV

This filter shall have a passband with $\Delta\rho = 0.0023125$ and a transition bandwidth $\Delta f = 0.0086875$. The desired error $\delta = 0.01$ (-40dB) in both bands. The scaling factor is 8; the resulting base filter has 31 taps, and the masking filter has 18 for a total count of 49 taps. The direct

approach would have required about 130 distinct multipliers (62% more). Figures 3.28 display both responses for this particular filter.

Sample Design V

The specifications are as follows : $\Delta\rho$ = 0.0025, Δf = 0.0065 and δ = 0.01 in both bands. The result is the filter of figure 3.29 with a total multiply count of 66 multiplications per output sample (Base 35 taps/ Mask 31 taps) as opposed to 130 for the direct approach (49% more).

Sample Design VI

The specs are as follows : $\Delta\rho$ = 0.005, Δf = 0.01 and δ = 0.01 in both bands. The result is the filter of figures 3.30 with a total multiply count of 52 multiplications per output sample (Base 34 taps and Mask 18

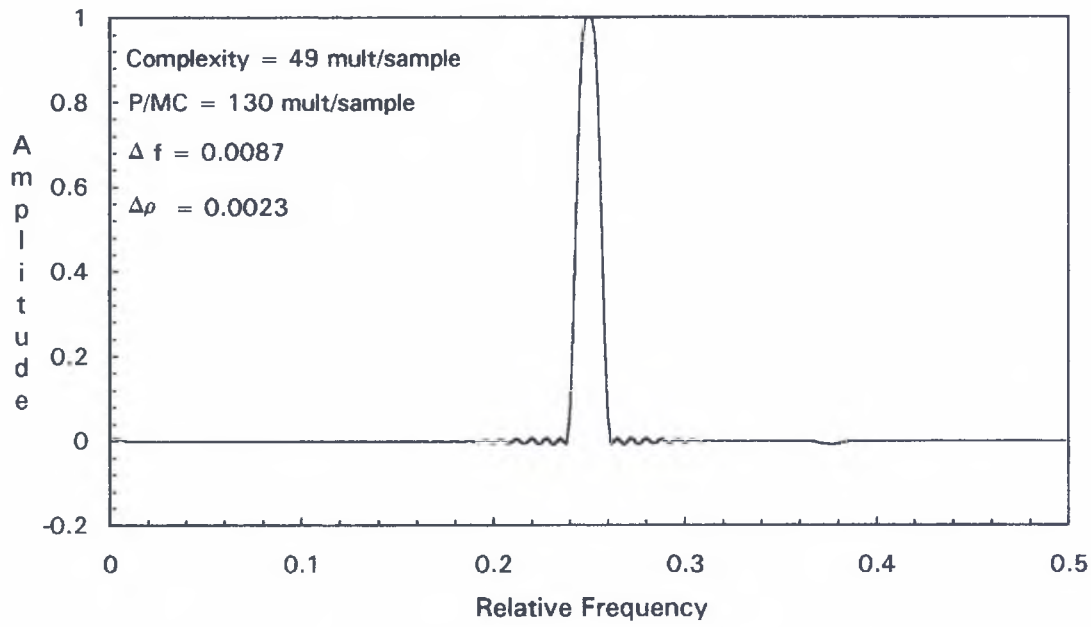

Fig. 3.28a Amplitude Frequency Response of Filter of Sample Design IV.

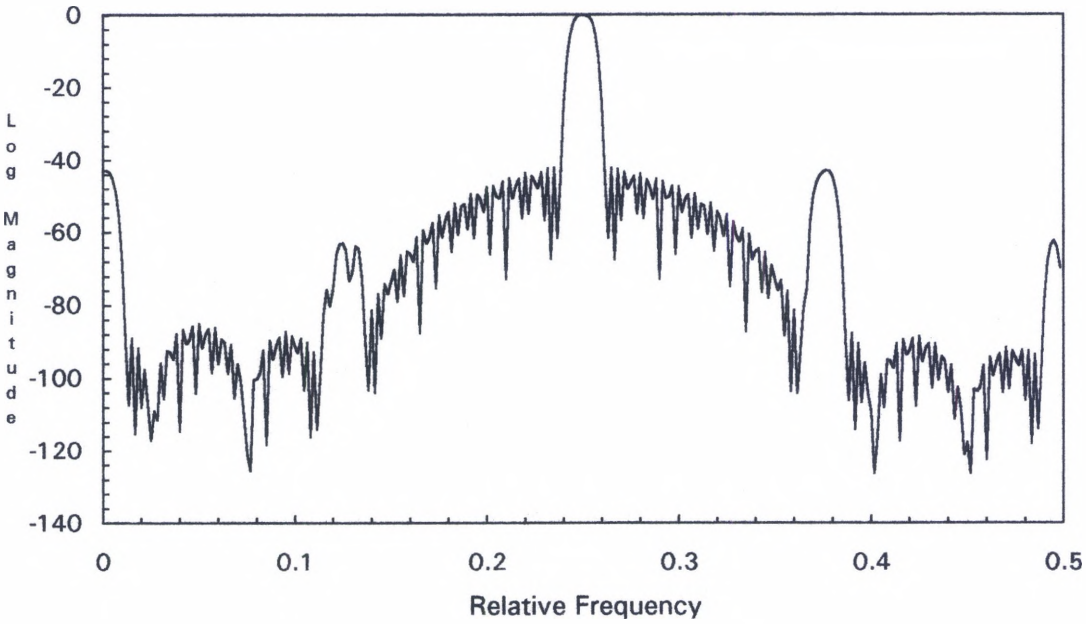

Fig. 3.28b Log Magnitude Response of Filter of Sample Design IV.

taps), as opposed to 90 with the direct approach (42 % more).

Other filters with flat tops are shown in figures 3.31 and 3.32 and in the first instance, Parks/McClellan takes about 45% more, whereas in the second case it takes some 43% more. The designs above show that there are advantages or gains of the two-branch structure over the direct approach for narrow-band bandpass filters.

Even though they appear different, these last two filters are essentially the same, the second filter was designed for a sampling rate half as great as that of the first, which makes the relative transition of the second twice as wide and therefore less complex to implement. Note that doubling the sampling rate does not mean doubling the complexity of the

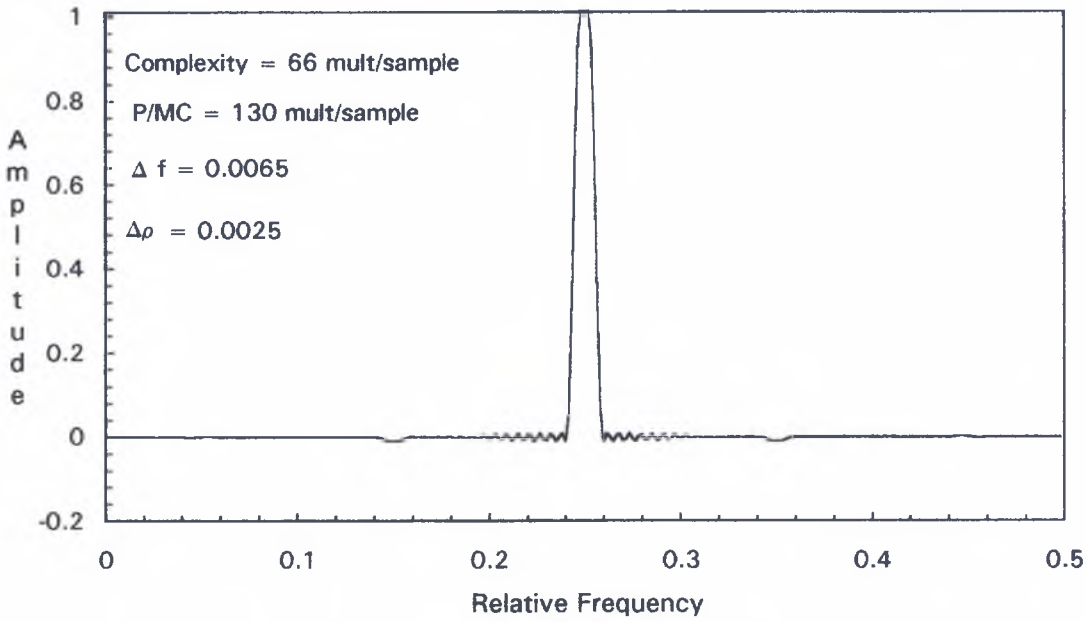

Fig. 3.29a Amplitude Frequency Response of Filter of Sample Design V.

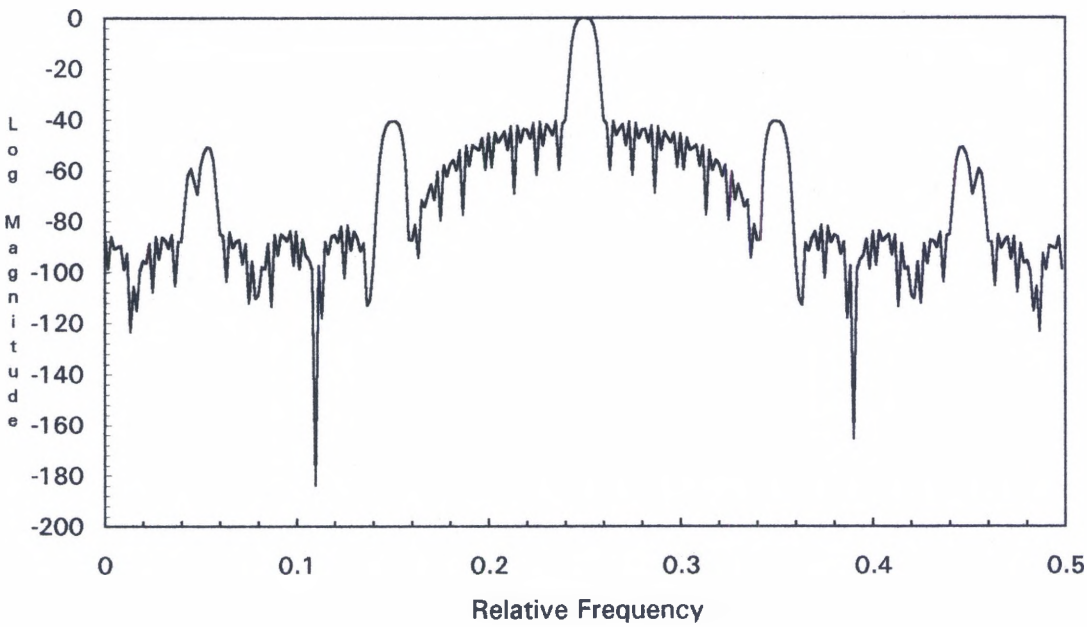

Fig. 3.29b Log Magnitude Response of Filter of Sample Design V.

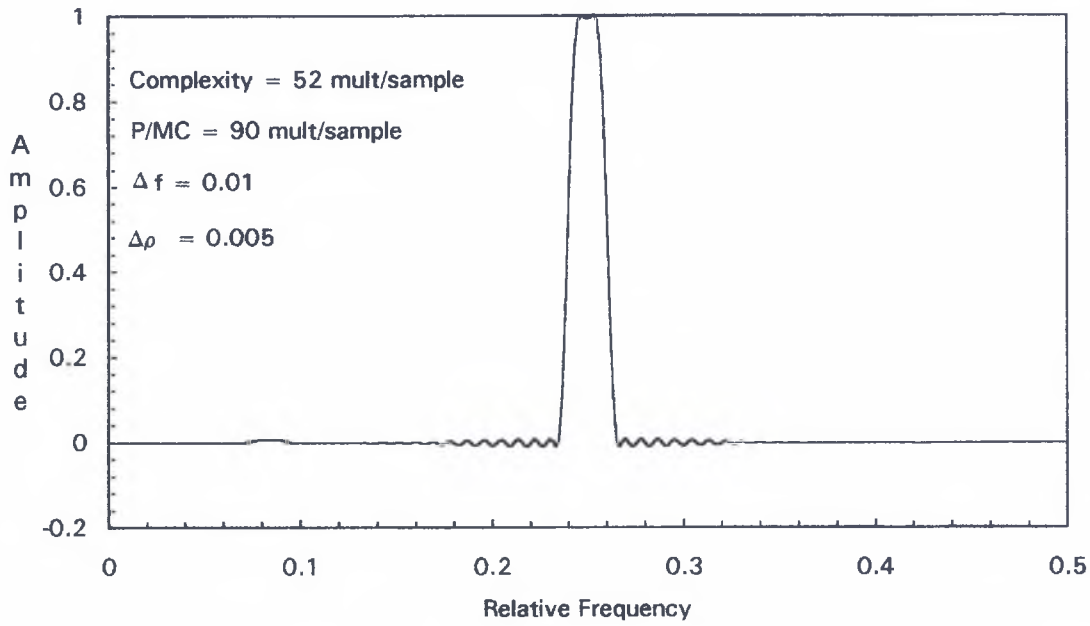

Fig. 3.30a Amplitude Frequency Response of Filter of Sample Design VI.

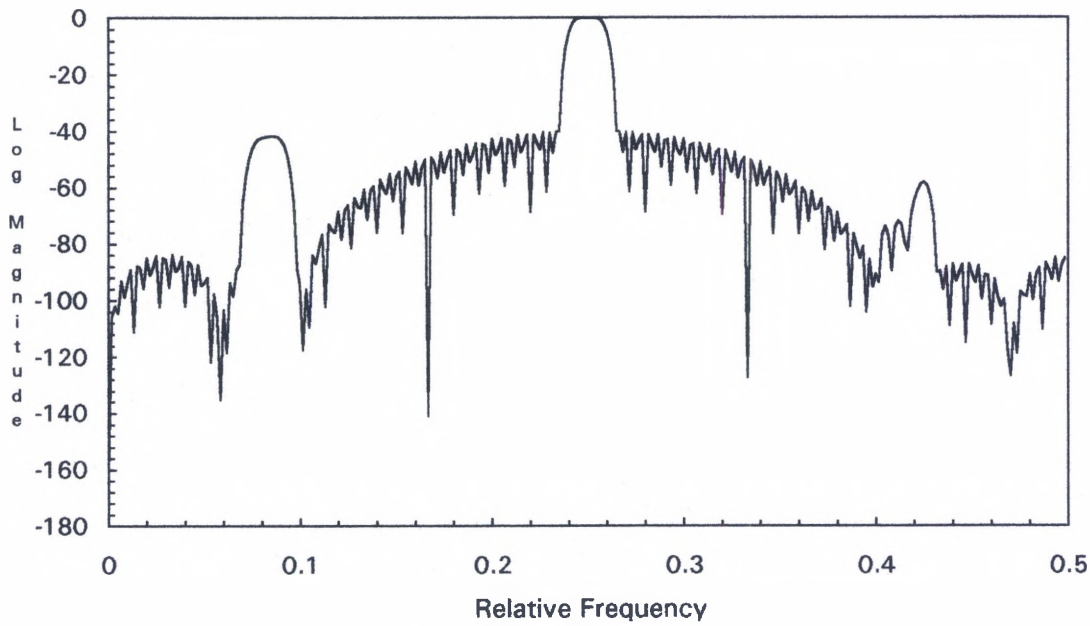

Fig. 3.30b Log Magnitude Response of Filter of Sample Design VI.

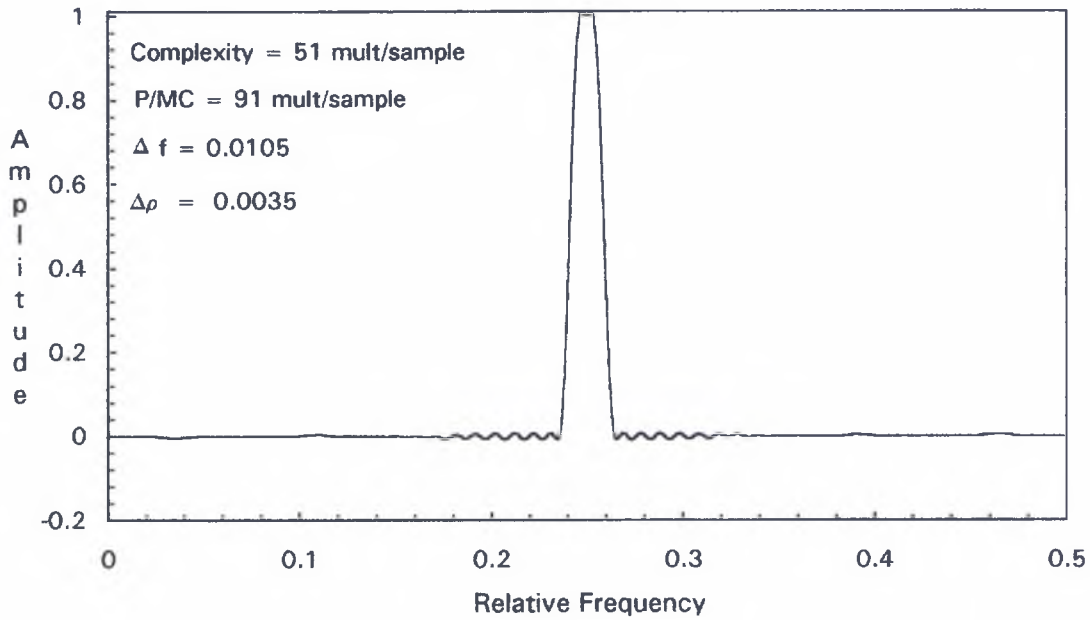

Fig. 3.31a Amplitude Frequency Response of Sample Narrow BP Filter.

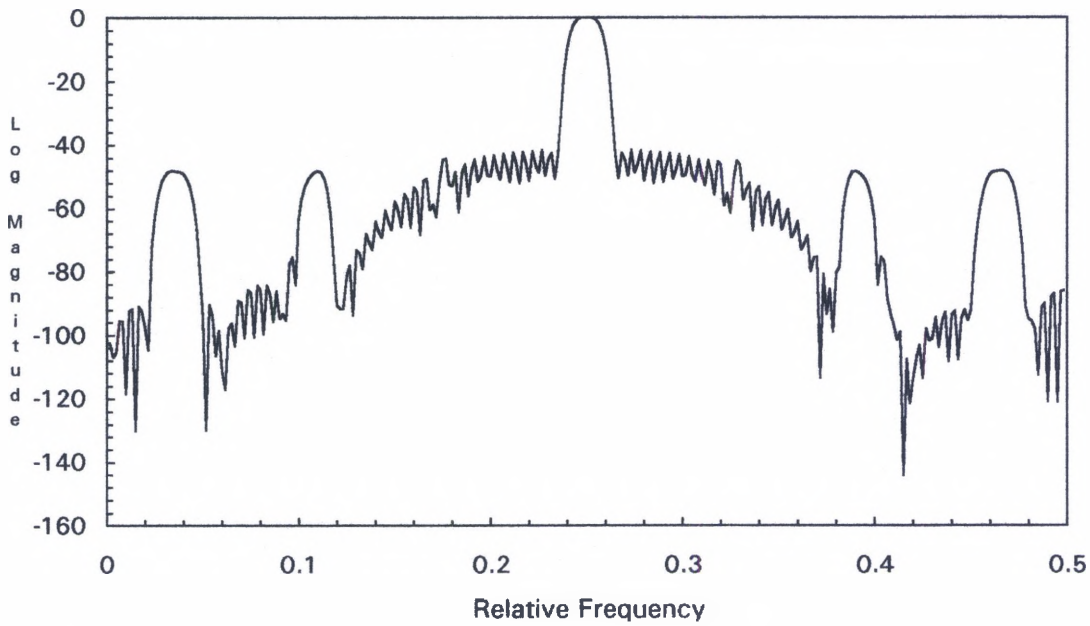

Fig. 3.31b Log Magnitude Response of Sample Narrow BP Filter.

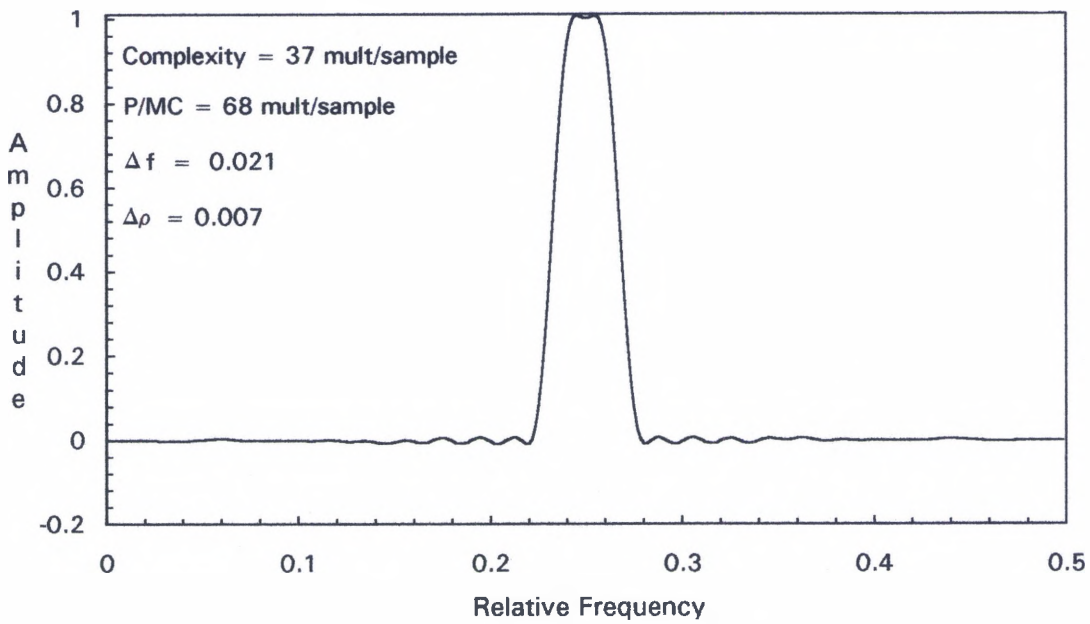

Fig. 3.32a Amplitude Frequency Response of Sample Narrow BP Filter.

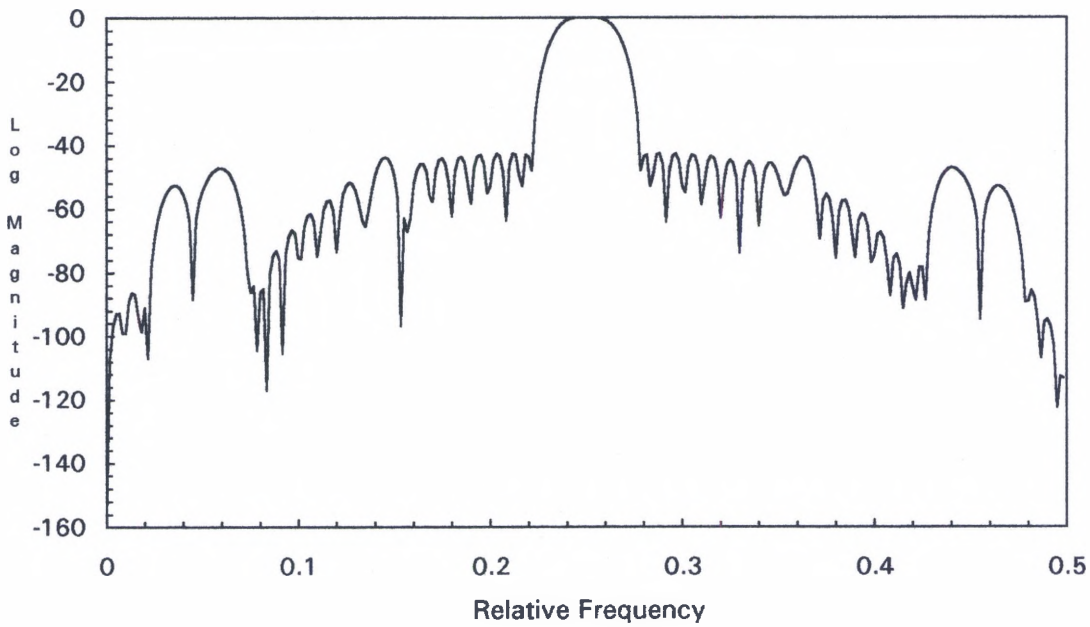

Fig. 3.32b Log Magnitude Response of Sample Narrow BP Filter.

filter, as in the direct approach, since the complexity is not in inverse proportion to the relative transition bandwidth but rather to $\sqrt{\Delta f}$ as indicated in equation 3.14. The following table gives a summary of the designs presented here, highlighting filter specifications and a comparison between the direct approach, or Parks/McClellan method, and the method described in this chapter.

Table 1. Complexity Comparison Between Direct and Indirect Methods.

Design	Transition Bandwidth	Passband Width	Two-Branch Structure	Parks and McClellan	Percent Improve-ment.
1	0.005	0.0	59	160	63
2	0.02	0.0	31	43	28
3	0.04	0.0	21	22	4.5
4	0.0027	0.0	72	320	76
5	0.0055	0.0	60	160	62.5
6	0.0109	0.0	46	80	42
7	0.0087	0.0023	49	130	62
8	0.0065	0.0025	66	134	50
9	0.01	0.005	52	90	42
10	0.0105	0.0035	51	91	44
11	0.021	0.007	37	68	45.5
12	0.01	0.005	85	150	43

3.4 Application of the Two-Branch Structure to Split Spectrum Processing

Let us now proceed to process ultrasonic signals previously encountered in Chapter II of this work by implementing the digital bandpass filtering with the structure of the preceding section. The digital filters designed here for such purpose have an approximation error δ of roughly 0.01(-40dB) in both passband and stopband so as to not adversely affect SNR performance, as suggested by figure 3.33, which shows how SNR performance deteriorates with increasing error in the approximation to the filter's frequency response. Consider, as a first example, the ultrasonic signal of figure 2.5 of duration $T = 25.6\ \mu s$. If this signal is processed with a filter bank made up of 26 filters such as the one designed above in sample IV ($\Delta\rho \approx \frac{1}{T}$ and $\Delta f = \frac{4.74}{T}$), which concentrates about 87% of its energy within the HPBW and using the minimization technique, the result is the signal of figure 3.34, which reveals the similar nature of the more generic filter type to that of the RAC filters used in chapter II. For comparison purposes refer to figure 2.10. The total multiply count is substantially less than would be needed in a direct implementation; however, FFT-based convolution would prove much more efficient than this approach; an N-point FFT requires about $\frac{N}{2}\log_2 N$ complex multiplies or $2N*\log_2 N$ real multiplies. The number of multiplies involved in an FFT convolution is then given by

$$M_{fft} = 2N*\log_2 N + N \qquad \textbf{(eq. 3.8)}$$

The FFT algorithm usually demands a power-of-two length sequence to operate on, and in practice it may be necessary to sample at rates higher than the Nyquist rate to prevent the introduction of high frequency harmonics. These two limitations are not exhibited by tapped-delay lines, and a convolution with tapped-delay lines requires a number of multiplications given by $M_{fir} = M_{os}*N$ where M_{os} is the number of multiplies per output sample of the filter. In the application of SSP with a filter bank of size K, and using the polarity thresholding algorithm, the number of multiplies for the FFT and digital filters are given by

$$TM_{fft} = (2N*\log_2 N + N)*K \qquad \textbf{(eq. 3.9)}$$

and

$$TM_{fir} = M_{os}*N*K - (\frac{N}{2})(\frac{K}{2})*M_{os}$$

where the second term comes from the fact that, on average, half the number of samples of the output signal are zero due to polarity reversals between any two samples in different channels and that, on average, these sign reversals will occur in the first half of the filter bank. The above equation reduces to

$$TM_{fir} = \frac{3\ M_{os}*N*K}{4} \qquad \textbf{(eq.3.10)}$$

Minimization would have required the full $M_{os}*N*K$ multiplies and not been so amenable to a real-time scheme for the technique. For the bandpass

filtering structure of the preceding section, M_{os} is given by equation 3.10 above.

As shown above, the polarity thresholding algorithm alone or polarity thresholding and minimization combined lend themselves better to a real-time implementation than minimization alone, since once a sign reversal is found between any two channels or bands in the filtering, the process can be restarted to compute the next output sample thereby bypassing a certain number of filters in the bank for a particular output sample. Also, polarity thresholding and minimization combined are more widely used than minimization alone due to an excellent SNR performance. Therefore, what follows will deal mainly with polarity thresholding.

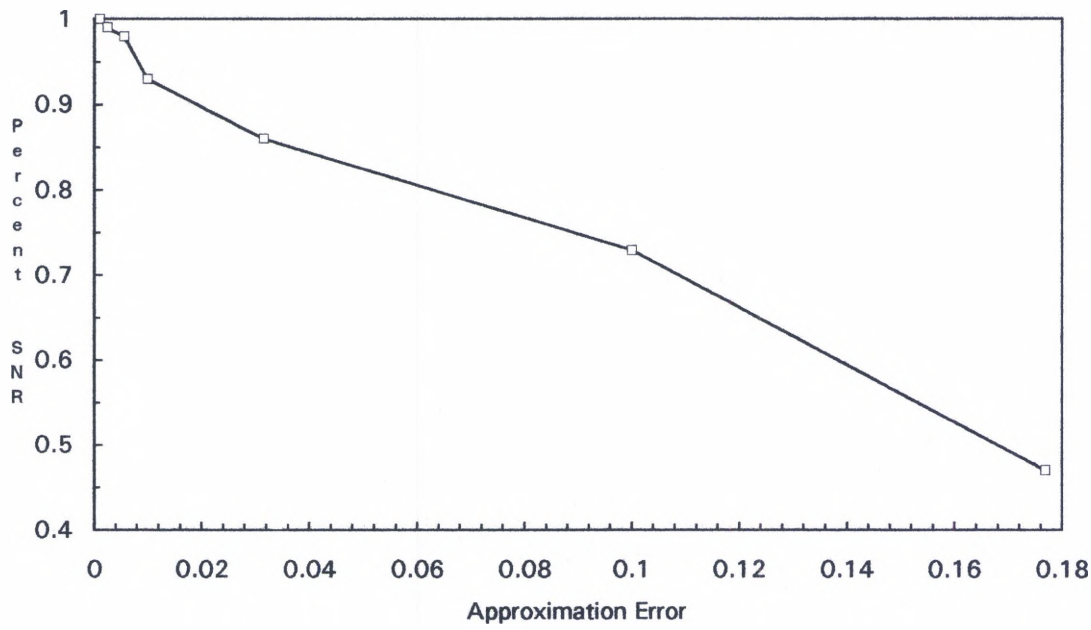

Fig. 3.33 Performance Degradation with Approximation Error δ.

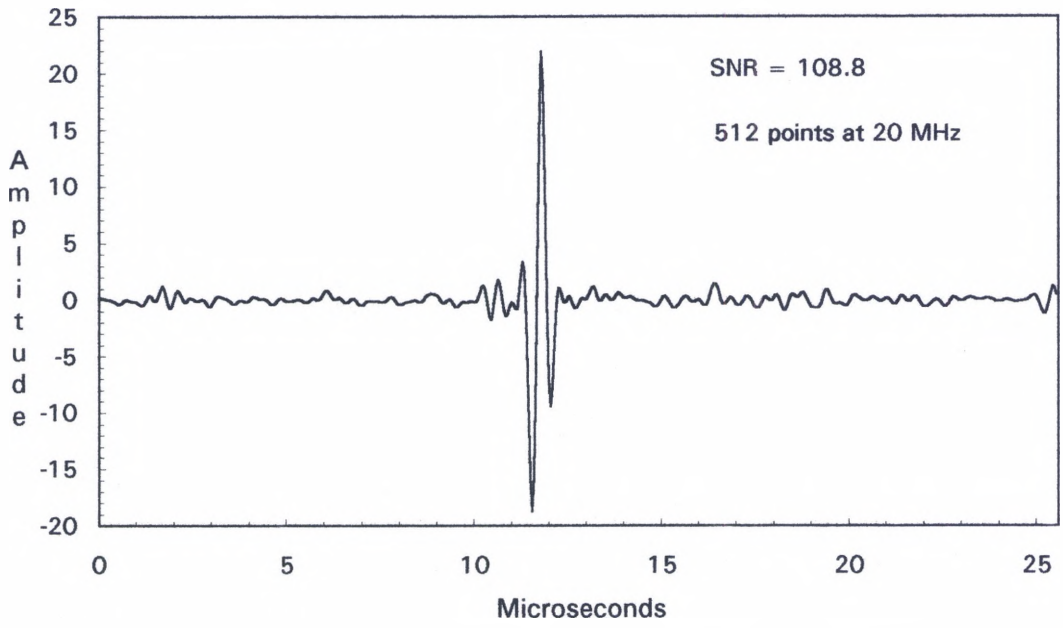

Fig. 3.34 Signal Processed with Two-Branch Filter Structure.

The preceding signal was originally sampled at a rate of 20 MHz which is a rate higher than actually needed to satisfy Nyquist sampling criterion. If this ultrasonic signal is processed with the polarity thresholding and minimization algorithms combined using 26 filters of the type in sample design V (72 multiplies/output sample), the result is the signal of figure 3.35a which shows an excellent view of the target; processing this signal with the same filter shape, but using only 10 filters also yields very good results as shown in figure 3.35b. If the signal is decimated by taking every other sample, the effective sampling rate is then 10 MHz (256 points) and the application of SSP with 10 filters such as the type in sample design VI (52 multiplies/output sample) results in the signal displayed in figure 3.35c clearly revealing the target. Using the 10 MHz sampling rate would lead to

a total multiply count of 99,840 (eq. 3.10), while the FFT approach, with the 20 MHz sampling rate and 26 filters without flat-tops, would require roughly 213,504 multiplies (eq. 3.9) for a similar performance. It is possible to use flat-top filters with the FFT, but FFT-resolution problems of the passband and skirt of the filter may arise that would require the observation time of the signal to be doubled or more for very sharp filters. If that were the case here, 1024 points would be needed and the result would be 205,824 multiplies for the entire 10 filters. This count is still significantly higher than that of the tapped-delay line. This example suggests that it may be possible, in the case a very narrow band filters of the type usually associated with the polarity thresholding algorithm, to improve processing time (over the FFT scheme), by using a tapped-delay line sampling as close as possible to the Nyquist sampling rate.

As another example of sampling-rate reduction, consider now processing the signal of figure 2.18 using the minimization algorithm. If the original 256 points are used (100 MHz) in association with the filter shape of figure 3.31, the result is the signal of figure 3.36a, whereas using only 128 points (50 MHz) in association with the filter shape of figure 3.32 results in the signal of figure 3.36b. Refer to figure 2.22 for comparison purposes. These sampling-rate reduction instances may allow a substantial decrease in the amount of processing that takes place in SSP and also in the amount of data that is stored. When these factors are combined, the appeal of the digital filter structure is quite evident.

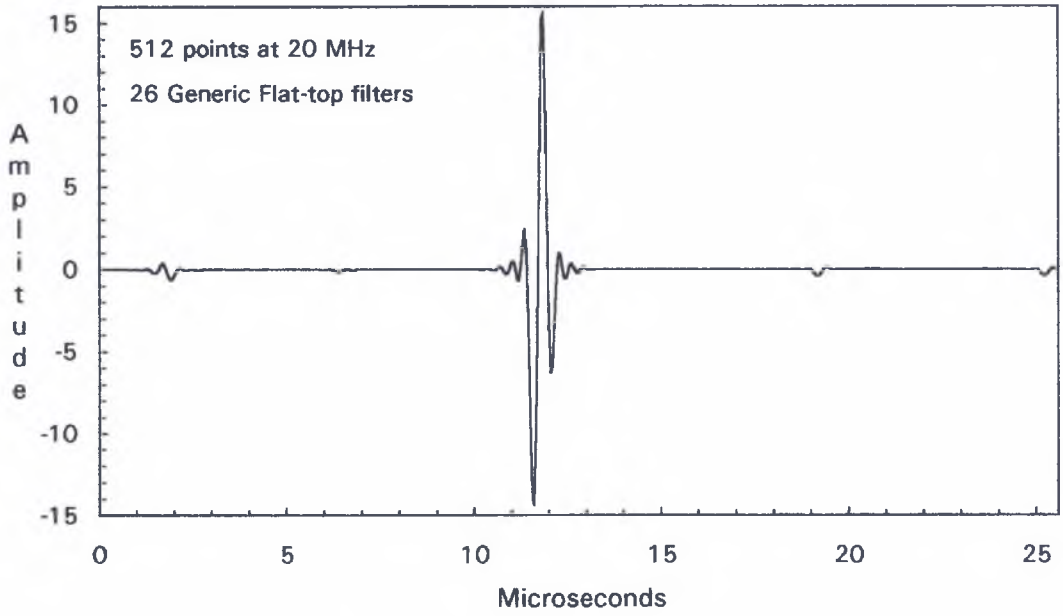

Fig. 3.35a Signal of Fig. 2.5 after Processing(26 Filters. Sample Design V).

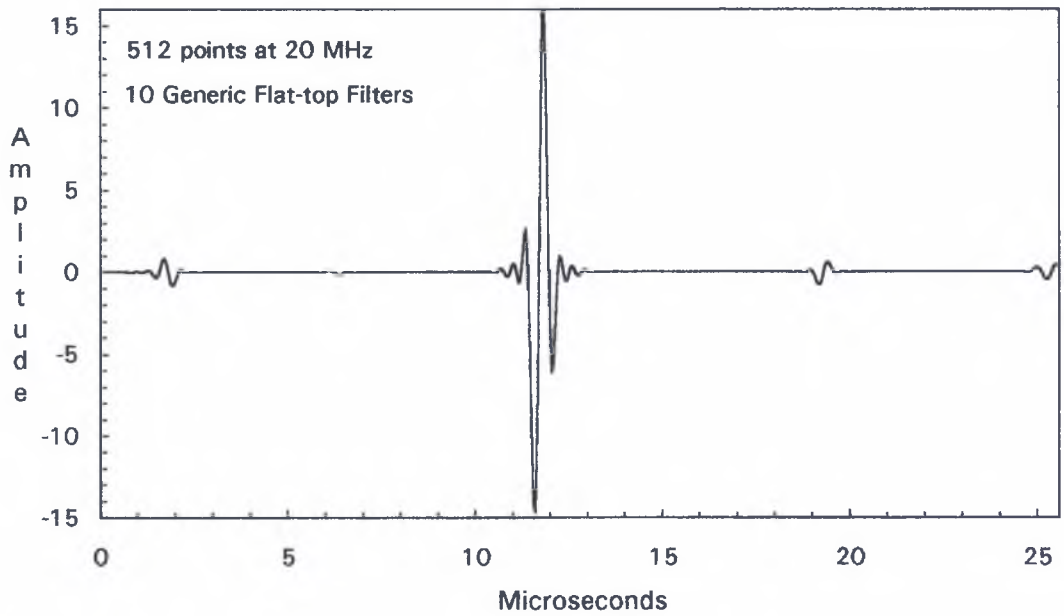

Fig. 3.35b Signal of Fig. 2.5 after Processing (10 Filters. Sample Design V).

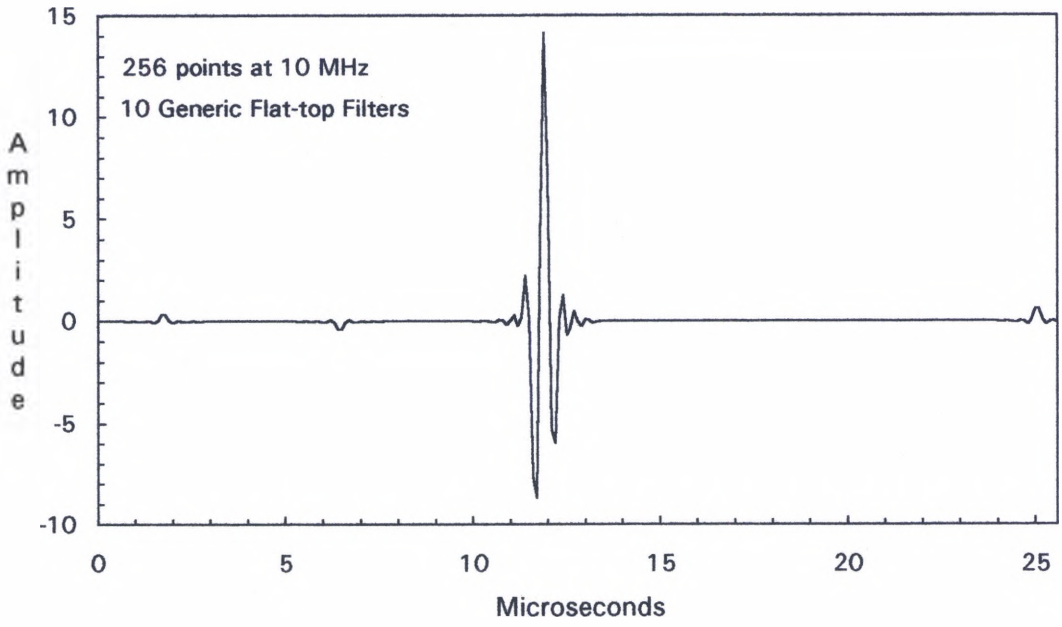

Fig. 3.35c Signal of Fig. 2.5 after Processing (10 Filters. Sample Design V).

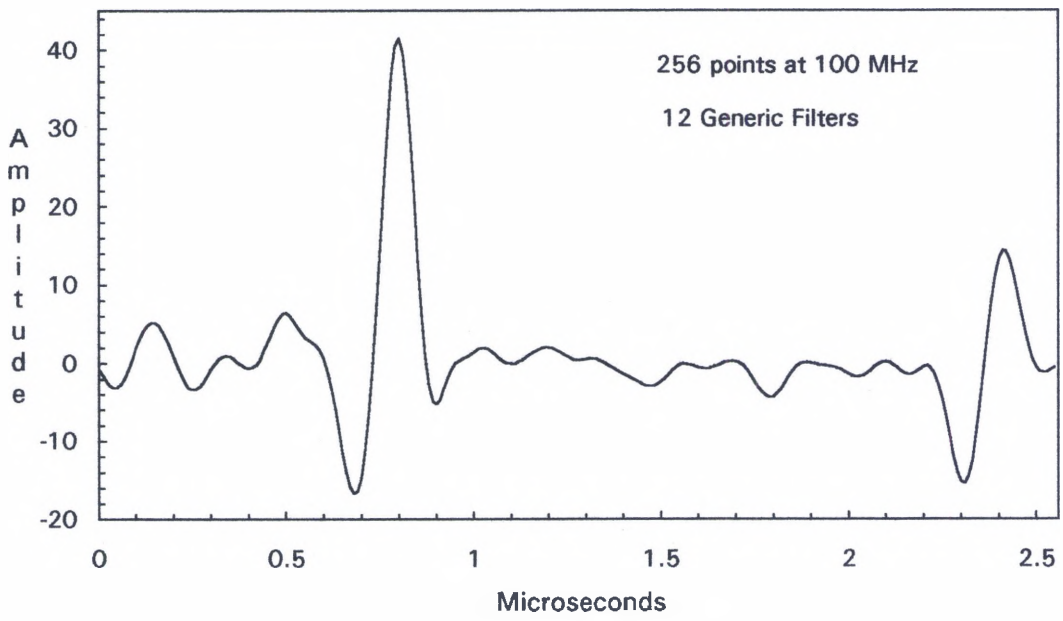

Fig. 3.36a Signal of Fig. 2.18 after Processing with 12 Filters(Fig. 3.31).

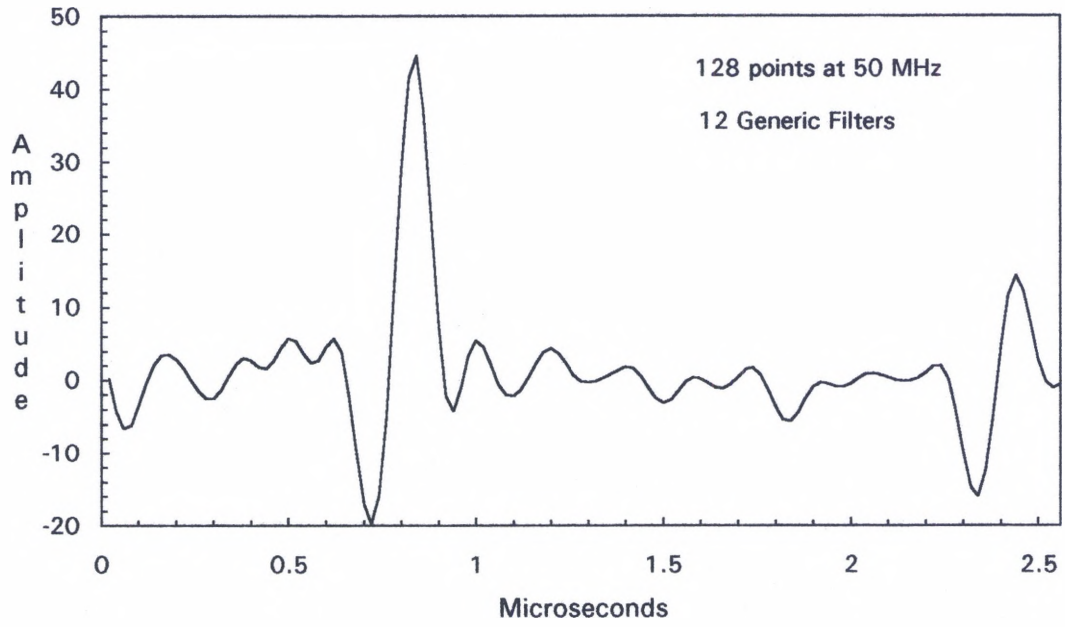

Fig. 3.36b Signal of Fig. 2.18 after Processing with 12 Filters(Fig. 3.32).

As a final example of sampling-rate reduction, consider processing the signal of figure 1.2 which exhibited very high amounts of clutter, using polarity thresholding/minimization. Processing the original signal of 1024 points at 100 MHz with the filter shape of figure 3.25 yields the signal of figure 3.37a, whereas processing at 50 MHz with the filter shape of figure 3.26 produces the signal of figure 3.37b. Finally, processing at 25 MHz yields the output in figure 3.37c. It can be seen that the three output signals provide excellent views of the target present in the clutter and that the computational advantages of processing at the much lower sampling rate are significant. As a matter of comparison, processing this signal with 13 filters at the original rate with the FFT would have taken about 267,264 multiplies for the filtering phase, whereas the tapped-delay line would take

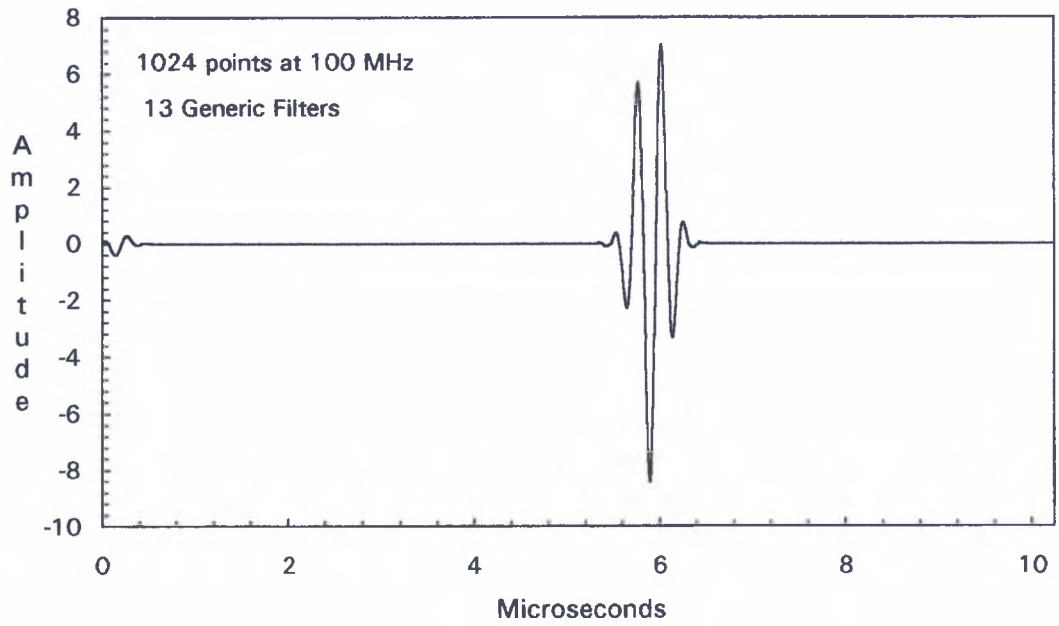

Fig. 3.37a Signal of Fig. 1.2 after Processing with 13 Filters(Fig. 3.25).

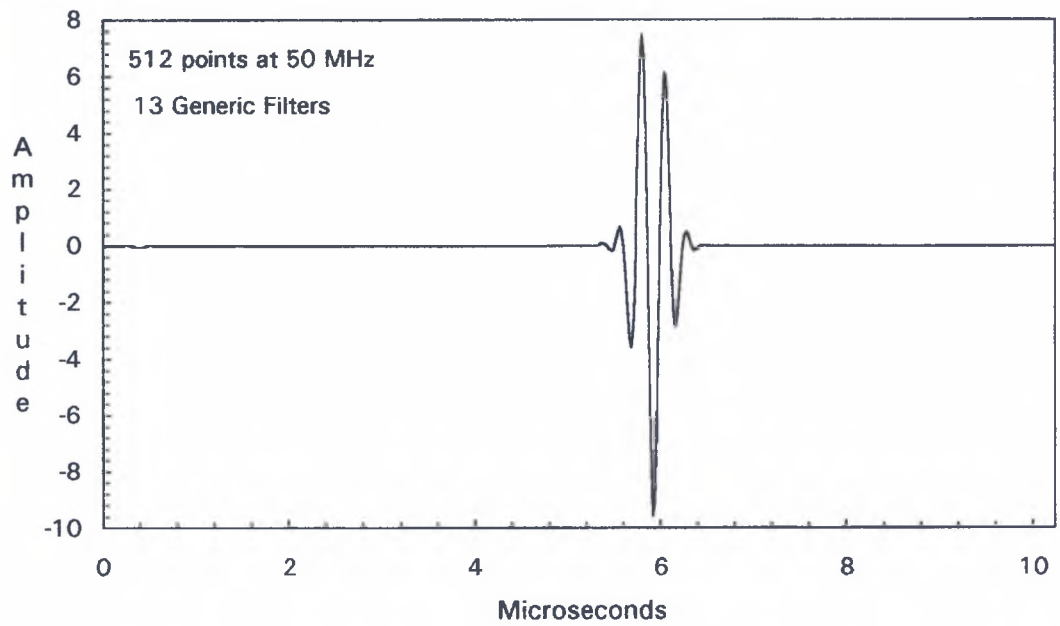

Fig. 3.37b Signal of Fig. 1.2 after Processing with 13 Filters(Fig. 3.26).

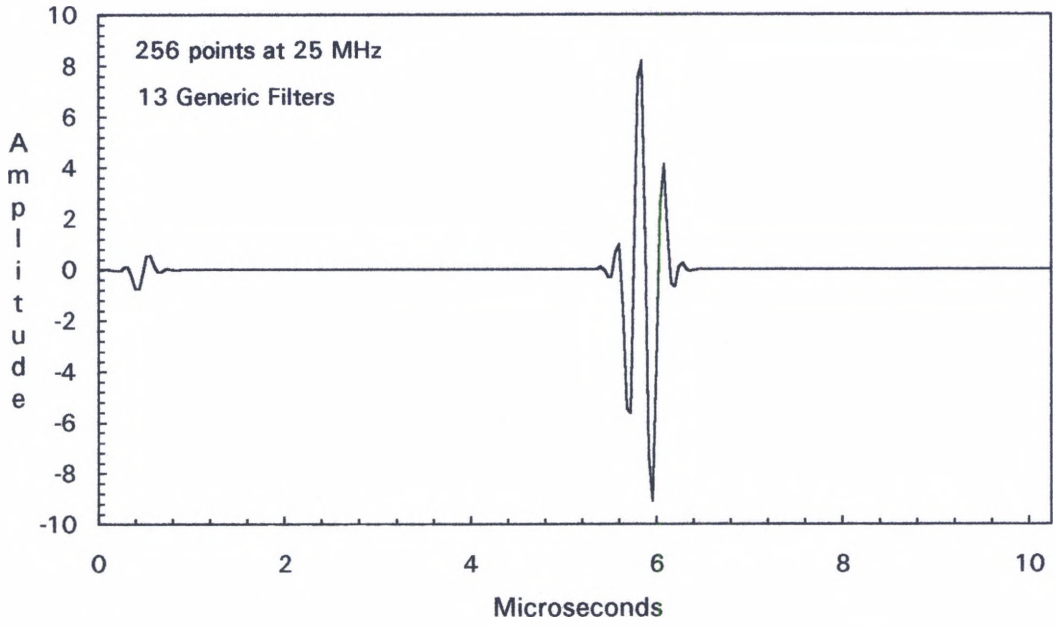

Fig. 3.37c Signal of Fig. 1.2 after Processing with 13 Filters(Fig. 3.27).

about 114,816 multiplies. Usually, in practice, much higher sampling rates are used with the FFT to prevent the introduction of high frequencies into the signal; digital filters do not pose this problem.

CHAPTER IV

CONCLUSIONS AND FUTURE WORK

The bulk of this work has been devoted to exploring alternative implementations of the split spectrum processing technique to reduce the processing time. Two avenues were considered. First, chapter II introduces a flat top to the conventional filter shape in order to boost SNR performance by preserving signal energy without substantially increasing correlation between neighboring filters, and possibly reduce the size of the filter bank to speed up processing. Hanning windows were used in the simulations, and eventually generic flat-top filters were employed. The results clearly indicate that, under certain conditions, a certain number of filters can be dropped without compromising SNR performance thereby reducing processing time. Second, chapter III considers the implementation of SSP with an FIR two-branch structure whose multiply count per output sample compares favorably to the well known direct method by Parks and McClellan. Following this approach, savings in excess of 70% in the multiply count of the digital filter, over that of the direct approach, can be obtained. Also, when a reduction in the filter bank, combined with the application of the polarity thresholding and minimization algorithms in tandem, is possible; then substantial improvements in the processing time of the technique can be achieved.

This work has demonstrated the effectiveness of other filter shapes such as raised-cosine filters, and the more generic frequency selective filters, as opposed to the more conventional Gaussian shape. Other shapes can also work just as well: Kaiser shape, for instance, could also be used.

Even though the feasibility of the reduction of the filter bank size has been demonstrated, the scope of this work has not allowed to study and clearly establish any general criteria, or guidelines for concrete conditions under which such reduction can be implemented without compromising performance, and what number of filters could be dropped. This work could be carried out by conducting extensive experiments on various different types of signals with varying degrees of noise levels and originating from different types of flaws and materials.

Another area for further work is the implementation of the technique of chapter III on any of the most recent DSP chips such as the TMS320 family, in order to ascertain hardware resources necessary such as buffers, data memory, code size, data flow for optimal performance etc., and be able to contrast it to an FFT-based implementation. The FFT has been long established as a very powerful processing tool, and specialized circuitry has been built into DSP chips for its efficient implementation; however, an investigation of the VLSI implementation of SSP with the FFT, as opposed to a two-branch filter structure mechanization of the technique, may be required to establish the merits and shortcomings of both.

Finally, as another option for future work, the bandpass filtering stage of SSP may be implemented by shifting the spectrum of the unprocessed signal, as opposed to shifting(tuning) the spectrum of the bandpass filter itself, by an appropriate amount to place or center the correct frequency bin about the zero-frequency axis. In this fashion, the filtering may be performed by a cascade of running-sum filters that would reduce the filtering to simple additions and subtractions. Of course, the resulting spectrum would have to be shifted back to the original place. However, the processing should proceed extremely fast.

APPENDIX A

```
C= = = = = = = = = = = = = = = = = = = = = = = = = = = = = = = = = = = = = = = = = = = = =
C
C     ROUTINE NAME : BPIFIR
C
C     ROUTINE TYPE: FORTRAN 77 SUBROUTINE
C
C     PURPOSE: THIS SUBROUTINE MECHANIZES THE TWO BRANCH
                    STRUCTURE OF FIGURE 3.12.
C
C     X  ----> INPUT SEQUENCE
C
C     H  ----> IMPULSE RESPONSE OF THE BASE FILTER
C
C     LH ---> LENGTH OF BASE FILTER
C
C     G -----> IMPULSE RESPONSE OF THE MASKING FILTER
C
C     LG ----> LENGTH OF MASKING  FILTER
C
C     F1----> 0 IF THE LENGTH OF H IS EVEN, 1 IF ODD
C
C     F2----> 0 IF THE LENGTH OF G IS EVEN, 1 IF ODD
C
C     IF----->  INTERPOLATION OR SCALING FACTOR
C
C     WO---> DESIRED CENTER FREQUENCY OF FILTER
C
C     Y ----> OUTPUT SEQUENCE
C
C     LY ----> LENGTH OF OUTPUT SEQUENCE
C              { LY = LX+(LH-1)*IF + LG - 1}
C
C     AUTHOR:  ORLANDO J. CANELONES
C
```

```
C= = = = = = = = = = = = = = = = = = = = = = = = = = = = = = = = = = = = = = =
C
      SUBROUTINE BPIFIR(X,LX,H,G,LH,LG,F1,F2,IF,WO,LY,Y)
C
      REAL X(0:3500), HA(0:80), HB(0:80),H(0:LH),G(0:LG), WO
      REAL GA(0:80), GB(0:80), Y(0:LY)
      REAL XA(0:2000), XB(0:2000), R1(0:80), R2(0:80)
      REAL P1(0:80), P2(0:80), MS, PI, PIE, J
      INTEGER IF, F1, F2
C
      PI = 3.141592654
      M = (LH-1)/2
      MS = (LH-1)/2.0
      PII = WO*(PI+PI)
      W = PII*IF
C
C= = = = = = = CENTERING OF THE BANDPASS FILTER= = = = = = = =
C
      DO 1 K = 0, M
      J = K-MS
      HA(K) = H(K)*COS(W*J)
      HB(K) = H(K)*SIN(W*J)
1     CONTINUE
C
      M = (LG-1)/2
      MS = (LG-1)/2.0
C
      DO 2 K=0,M
      J = K - MS
      GA(K) = G(K)*COS(PII*J)
      GB(K) = G(K)*SIN(PII*J)
2     CONTINUE
C
      L = (LH-1)*IF
      LL = LG-1
      LAB = LX+L
      M1 = L/2
      M2 = LG/2
C
      DO 40 I = 0, LG
      R1(I) = 0.0
      R2(I) = 0.0
```

```
40    CONTINUE
C
C= = = = = = = = = = = = = = = = =SECTION I= = = = = = = = = = = = = =
C
      DO 10 N = 0, LAB-1
      XA(N) = 0.0
      XB(N) = 0.0
      I = 0
C
      DO 20 K = 0, M1-1, IF
      I1 = N+K
      I2 = N-K+L
      IF (X(I1).EQ.0.0.AND.X(I2).EQ.0.0) GOTO 3
      XA(N) = XA(N) + HA(I)*(X(I1) + X(I2))
      XB(N) = XB(N) + HB(I)*(X(I2) - X(I1))
3     I = I + 1
20    CONTINUE
      IF (F1.EQ.1) XA(N) = XA(N) + HA(I)*X(I1+IF)
C
C = = = = = = = = = = = = = = = = =SECTION II= = = = = = = = = = = = = =
C
      DO 60 K = 0, M2 - 1
      P1(K) = GA(K)*XA(N)
      P1(LL-K) = P1(K)
      P2(K) = GB(K)*XB(N)
      P2(LL-K) = -P2(K)
60    CONTINUE
C
      IF (F2.EQ.1) THEN
            P1(M2) = GA(M2)*XA(N)
            P2(M2) = 0.0
      ENDIF
C
      DO 70 K = 0, LG - 1
      I = K+1
      R1(K) = P1(K) + R1(I)
      R2(K) = P2(K) + R2(I)
70    CONTINUE
      Y(N) = R1(0) - R2(0)
10    CONTINUE
C
      DO 80 N = LAB, LY - 1
```

```
      DO 110 K =0, LG - 1
      I = K+1
      R1(K) = R1(I)
      R2(K) = R2(I)
110   CONTINUE
      Y(N) = R1(0) - R2(0)
80    CONTINUE
      RETURN
      END
C=====================================
```

A sample digital filter designed with the technique introduced in chapter III with the help of the above subroutine is presented next. The specifications for this filter are : desired approximation error $\delta = 0.001$ (-60 dB) in both passband and stopband. The passband width $\Delta\rho = 0.005$ and the transition bandwidth $\Delta f = 0.01$. Following the instructions laid out in chapter III, the scaling factor is chosen to be 8 and the errors are selected such that $\delta_{\beta p} = \delta_{\mu p} = \delta_{\mu s} = 0.0005$ and $\delta_{\beta s} = 0.001$. The cut-off frequencies for the base filter are as follows:

$f_{\beta p} = 8x0.005 = 0.040$ (passband cut-off frequency)

$f_{\beta c} = 8x0.015 = 0.12$ (stopband cut-off frequency)

and those of the masking filter are

$f_{\mu p} = 0.015$ (passband cut-off frequency)

$f_{\mu c} = \frac{1}{8} - 0.015 = 0.11$ (stopband cut-off frequency)

The filter that results is shown figures A.1. The base filter is realized with 45 taps while the masking filter takes 40 taps. Note that the direct approach demands about 43% more multiplies per output sample. Also, note that the error is no longer equiripple.

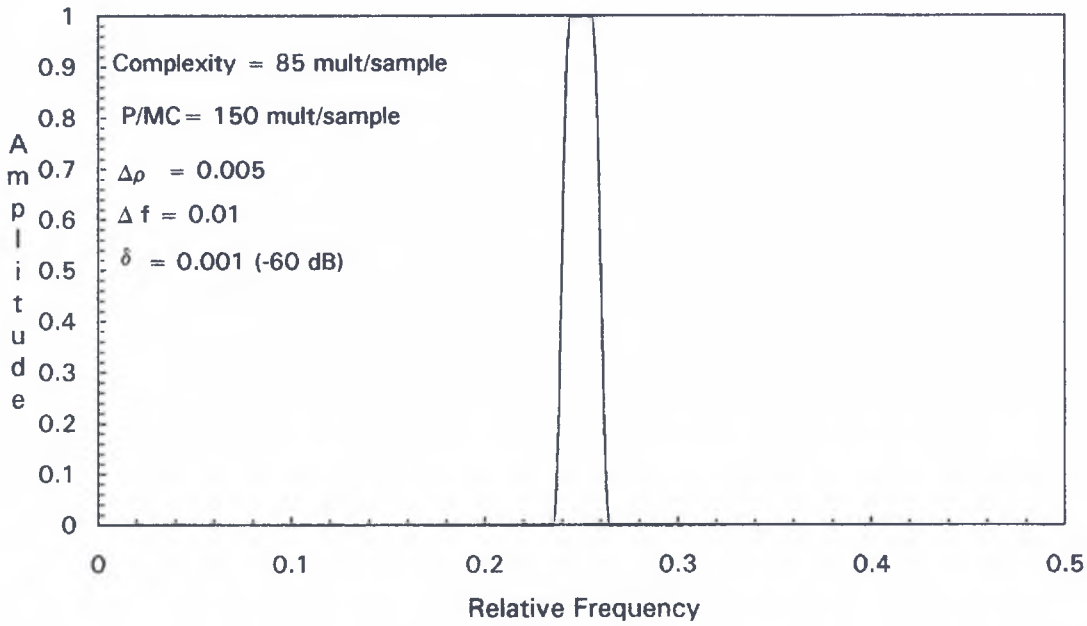

Fig. A.1a Amplitude Frequency Response of Digital Filter.

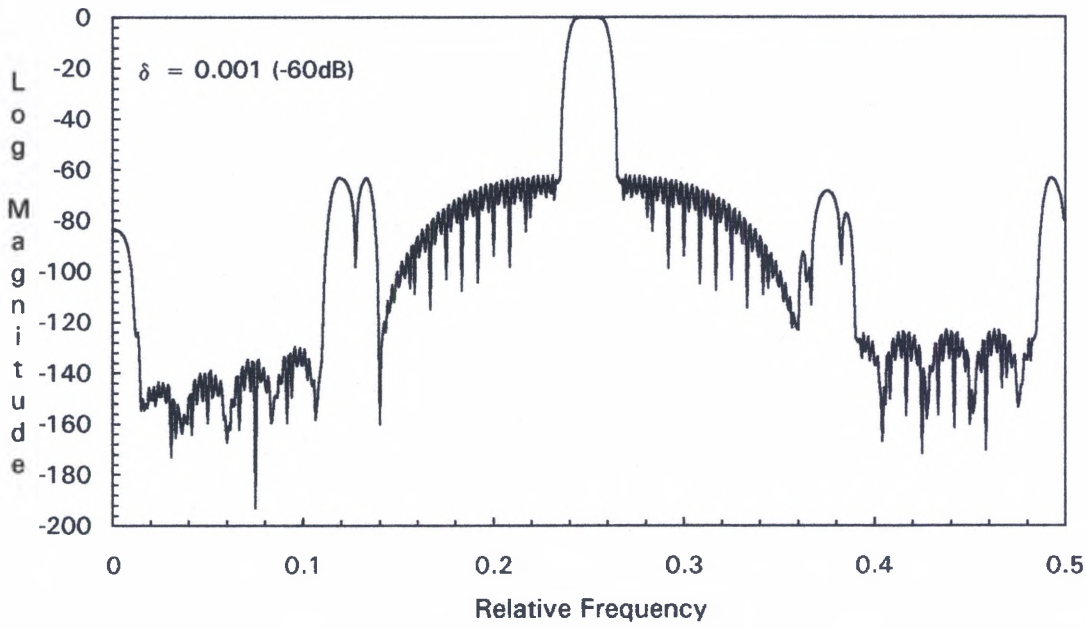

Fig. A.1b Log Magnitude Frequency Response.

```
C= = = = = = = = = = = = = = = = = = = = = = = = = = = = = = = = = = = = = =
C
C      ROUTINE NAME : RAC
C
C      TYPE OF ROUTINE: FORTRAN 77 SUBROUTINE
C
```

C **PURPOSE**: RETURNS THE COEFFICIENTS FOR THE IMPULSE OF A BANDPASS RAISED-COSINE FILTER. THE LENGTH OF THE IMPULSE RESPONSE IS GIVEN BY 'L' (ODD OR EVEN), THE WIDTH OF THE TRANSITION BAND IS 'TBW' AND THAT OF THE PASSBAND IS 'PBW'. THE CENTER FREQUENCY IS GIVEN IN 'FCE' AND THE COEFFICIENTS ARE RETURNED IN 'H(K)' WITH 'H(0)' HOLDING THE POINT OF SYMMETRY. IF 'FCE' = 0.0 A LOWPASS FILTER CAN BE DESIGNED, AND IF 'FCE' = 0.5 A HIGHPASS FILTER CAN BE DESIGNED.'FCE', 'TBW' AND 'PBW' MUST ALL BE NORMALIZED WITH RESPECT TO THE SAMPLING FREQUENCY.

```
C
C      AUTHOR:     ORLANDO J. CANELONES
C
C= = = = = = = = = = = = = = = = = = = = = = = = = = = = = = = = = = = = = =
C
      SUBROUTINE RAC(FCE,TBW,PBW,L,H)
C
      REAL H(0:L), FCE, PBW, PI, PII, TBW, LHP
C
      PI = 3.141592654
      PII = PI+PI
      LHP = 1.0
C
      IF (FCE.EQ.0.0.OR.FCE.EQ.0.5) LHP = 0.5
      OS = 0.0
      IT = MOD(L,2)
      M = L/2
```

```
      IF (IT.EQ.0) THEN
      OS = 0.5
      IK = 0
      ELSE
      IK = 1
      OS = 0.0
      H(0) = 4*PBW+TBW+TBW
      H(0) = LHP*H(0)
      ENDIF
C
      DO 10 K = IK, M
      T = K+OS
      FAC = PII*T
      TT = T*(TBW+TBW)
      IF (TT.NE.1.0) THEN
      H(K) = (SIN(FAC*(PBW+TBW)) + SIN(FAC*PBW))*COS(FAC*FCE)
      H(K) = LHP*H(K)/(PI*T*(1 - TT*TT))
      ELSE
      H(K) = LHP*TBW*COS(PBW*PI/TBW)*COS(PI*FCE/TBW)
      ENDIF
10    CONTINUE
      RETURN
      END
C= = = = = = = = = = = = = = = = = = = = = = = = = = = = = = = = = = = = = = = =
```

A sample of a digital lowpass, bandpass, and highpass filters of the raised-cosine type designed with the subroutine **RAC** above are shown in the figures A.2 below.

```
C= = = = = = = = = = = = = = = = = = = = = = = = = = = = = = = = = = = = = = = =
C
C     NAME: GAUSSIAN
C
C     TYPE OF ROUTINE: FORTRAN 77 SUBROUTINE
C
```

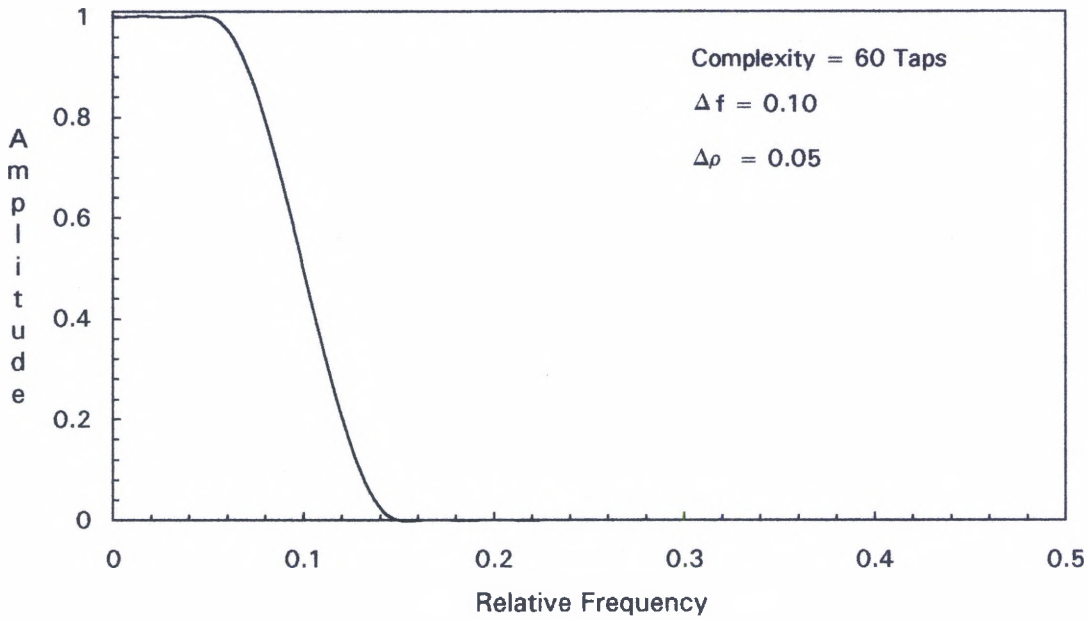

Fig. A.2a Lowpass RAC Filter.

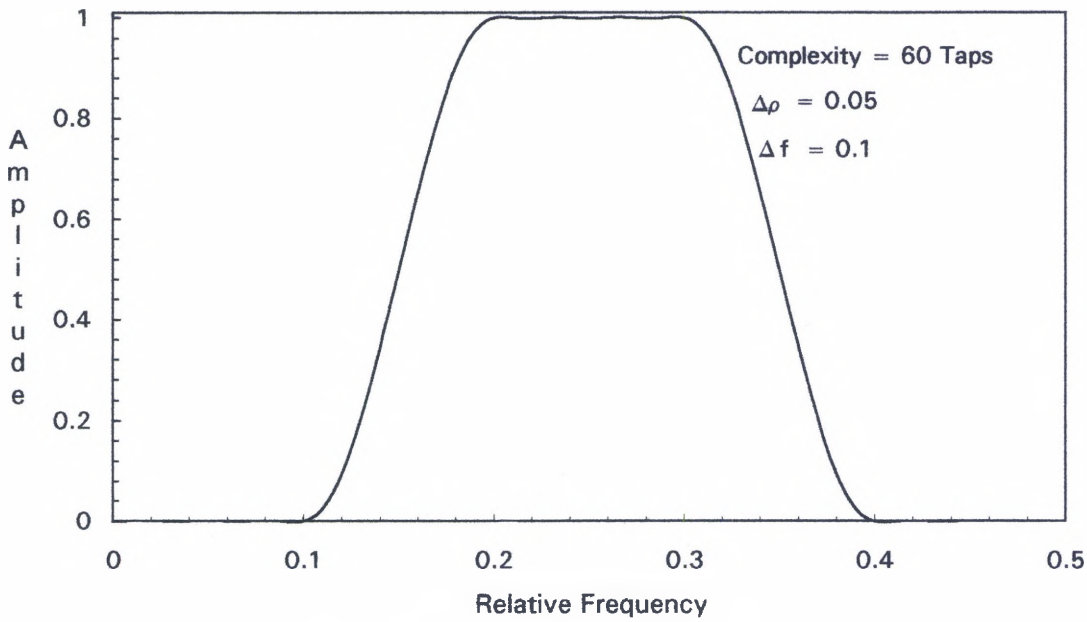

Fig. A.2b Bandpass RAC Filter.

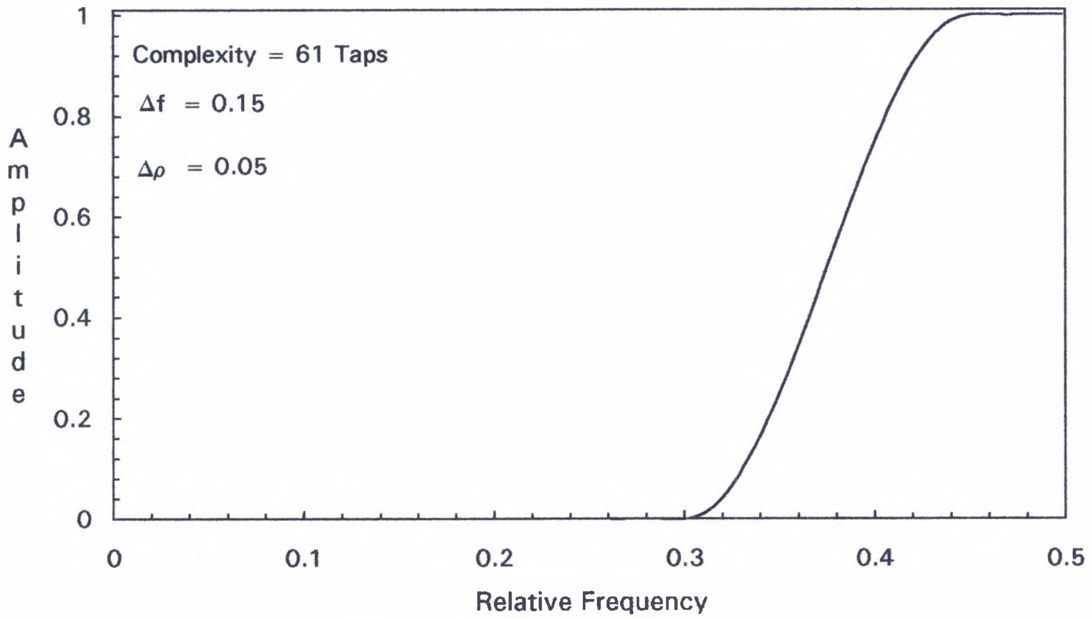

Fig. A.2c Highpass RAC Filter.

```
C     PURPOSE: RETURNS THE COEFFICIENTS OF THE IMPULSE
RESPONSE FOR A BP GAUSSIAN FILTER WITH BANDWIDTH 'BW' AND
CENTER FREQUENCY 'FCE' BOTH NORMALIZED WITH RESPECT TO THE
SAMPLING FREQUENCY. 'H(K)' HOLDS THE IMPULSE RESPONSE WITH
'H(0)' CONTAINING THE POINT OF SYMMETRY. THE USER SPECIFIES
THE LENGTH 'L'. (SEE FIG. A.3)
C
C     AUTHOR: ORLANDO J. CANELONES
C
C=====================================
C
      SUBROUTINE GAUSSIAN(L,BW,FCE,H)
C
      REAL BW, FCE, H(0:L), LP
C
```

```
      LP = 1.0
      IF (FCE.EQ.0.0) LP = 0.5
      PI = 3.141592654
      V1 = 1.7*BW*1.772453851
      V2 = 2.67*BW
      V3 = (PI+PI)*FCE
      REMAINDER = MOD(L,2)
      OS = 0.0
      IF (REMAINDER.EQ.0) OS = 0.5
      M = (L-1)/2
C
      DO 10 K=0,M
      H(K) = V1*EXP(-(V2*(K+OS))**2)
      H(K) = LP*H(K)*COS(V3*(K+OS))
10    CONTINUE
      RETURN
      END
C
C= = = = = = = = = = = = = = = = = = = = = = = = = = = = = = = = = = = = = = = =
C
C     NAME: GAUSSRAND
C
```

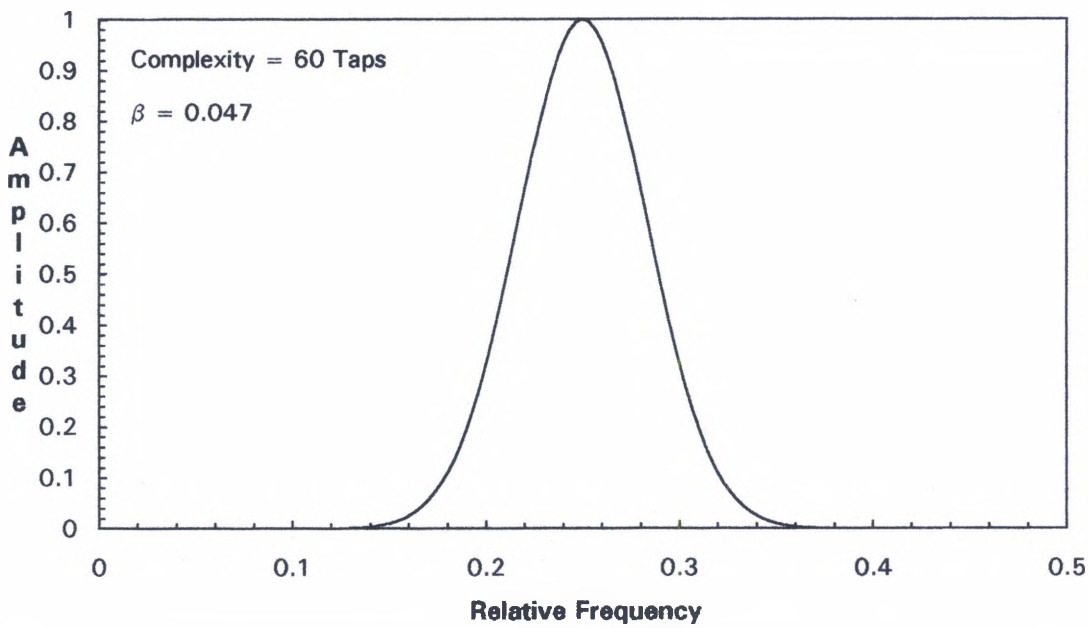

Fig. A.3 Gaussian Bandpass Filter Designed with Subroutine *Gaussian*.

```
C     TYPE OF ROUTINE: FORTRAN 77 SUBROUTINE
C
C     PURPOSE: GENERATES A RANDOM SEQUENCE WITH A GAUSSIAN
DISTRIBUTION WITH MEAN AND STANDARD DEVIATION SPECIFIED BY
THE USER. THE ARRAY 'RN(K)' HOLDS THE RANDOM SEQUENCE. FOR
THE GENERATION OF THE SEQUENCE, FIVE HUNDRED RANDOM
NUMBERS WITH A UNIFORM DISTRIBUTION ARE ADDED TOGETHER. THE
MEAN OF THE UNIFORM DISTRIBUTION IS 0.0775 AND ITS VARIANCE IS
0.002 APPROXIMATELY.
C
C     AUTHOR:  ORLANDO J. CANELONES
C
C= = = = = = = = = = = = = = = = = = = = = = = = = = = = = = = = = = =
C
      SUBROUTINE GAUSSRAND(MEAN,STD,NS,SEED,RN)
C
      REAL MEAN, STD, RN(NS), Z
      INTEGER*4 SEED
C
      DO 10 K=1,NS
      SUM = 0.0
      DO 20 J=1,500
      SUM = SUM+0.155*RAN(SEED)
20    CONTINUE
      Z = SUM-38.75
      RN(K) = MEAN+STD*Z
10    CONTINUE
      RETURN
      END

C= = = = = = = = = = = = = = = = = = = = = = = = = = = = = = = = = = =
C
C     NAME: UNIRAND
C
C     TYPE OF ROUTINE: FORTRAN 77 SUBROUTINE
C
```

```
C     PURPOSE : GENERATES A UNIFORMLY DISTRIBUTED SEQUENCE
OF RANDOM NUMBERS. THE USER SPECIFIES THE BOUNDS, UPPER AND
LOWER ('UL' AND 'LL'), THE NUMBER OF POINTS IN THE SEQUENCE
'NS' AND THE 'SEED'. TO OBTAIN DIFFERENT SEQUENCES, DIFFERENT
SEEDS MUST BE GIVEN. THE RANDOM SEQUENCE IS RETURNED IN
'RN(K)'.
C
C     AUTHOR: ORLANDO J. CANELONES
C
C= = = = = = = = = = = = = = = = = = = = = = = = = = = = = = = = = = = = =
C
C     SUBROUTINE UNIRAND(UL,LL,NS,SEED,RN)
C
      REAL UL, LL, RN(NS)
      INTEGER*4 SEED
C
      DO 10 I=1,NS
      RN(I) = LL+(UL-LL)*RAN(SEED)
10    CONTINUE
      RETURN
      END
C= = = = = = = = = = = = = = = = = = = = = = = = = = = = = = = = = = = = =
```

BIBLIOGRAPHY

1. Karpur, P. , Shankar, P.M., Rose, J.L. and Newhouse, V.L. "Split Spectrum Processing: Optimizing the Processing Parameters Using Minimization." Ultrasonics, Vol. 25, pp. 204-208, 1987.

2. Aussel, J.D. "Split Spectrum Processing with Finite Impulse Response Filters of Constant Frequency-to-bandwidth Ratio." Ultrasonics, Vol. 28, pp. 229-240, July 1990.

3. Oran, Brigham E. "The Fast Fourier Transform and its Applications." Prentice Hall, Englewood Cliffs, N.J.,1990.

4. Karpur, Prasanna. "Split Spectrum Processing: Process Modeling and the Evaluation of Polarity Thresholding Algorithm for Material Noise Reduction in Ultrasonic NDE." Ph.D. Dissertation, Drexel University, Philadelphia, 1987.

5. Rose, J.L., Karpur, P., and Newhouse, V.L. "Utility of Split-Spectrum Processing in Nondestructive Ultrasonic Evaluation." Materials Evaluation, Vol. 46, pp. 114-122, January 1988.

6. Shankar, P.M., Bencharit, U., Bilgutay, N.M., and Saniie J. "Grain noise Suppression through Bandpass Filtering." Materials Evaluation, Vol. 46, pp.1100-1118, July 1988.

7. Oppenheim, Alan V., and Schafer, Ronald W. "Discrete Time Signal Processing." Prentice Hall, N.J., 1990.

8. Higgins, Richard J. "Digital Signal Processing in VLSI." Prentice Hall, N.J., 1990.

9. Saramaki, T., Neuvo, Yrjo, and Mitra, S.K. "Design of Computationally Efficient Interpolated FIR Filters." IEEE Transactions on Circuits and Systems, Vol. 35, No.10, pp. 70-88, January 1988.

10. Yan, R., Liu, B. and Lim, Y.C. "A New Structure of Sharp Transition FIR Filters Using Frequency Response Masking." IEEE Transactions on Circuits and Systems, Vol. 35, No.8, pp. 955-966, August 1988.

11. Adams, J.W. and Wilson, A.N. "A New Approach to FIR Digital Filters with Fewer Multipliers and Reduced Sensitivity." IEEE Transactions on Circuits and Systems, Vol. CAS-30, No. 5, pp. 277-283, May 1983.

12. Jing, Z. and Fam, A.T."A New Structure for Narrow Transition Band, Lowpass Digital Filter Design." IEEE Transactions on Acoustics, Speech, and Signal Processing, Vol. ASSP-32, No. 2, pp. 362-370, April 1984.

13. Saramaki, T. "Design of FIR Filters as a Tapped Cascaded Interconnection of Identical Subfilters." IEEE Transactions on Circuits and Systems, Vol. CAS-34, No. 9, pp. 1011-1029, September 1987.

14. McClellan, J.H., Parks, T.W. and Rabiner, L.R. "A Computer Program for Designing Optimum FIR Linear Phase Digital Filters." IEEE Transactions on Audio and Electroacoustics, Vol. AU-21, No.6, pp. 506-526, December 1973.

15. Draheim, W.A. and Furgason, E.S."A Two Dimensional Approach to Clutter Rejection in Ultrasonic Images." IEEE Ultrasonics Symposium, 1983.

16. Rabiner, L. and B. Gold, "Theory and Application of Digital Signal Processing." Prentice Hall, Englewood Cliffs, N.J., 1975.

17. Lim, Y. C. "A Digital Filter Bank for Digital Audio Systems." IEEE Transactions on Circuits and Systems, Vol. CAS-33, No. 8, August 1986.

18. Bilgutay N.M. "Split-spectrum Processing for Flaw-to-Grain Echo Enhancement in Ultrasonic Detection." PhD. Thesis, Purdue University, Laffayatte, 1981.

19. Bilgutay N.M., E.S. Furgason, and V.L. Newhouse, "Evaluation of Random Signal Correlation System for Ultrasonic Flaw Detection." IEEE Transaction on Sonics and Ultrasonics, Vol.SU-23,pp.329-333, September 1976.

20. E.S. Furgason, V.L. Newhouse, Bilgutay N.M. and G.R. Cooper, "Application of Random Signal Correlation Technique to Ultrasonic Flaw Detection." Ultrasonics, Vol.13, No. 1, pp.11-17, Butterworth Scientific, Guildford, U.K., January, 1975.